Microlensing towards M31

Microlensing towards M31

Matthias Martin Schmid
ETH Zürich

September 2002

Diploma Thesis

carried out at the Institute of Theoretical Physics of the University of Zürich under supervision of Prof. Philippe Jetzer.

Abstract

Many astrophysical observations imply, that a significant fraction ($\approx 90\%$) of the matter present in the Universe is dark. In particular, the rotation curves of many spiral galaxies suggest that the dark matter is the dominant constituent of the galaxies and forms approximately spherical dark haloes around them. The nature of this dark matter is still unknown.
Plausible candidates for a baryonic nature of the dark matter are brown dwarfs, or more general massive compact objects (MACHOs). Gravitational microlensing is a useful method to detect MACHOs in the halo of our Galaxy. A natural expansion of this method is the pixel lensing technique, where the monitored stars need not to be resolved. Using this powerful technique it is possible to probe the haloes around nearby galaxies for MACHOs.
In the present diploma thesis I calculate the optical depth, the event rate and the expected number of events for a pixel lensing survey of M31, the Andromeda Galaxy. I consider microlensing by MACHOs in the M31 halo and the Galactic halo, as well as self-lensing of M31 stars. The results are compared with the observational data of four microlensing events reported by the POINT-AGAPE collaboration. From this data I estimate the measured optical depth using both the Einstein time t_E and the full width at half maximum timescale t_{fwhm} and I obtain similar results. Using the method of dark mass moments I calculate the mean lens mass and the fraction of dark matter in form of MACHOs, implied by the four events.
As a major novelty, I propose a generalization of the method of dark mass moments to the case of pixel lensing, where t_E is in general not known and only t_{fwhm} can be used. The developed method is tested with the four POINT-AGAPE events and I obtain similar results for the mean lens mass, but systematically higher MACHO fractions.

Contents

List of Figures

List of Tables

Chapter 1

The Dark Matter Problem

An important problem of contemporary astrophysics and cosmology is the determination of the amount and the nature of matter in the Universe. From many astrophysical observations, there is ample evidence that over 90% of the matter present in the Universe is actually dark and, therefore, cannot be detected using telescopes. It was first the Swiss astrophysicist Fritz Zwicky, who pointed out in 1933 that luminous matter makes up only a small fraction of the mass in large-scale structures (Zwicky, 1933). He observed that the dispersion velocities of clusters of galaxies like the Coma cluster implied masses far in excess of the luminous matter. This is called the *missing mass problem*. Furthermore, observations of single galaxies have shown that the *dark matter* dominates the visible matter on galactic distance scales as well. A different point of view comes into play from primordial nucleosynthesis of the light elements, which is predicted in the context of the standard model of cosmology. By comparing the measured abundances of the primordial light elements (H, He, Li, etc.) to the predictions from the theory one can put constraints on the density of baryons[1] in the Universe.
On the other hand, these predictions for the density of baryons can be confronted with the estimations of the mass densities of galaxies and clusters of galaxies. From this, it is clear, that the total amount of matter cannot be provided with baryons only - there must be a form of matter in the Universe, that is *non-baryonic*. Furthermore, some part of the baryons must be dark, since the estimated baryon density seems to be higher than the density of the visible content of the Universe. Therefore, the dark matter problem poses actually two fundamental questions. First, what is the nature of the non-baryonic dark matter? And second, what form has the baryonic dark matter?

The dark matter problem is present on various distance scales, from the

[1] Baryons are called those particles, that take part at the strong interaction and have half-integer spin. Today it is known, that baryons are made up of three quarks. Since the proton and the neutron are the lightest baryons and are stable within the nuclei of atoms, the bulk of the mass of ordinary matter is provided by the baryons.

large superclusters of galaxies with hundreds of Mpc diameter down to the local solar neighbourhood of a few hundred pc. Thus, a third question is, how the dark matter is distributed on the different distance scales. In this work, we will restrict ourselves to the dark matter in the haloes around galaxies. In section 1.2 we present a few candidates for the galactic dark matter.

In section 1.3 we will introduce the so-called *microlensing* method to detect massive compact objects, which are a particular candidate for dark matter in the haloes around galaxies. This method is based on the deflection of light rays in the gravitational fields of dark massive objects, which is predicted by Einstein's theory of General Relativity. It was again Zwicky who proposed to use this effect to measure the mass of an astrophysical system that acts as a lens and changes the image of a luminous source. The first effect was seen in 1979 in form of a multiply-imaged quasar (Walsh, Carswell & Weymann 1979). This has opened an independent way to measure the mass of astrophysical systems. Microlensing is a special case of gravitational lensing and is characterized by the fact that the source is a single star in the Milky Way or in a nearby galaxy and the lens is a dark compact object between the source star and the observer. In this case, the multiple images are not resolved and the deflection of light rays leads to a time-dependent brightening of the source star, while the lens passes in front of the source star.

1.1 Observational Indications

The dark matter problem is embedded in the framework of the standard model of cosmology, which is essentially the Big Bang model based on the theory of general relativity. In the standard model, the spacetime is assumed to be isotropic and homogenous.[2] The homogenous density of the Universe is usually denoted by

$$\Omega = \frac{\rho}{\rho_c} \ , \tag{1.1}$$

where the critical density is

$$\rho_c = \frac{3H_0^2}{8\pi G} = 2.78 \times 10^{11} \ h^2 \ \mathrm{M}_\odot \mathrm{Mpc}^{-3} \ . \tag{1.2}$$

$H_0 = 100 \ h$ km s^{-1} Mpc^{-1} is Hubble's constant and G is Newton's constant. The value of the dimensionless parameter h lies between 0.5 and 1 and present measurements suggest $h \approx 0.65$. The critical density is the

[2] Actually, it is sufficient to postulate isotropy. It can be shown that homegenity follows from isotropy, but not vice-versa (see e.g. Straumann 1974).

density of a Universe described by the 'flat' Friedmann-Lemaître model.[3] A universe with a density above this critical value will be spatially closed, whereas a lower-density universe will be spatially open. It is quite common in cosmology to express the different estimations to the density paramater in a notation of the form (1.1) by writing $\Omega_i = \rho_i/\rho_c$, where the subscript i stands for the considered astrophysical system.
Unfortunately, the Hubble parameter h enters most of the density estimations. Therefore, an accurate measurement of it is still an important issue of present observational cosmology. For the estimations of the masses of galaxies and clusters of galaxies, the ratio M/L between the (dynamical) mass M and the luminosity L characterizes the system. Since $M \propto h^{-1}$ and $L \propto h^{-2}$ we have $M/L \propto h$. The same Hubble parameter h affects also the predictions from primordial nucleosynthesis for the baryon density. These predictions are usually quoted in cosmology as the reciprocal of the entropy per baryon

$$\eta := \frac{n_p + n_n}{n_\gamma} = 2.74 \times 10^{-8} \left(\frac{T}{2.73\ K}\right)^{-3} \Omega_B h^2 \ , \qquad (1.3)$$

which is just the ratio between the number of baryons and the number of photons.

1.1.1 Mass estimations

The observation of astrophysical systems like galaxies or clusters of galaxies makes it possible to estimate the mass of the visible matter by determining their luminosities, but also the dynamical mass, by measuring the internal velocities of the systems.
The dark matter shows its existence just by gravitational effects, it determines the potentials of the observed astrophysical system. The dark matter content of an astrophysical system is defined as the difference between the dynamical mass and the visible mass. The mass estimations are made on different distance scales from $\approx$ 100 Mpc in the super-clusters to $\approx$ 100 pc in the solar neighbourhood. We begin on the largest scale.

Clusters and groups of galaxies

Historically, the first detection of dark matter was made by Zwicky (1933). He looked at the dispersion of velocities in the Coma cluster and deduced $M/L \approx 300h\ M_\odot/L_\odot$ from application of the virial theorem. Modern techniques are able to probe the mass distribution in rather more detail, but end

[3] The Friedmann-Lemaître model describes an isotropic, matter containing Universe provided with the Robertson-Walker metric $g = c^2dt^2 - R^2(t)\left(\frac{dr^2}{1-kr^2} + r^2 d\Omega\right)$.

up with very much the same answer. With these methods a total mass of

$$M_{Coma} = 6 \times 10^{14}\ h^{-1}\mathrm{M}_{\odot}\ , \tag{1.4}$$

is found for the Coma cluster implying $\Omega \approx 0.2 - 0.3$. The visible mass in form of stars in the galaxies of the Coma cluster is only $M_{stars} \approx 3 \times 10^{13}\ h^{-1}\ \mathrm{M}_{\odot}$, i.e. the fraction of the visible matter is only 5%.
This dark matter problem on larger scales was partially solved by the discovery of hot intergalactic gas between the galaxies that is visible in X-rays. With observations from X-ray satellites as ROSAT one could estimate the mass of this intergalactic gas for different clusters of galaxies. Adding this mass to the mass of the stars in the galaxies of the cluster, we then get a better measure for the mass of the luminous content of the cluster. For the Coma cluster the mass of the hot intergalactic gas is $M_g \approx 3 \times 10^{13}\ h^{-5/2}\ \mathrm{M}_{\odot}$ and thus we obtain

$$\frac{M_{lum}}{M_{tot}} \approx 0.01 + 0.05 h^{-3/2}\ . \tag{1.5}$$

For $h = 0.65$ the luminous mass is only 11% of the total mass (less than 3% of the critical density). Thus, on larger scales, about 90% of the total mass is supplied by dark matter and its nature is unkown until the present day.

Spiral galaxies

Another important evidence for the existence of large quantities of dark matter on smaller scales comes from the measured rotation curves of several hundreds of spiral galaxies. Many of the spiral galaxies show flat rotation curves. If there were no matter beyond the visible edge of the spiral galaxies, the measured rotation curve should show a Keplerian fall-off ($v_{rot} \propto 1/r$). But measurements of the rotation velocity of stars up to the visible edge and of atomic hydrogen gas in the galactic discs imply that the rotation velocity remains constant out to very large distances (≈ 100 kpc).[4] This is the main evidence for dark haloes around spiral galaxies.
However, the need for massive dark haloes around spiral galaxies was in fact originally suggested before most of the data on galaxy rotation curves were available (Ostriker, Peebles & Yahil 1974). The theoretical argument comes from the stability of self-gravitating discs. Numerical studies indicate that discs can in many circumstances be unstable and generate a nearly linear structure in their centres. One way of understanding this is, that the visible matter in the disc orbits passively in the potential well defined by approximately spherical haloes of dark matter. However, this theoretical argument has been weakened by the discovery of many spiral galaxies (even the Milky Way) with barred structures in their centres.

[4]The radial velocity of the atomic hydrogen can be measured via the Doppler shift of the 21 cm hyperfine structure emission line of neutral hydrogen.

Elliptical galaxies

The kinematics of elliptical galaxies are much more difficult to study than that of spiral galaxies. However, in some cases ellipticals contain sufficient neutral hydrogen gas at large distances, that measurements of the rotation velocity can be made, which suggest the existence for a dark halo for elliptical galaxies as well. For the great elliptical galaxy M87 in the center of the Virgo cluster, there is clear evidence for a dark halo from the dynamics of globular clusters orbiting M87.

1.1.2 Baryon density

Primordial nucleosynthesis in the context of the standard model of cosmology gives us an estimation for Ω_B, the fraction of the critical density of the Universe in form of baryons. This estimation supplies us with two important informations. First, comparing Ω_B to the density of the visible mass, we can estimate the amount of dark matter in form of baryons. Second, confronting Ω_B to the estimated total matter density Ω yields the non-baryonic contribution to the dark matter.

Primordial nucleosynthesis takes place in the era of the evolution of the Universe, when radiation dominates matter. During this epoch the relation between the time evolution of the Universe and the temperature is

$$kT \propto t^{-1/2}. \tag{1.6}$$

For kT measured in MeV and t measured in s after the Big Bang, the proportionality can be approximated by taking $kT \approx 1$ MeV for $t = 1$ s.
At the beginning of the nucleosynthesis era, the Univers consists of photons, protons, neutrons, electrons and three species of neutrinos. The first step in primordial nucleosynthesis must therefore be the synthesis of deuterium by the reaction

$$n + p \leftrightarrow D + \gamma. \tag{1.7}$$

Since the ratio between nucleons and photons is so small ($n_B/n_\gamma < 10^{-9}$) and the cross section for the dissociation of the deuterium is high, the formation of heavy elements is largely suppressed at high temperatures ($kT > 0.3$ MeV). This phenomenon is called the deuterium bottleneck. At a temperature higher than about 1 MeV, protons and neutrons are in thermical equilibrium through the reactions

$$n \leftrightarrow p + e^- + \bar{\nu}_e \tag{1.8}$$

$$n + \nu_e \leftrightarrow p + e^- \tag{1.9}$$

$$n + e^+ \leftrightarrow p + \bar{\nu}_e \tag{1.10}$$

The ratio between the number of neutrons and protons depends on their mass difference $\Delta(mc^2) = 1.29$ MeV and on the temperature T

$$\frac{n}{p} \propto e^{-\Delta(mc^2)/kT} \ . \tag{1.11}$$

When the temperature falls below 0.3 Mev the deuterium bottleneck is overcome and the synthesis of the primordial light elements begins. Primordial nucleosynthesis produces almost only ^{4}He together with traces of D, ^{7}Li and ^{3}He. During the synthesis all neutrons are built into the produced nuclides or decay. Since there are no stable nuclides of atomic mass 5 and 8 and since the binding energy of ^{4}He is large, the synthesis of heavier elements than ^{4}He is almost prevented. Primordial nucleosynthesis ends at a temperature of 0.07 MeV or $t = 3$ min, when the Coulomb barrier becomes important. The kinetic energy of the protons is then too small to continue nucleosynthesis.
The observational data on the abundances of deuterium and the other primordial light elements favour a low density $\Omega_B h^2 \approx 0.02$. The constraint obtained from a comparison between nucleosynthesis predictions and observational data is rather tight:

$$0.01 \lesssim \Omega_B h^2 \lesssim 0.015 \ , \quad \text{or} \tag{1.12}$$

$$0.024 \lesssim \Omega_B \lesssim 0.036 \tag{1.13}$$

for $h = 0.65$. This comparison is of course non-trivial, because we can only observe abundances in present-day stars and gas, rather than in primordial material. And it is clear that during the evolution of the Universe ^{4}He is produced and D and ^{7}Li are destroyed within stars. ^{3}He is not destroyed but produced by the destruction of D within the stars.
In any case, since the total mass density of the Universe Ω is at least 0.2 from the different mass estimations, one is forced towards a new form of matter, non-baryonic in nature. Since the uncertainties in the observed abundances of the primordial light elements is still large, one might contemplate a baryonic contribution of at most $\Omega_B = 0.1$. It is clear that this amount of baryonic matter is larger than would be inferred by taking into account only the luminous matter. Thus, it is also evident, that a large fraction of the baryonic matter in the Universe must be dark in the sense that they do not emit detectable electromagnetic radiation.

1.2 Search for galactic dark matter

On the distance scale of galaxies the dark matter exceeds the visible matter by roughly a factor 10. On the other hand, on the galactic scale the dark matter is more dense and thus might be detected in a simpler way. In this section we describe a few candidates for dark matter in the galactic haloes. Some of these are objects of present research.

1.2.1 Non-baryonic dark matter

While the nonbaryonic dark matter almost certainly dominates on intergalactic scales, it could also dominate the mass of single galaxies. According to the standard model of cosmology the matter content of the universe at nucleosynthesis consisted of baryons (plus electrons), photons and three species of neutrinos. There are therefore two distinct ways forward: either the neutrinos have mass, or there must exist some additional particle species that is a frozen-out relic from an earlier stage of the Big Bang. A small mass for neutrinos would not affect nucleosynthesis, as the neutrinos would be ultrarelativistic when they decouple and are thus referred to hot dark matter (HDM) in the literature. Recent results of neutrino oscillation experiments, which also support current models for the nuclear reactions within the sun, show that the neutrinos indeed possess mass, but their mass will be much less than 10 eV. Therefore, the neutrinos as the major constituent of the non-baryonic dark matter are ruled out.
Other relic particles outside of the framework of the standard model would have to be either very rare or extremely weakly coupled (even more weakly than neutrinos) in order not to affect nucleosynthesis. Possible candidates are the axion[5] and the lightest supersymmetric particle (LSP), probably the neutralino. The LSPs are predicted in the framework of supersymmetric extensions of grand unified theories for the interactions between elementary particles.[6] There are important efforts underway to search for LSPs and the axion using existing and planned particle accelerators. The axion or the LSPs decouple when nonrelativistic and are thus cold dark matter (CDM). A common term for all the relic particle candidates for nonbaryonic dark matter is **WIMP**s, standing for **W**eakly **I**nteracting **M**assive **P**articles.

1.2.2 Baryonic dark matter

The simplest hypothesis about the dark matter in the haloes is, that it may be baryonic, in which case the question arises, why this matter is not incorporated onto stars. There are several possibilities for answering this question:

Hot ionized hydrogen gas

If ionized hydrogen gas is the major contribution to the halo dark matter, we would see a large X-ray flux, which would have been detected by X-ray

[5]The axion is the Goldstone boson of the Peccei-Quinn symmetry, a global symmetry introduced to solve the strong CP problem in QCD. The axion would explain, why the CP violation in the strong interaction is so small.

[6]Supersymmetry could, apart from many other advantages, answer the question, why the vacuum energy density Ω_Λ is so small (compared to the predictions of quantum field theory).

satellites. The data of the X-ray satellites imply that at most about 4-5% of the total dark matter is of this form.

Neutral atomic hydrogen gas

From the measurement of the 21 cm hyperfine emission line, we know that the contribution of neutral hydrogen gas is extremely small, probably less than 1%.

Cold molecular hydrogen gas

The observation of cold clouds of molecular hydrogen gas is very difficult. Therefore, there are currently no constraints on this contribution. On contrary, indirect observation even suggest the existence of such clouds. Cosmic ray photons, generated in the Galactic centre and in the disc, are scattered on the protons in the molecular clouds. This scattering process produces energetic gamma-rays which have been detected by satellites.

Massive compact objects

Baryons could have condensed into compact objects, the so-called **MACHOs** (**M**assive **A**strophysical **C**ompact **H**alo **O**bjects). MACHOs are the most promising opponent of the nonbaryonic WIMPs. The term MACHO collects different types of compact objects that could contribute to the mass of the dark haloes of galaxies:

- Low-mass stars
  MACHOs might be low-mass (0.1-0.3 $M_\odot$) hydrogen burning stars (also called M-dwarfs). However, several searches for low-mass stars both in the disc and in the halo of our galaxy have found no evidence that the halo consists mostly of hydrogen burning main-sequence M-dwarfs.

- White dwarfs
  Also a scenario with white dwarfs as a major constituent of the dark haloes has been explored, but it would require an initial mass function[7] (IMF) sharply peaked at 2-6 $M_\odot$.

- Neutron stars
  A substantial component of neutron stars and black holes with masses above that of the sun can be excluded, for they would lead to an overproduction of heavy elements relative to the observed abundances.

[7]The initial mass function states the number of stars per unit mass as a function of their mass ('initial' since the mass distribution is set during the process of star formation).

- Primordial black holes
  Black holes, formed prior to the nucleosynthesis epoch are an interesting dark matter candidate. Such objects could even be made from baryons originally, but they would not count against the nucleosynthesis bound. In this scenario, there is no need for non-baryonic dark matter at all, as the missing mass is hidden in black holes. From certain cosmological models it seems plausible that solar mass black holes might be formed at a temperature of about 100 MeV and this is before the nucleosynthesis era.

- Brown dwarfs
  Brown dwarfs are objects too light for the gravitational pressure to ignite nuclear reactions and are thus a natural candidate for the dark matter in the galactic haloes. If brown dwarfs are a major constituent of the baryonic dark matter, they will have to be primordial and thus will be composed of hydrogen and helium with primordial abundances. Brown dwarfs are defined to have a mass between $M_{ev} \approx 10^{-7}$ $M_\odot$, below which they would evaporate away in a galactic time-scale (De Rújula et al. 1992), and the hydrogen-burning limit of 75 M_J (0.07 $M_\odot$).[8] Radial velocity searches have detected giant planets from 0.25 M_J to 75 M_J in orbits around solar-type stars. Studies of young star-forming regions by infrared observations have found evidence for isolated brown dwarfs in a mass range of 5-75 M_J. The frequency of such objects is not known, but they seem to be sufficiently numerous that the IMF must certainly be continued below the hydrogen-burning limit.

1.3 Microlensing

Direct searches for brown dwarfs can at best explore the solar neighbourhood. To detect brown dwarfs further out, it was proposed by Paczyński (1986) to search for dark objects through gravitational lensing. When a MACHO passes near the line of sight of a background star, the luminosity of this star will be temporarily increased in a characteristic way. Several experiments have been implementing this idea since 1990 and have indeed seen microlensing events.
The MACHO collaboration discovered 13-17 microlensing events towards the LMC. Assuming that all events are due to MACHOs in the halo, about 20% of the halo dark matter resides in the form of MACHOs with a mass in the range 0.15-0.9 $M_\odot$. The EROS[9] collaboration observed 6 microlensing

[8] Sometimes brown dwarfs below the deuterium-burning threshold of 13 M_J (0.01 $M_\odot$) are numbered among the planets. But we prefer to call 'planets' just those objects related to protoplanetary discs around young stars.

[9] **E**xpérience de **R**echerce d'**O**bjets **S**ombre

events, 5 in the direction of the LMC and 1 in the direction of the SMC. These observations place an upper limit on the halo dark matter fraction in the form of MACHOs. In particular, they exlude, that more than 40% of the halo is composed of compact objects in the mass range 10^{-7} to 1 $M_\odot$.

A natural extension of the microlensing observational technique consists of observing dense stellar fields even if single stars cannot be resolved. For this purpose the so-called *pixel lensing* technique has been proposed by Crotts (1992) and Baillon et al. (1993). In pixel lensing the measurement of the luminosity of single pixels of the CCD permits to detect a microlensing event, even when single stars are not resolved. The pixel lensing technique makes it possible to look at more dense stellar fields like globular clusters or more distant galaxies like the Andromeda Galaxy (M31) or the elliptical galaxy M87, that is known to possess a dark halo as well.

1.3.1 Microlensing towards M31

Using M31 as a target for microlensing searches is of particular interest because of three main reasons:

- By monitoring external galaxies, their own haloes can be studied globally, while the Milky Way halo always can be probed along one single line of sight.

- The disc of M31 is tilted relative to the line of sight. The inclination is so large, that we see the M31 disc nearly from edge-on. Therefore, more events should be seen looking on the far side of the disc than on the near side, since on the far side, the line of sight penetrates the dark halo on a longer way and in addition the denser inner part of it. Therefore, microlensing events caused by MACHOs in the M31 halo could be disentangled from Galactic halo events and the so-called *self-lensing* events. Self-lensing events are those microlensing events, where the source star in the target galaxy is lensed by an ordinary star as well in the target galaxy, and not by a MACHO in the halo. The self-lensing events should be detected in any case, even if there were no MACHOs at all in the haloes of M31 and the Milky Way. In this case, the self-lensing could be used to test the initial mass function in the regime of low mass stars ($M < 1$ $M_\odot$), where the IMF is not known well.

- The Milky Way halo can be probed along an additional line of sight different from those towards the LMC, SMC and the Galactic centre used by the previous microlensing surveys. M31 is located about 20° from the Galactic plane (towards the southern galactic pole) and about 120° from the Galactic centre.

In the past few years several collaborations began to observe M31 using different ground-based telescopes. The MEGA[10] collaboration has reported totally 14 microlensing candidate events so far, together with its precessor the Columbia/VATT[11] collaboration (Crotts & Tomaney 1996, Crotts et al. 2000). The French collaboration AGAPE[12] presented AGAPE Z1, probably a large-amplification microlensing event (Ansari et al. 1999).
In 1999 the joint-venture POINT-AGAPE[13] began its systematical observations of M31. POINT-AGAPE carried out a survey of M31 for pixel lensing events at the Isaac Newton Telescope (INT) at La Palma during 1999 and 2000. From these observations they recently reported a subset of four short-timescale microlensing candidates (Paulin-Henriksson et al. 2002).
In addition, there are a German project called WeCapp[14] and the joint-venture of AGAPE with the Swiss-Italian SLOTT[15] collaboration. SLOTT-AGAPE reported 5 pixel lensing candidate events, already (Calchi Novati et al. 2002).

[10] **M**icrolensing **E**ploration of the **G**alaxy and **A**ndromeda
[11] **V**atican **A**dvanced **T**echnology **T**elescope
[12] **A**ndromeda **G**ravitational **A**mplification **P**ixel **E**xperiment
[13] **P**ixel **O**bservations with **I**saac **N**ewton **T**elescope
[14] **W**endelstein **C**alar **A**lto **P**ixellensing **P**roject
[15] **S**ystematic **L**ensing **O**bservations at **T**oppo di Castelgrande **T**elescope

Chapter 2

Microlensing Theory

2.1 Principle of Microlensing

The general theory of relativity predicts that the paths of light rays are deflected in the presence of massive objects. Any phenomenon which differentially deflects light rays can act as a lens, magnifying or demagnifying the image of an object.
The magnification caused by a point mass lens was first derived by Einstein (1936). In the weak field limit, a light ray having a minimum impact parameter b to a point mass is deflected by an angle

$$\alpha = \frac{2R_s}{b} = \frac{4GM}{bc^2} \ . \tag{2.1}$$

We take an angular coordinate system with the lens at the origin. We define the true angular position of the source as $\mathbf{z}$ and the apparent angular position of the source as $\mathbf{y}$. The distance to the source is D_{os}, to the lens is D_{ol} and between the lens and the source is D_{ls}. The lens equation is then

$$\mathbf{z} = \mathbf{y} - \frac{D_{ls}}{D_{os}} \, \boldsymbol{\alpha}(\mathbf{y}) \ . \tag{2.2}$$

Since $\mathbf{y} = \mathbf{b}/D_{ol}$ we can define the Einstein radius and angle as follows

$$R_E = \sqrt{\frac{4GM}{c^2}\frac{D_{ol}D_{ls}}{D_{os}}}, \qquad \theta_E = \sqrt{\frac{4GM}{c^2}\frac{D_{ls}}{D_{os}D_{ol}}} \ . \tag{2.3}$$

Finally, we can take the lens equation for a point mass lens in the plane containing the observer, source and lens as

$$z = y - \frac{\theta_E^2}{y} \ \Rightarrow \ y_\pm = \frac{1}{2}\big(z \pm \sqrt{z^2 + 4\theta_E^2}\big) \ . \tag{2.4}$$

Thus we see that the point mass lens produces two images of the source, separated by an angle $\sqrt{z^2 + 4\theta_E^2}$.

Because the surface brightness is conserved, we only need to calculate the relative area of lensed and unlensed images to determine the magnification that a lens causes. The magnification factor A is therefore given by

$$A = \left(\det \frac{\partial \mathbf{z}}{\partial \mathbf{y}}\right)^{-1} = \frac{y}{z}\frac{dy}{dz} = \frac{y^4}{y^4 - \theta_E^4} \ . \tag{2.5}$$

If the images are not resolved, the apparent magnification of the source is just the sum of the absolute values of the magnifications of each image.

$$A = A_+ - A_- = \frac{1}{2}\left(\frac{\sqrt{z^2+4\theta_E^2}}{z} + \frac{z}{\sqrt{z^2+4\theta_E^2}}\right) = \frac{z^2+2\theta_E^2}{z\sqrt{z^2+4\theta_E^2}} \ . \tag{2.6}$$

The functional form of the magnification is important and thus we denote

$$f(x) := \frac{2+x}{\sqrt{x(4+x)}} - 1. \tag{2.7}$$

We now define $u := z/\theta_E$, the impact parameter in terms of the Einstein angle. The magnification is thus

$$A(u) = \frac{2+u^2}{u\sqrt{4+u^2}} = 1 + f(u^2) \ . \tag{2.8}$$

Since we want to use microlensing to detect MACHOs in both the M31 and the Galactic dark halo, we are concerned with detecting dark objects with masses of order 10^{-1} $M_\odot$. To get a rough idea of the sort of lensing we can expect, we plug some likely numbers for M31 ($M = 0.1$ $M_\odot$, $D_{os} =$ 770 kpc, $D_{ol} = 20$ kpc or 750 kpc) into (2.3), finding

$$R_E \approx 2.856 \text{ AU}\sqrt{\left(\frac{M}{M_\odot}\right)\frac{D_{ol}(D_{os}-D_{ol})}{D_{os}[\text{kpc}]}} \approx 4.0 \text{ AU} \ . \tag{2.9}$$

Thus, it is clear that the images will not be resolved, as they have milliarcsecond separations.

We define a *classical* microlensing event as when a lens object has a minimum impact parameter in units of the Einstein angle $\beta := u_{min} \leq 1$. At this impact parameter, the magnification is $A = 3/\sqrt{5} \approx 1.342$, easily detectable for a resolved star being monitored by a ground-based observatory. For pixel lensing, where the source stars are not resolved, we will have to modify this definition.

We are interested in transient events as the lenses and sources move in the gravitational potential of galaxies. We consider lensing in the frame where the observer and the source are stationary, the so-called *microlensing tube*. Thus, in the microlensing tube the lens is the only moving object. The lens

has some velocity transverse to the tube $v_\perp$. Since the physical distance of the lens from the line of sight is $R_E u$, we can define the Einstein time,

$$t_E := \frac{R_E}{v_\perp} \tag{2.10}$$

This is the time the source would take to cross half of the Einstein ring, if it had a minimum impact parameter of $\beta = 0$. Based on the estimates in (2.9) and on the assumption $v_\perp \approx 200$ km/s, typical for motions in galaxies, we see the Einstein time is of order

$$t_E \approx \frac{4942 \text{ km/s}}{v_\perp} \sqrt{\left(\frac{M}{M_\odot}\right) \frac{D_{ol}(D_{os} - D_{ol})}{D_{os}[\text{kpc}]}} \text{ days} \approx 34 \text{ days} . \tag{2.11}$$

Using the Einstein time, we now describe the rectilinear motion of the source. The position of the source in terms of the Einstein angle is

$$u(t) = \sqrt{\beta^2 + \left(\frac{t - t_0}{t_E}\right)^2}, \tag{2.12}$$

where t_0 is the time of maximum magnification A_{max}. This allows us to determine the lightcurve of the microlensing event. The excess flux of the source star during an ongoing microlensing event is

$$\Delta F(t) = F \; f\left[u^2(t)\right] , \tag{2.13}$$

where F is the flux of the source star in the absence of lensing. Eq. (2.13) is valid wether or not the source star is resolved. Of course, at the maximum magnification (2.13) becomes

$$\Delta F_{max} = F \; f(\beta^2) , \tag{2.14}$$

where β is the minimum impact parameter.
In a classical microlensing experiment, where the source star is resolved, the maximum excess flux ΔF_{max}, the unlensed flux of the source star F and the full width at half maximum time duration t_{fwhm} are measured. From (2.14) we find immediately

$$\beta = \sqrt{2 \; f\left(\frac{2 \; \Delta F_{max}}{F}\right)} , \tag{2.15}$$

where we have used the important relation $f^{-1}(x) = 2f(2x)$ (see Appendix A). From (2.12) and (2.14) we find the relation between t_{fwhm} and the Einstein time t_E:

$$t_{fwhm} = t_E \; w(\beta) , \tag{2.16}$$

with

$$w(\beta) := 2 \sqrt{2f\left[f(\beta^2)\right] - \beta^2} , \tag{2.17}$$

which is derived in Appendix A as well.

2.1.1 Finite source size effects

The microlensing formulae assume that the lens and the source are pointlike. Since $f(u^2) = 1/u$ for $u \ll 1$, the excess flux in (2.13) becomes infinite, if the lens passes exactly the line of sight. This is obviously not the case, since the source star has a nonzero radius. The lens has a finite radius as well, but this has not an important influence. However, the finite size of the source leads to a maximum magnification (Baltz & Silk 2000)

$$A_{max} = \sqrt{\frac{4R_E^2}{R_*^2} + 1}, \tag{2.18}$$

which is obtained by integrating the magnification over the disc of the star:

$$A_{max} = \frac{\int_0^{R_*} \mu_*(R) A(R/R_E) R dR}{\int_0^{R_*} \mu_*(R) R dR} \ . \tag{2.19}$$

If we substitute $u = R/R_E$ and assume the source star to have a uniform surface brightness, we obtain

$$A_{max} = 2\frac{R_E^2}{R_*^2} \int_0^{R_*/R_E} \frac{2+u^2}{\sqrt{u^2+4}} du = \sqrt{\frac{4R_E^2}{R_*^2} + 1} \approx \frac{2R_E}{R_*} \ , \tag{2.20}$$

where the approximation holds if $R_* \ll R_E$.
This can be immediately translated in a minimum value for β, namely

$$\beta_{min} := \sqrt{f^{-1}\left(A_{max} - 1\right)} = \sqrt{2f\left(2\sqrt{\frac{4R_E^2}{R_*^2} + 1} - 2\right)} \approx \frac{R_*}{2R_E} \ . \tag{2.21}$$

It is important to note, that β_{min} is a function of the source and lens positions D_{os} and D_{ol} and of the lens mass M through its dependence on R_E. The source radius is unknown a priori, but it can be related to the absolute magnitude of the source star (see Table 2.1).

2.2 Pixel lensing

The majority of microlensing surveys are searching for microlensing of resolved stars. While this requirement allows for relatively simple identification of microlensing events, it poses some problems. First, blending of stellar images and crowding in stellar fields are always a difficulty in microlensing surveys. Second, the requirement that the source stars have to be resolved limits the number of target fields to very nearby galaxies, satellites of the Milky Way.
It is possible to relax the requirement that the source stars have to be

M_I $[mag]$	Radius $[R_\odot]$
1.0	7
0.5	9
0.0	13
-0.5	17
-1.0	23
-1.5	33
-2.0	46
-2.5	64
-3.0	90

Table 2.1: Radii of stars having a given absolute magnitude in the I band. These values are taken from Gould (1995).

resolved. This was first suggested by Crotts (1992) and Baillon et al. (1993). The basic idea is that the flux difference between successive images may be detectable, even if the source star is not resolved. The technique of microlensing of unresolved stars is known as pixel lensing, because the lightcurves of individual pixels of CCD cameras reveal the microlensing events on the stars whose light they collect.
In the pixel lensing technique the flux in a given detector element is monitored rather than the flux from individual sources. If a star is magnified sufficiently due to a lens passing close to the line of sight, then the total flux in the detector element containing the source star, other nearby unlensed stars and the sky bakcground will rise significantly above the noise level and will be recorded as an event.

2.2.1 Problem of pixel lensing

We now consider the lightcurve of some detector element in a microlensing survey. The differential lightcurve is again given by (2.13). To detect an event in pixel lensing, one usually needs a large magnification, i.e. u becomes small. If we use $f(u \ll 1) \approx 1/u$, we obtain for a high magnification event the following lightcurve from (2.12) and (2.13)

$$\Delta F(t) = \frac{F}{\beta}\left(1 + \frac{(t-t_0)^2}{\beta^2 t_E^2}\right)^{-1/2} . \tag{2.22}$$

At this order, we see that of the parameters F, β, and t_E, only the combinations F/β and βt_E are measured from the shape of the lightcurve. In essence, there is less information in the shape of the lightcurve.
In classical microlensing, an additional measurement is made, namely the unlensed flux of the star, F, can be measured from long term monitoring.

Characteristic	INT WFC
Sky background	$\mu_{sky} = 21.9$ mag arcsec^{-2}
Zero point	$m_0 = 25.6$ mag
Exposure time	$t_{int} = 760\ s$
Pixel field of view	0.33"
Superpixel dimensions	7×7 pixels
Best seeing	0.8"
Worst seeing	2.4"
Average seeing	1.5"
Field dimensions	4 rectangles of $22.8' \times 11.4'$
Northern field	$\alpha = 00^h44^m00^s$ $\delta = 41°34'00''$
Southern field	$\alpha = 00^h43^m10^s$ $\delta = 40°58'15''$

Table 2.2: Adopted characteristics of the INT telescope, the observing site on La Palma and the used Wide-field Camera (WFC). The zero point is given in terms of the apparent magnitude of a source, which results in a 1 photon/s detection rate. The magnitudes are for the V-band.

The fundamental point is that it is difficult to determine the Einstein time t_E without an independent measurement of F, which of course is not possible when the observed field is very crowded. Since the Einstein time most clearly expresses the parameters of the source-lens system, this is a serious difficulty that must be addressed if pixel lensing has to be a useful technique.

2.2.2 Superpixel photometry

A major pixel lensing observing program towards M31 is performed with the Isaac Newton Telescope (INT) on La Palma using the Wide-field Camera (WFC). The POINT-AGAPE collaboration used INT WFC to monitor two 0.3 deg^2 fields of view to map the distribution of microlensing events across a large region of M31. There is a northern field centered nearly on the major axis and a southern field centered on the far side of the disc, which covers the dwarf galaxy M32 as well. The main characteristics of the INT WFC and the observing site at La Palma are given in Table 2.2.

To minimize the effects of seeing, *superpixel photometry* was developed. In this technique the base detector element is defined to be a *superpixel*: a square array of pixels. A superpixel is defined for each pixel, with that pixel lying at the centre, so that neighbouring superpixels overlap with an offset of one pixel. The optimal size of the superpixel array is set by the ratio of the size of the seeing disc on images obtained in poor seeing to the individual pixel size. The INT WFC has a pixel scale corresponding to 0.33 arcsec on the sky, whilst poor seeing at La Palma is ≈ 2 arcsec. Adopting a very conservative value of 2.4 arcsec for the worst seeing leads to an optimized choice of 7×7 pixels for the superpixel array. A larger array would dilute

source variations and a smaller array would be too sensitive to changing observing conditions.

2.2.3 Threshold minimum impact parameter

The detection of events in a pixel lensing dataset is a complex issue. The problem is, that in pixel lensing, only a small fraction of the classical microlensing events are detectable, because there must be some minimum of additional flux detected so that the event becomes distinguishable from the background. This minimum of additional flux corresponds to a threshold β_T of the minimum impact parameter β. There are several possible definitions, what the threshold β_T for a detected event might be. In this work we want to restrict ourselves on the 'peak threshold' of Baltz & Silk (2000) and the 'noise level threshold' of Kerins et al. (2001).

Peak threshold

We now derive an expression for β_T following Baltz & Silk (2000). First, we define some basic parameters. The first is the fiducial flux S_0 for the telescope-CCD system. This is the number of photons collected per second of an apparent magnitude zero star. We calculate $S_0 = 10^{0.4m_0} = 1.74 \times 10^{10}$ s^{-1} from Table 2.2. Furthermore, only a fraction f_{psf} of these photons falls within the given superpixel. In practice, the value of f_{psf} is determined from the point spread function (PSF) of the telescope-CCD system. We simplified the computation of the seeing fraction f_{psf} by adopting a two-dimensional Gaussian PSF (normalized to 1)

$$PSF := \frac{1}{\pi a^2}\, e^{-(x^2+y^2)/a^2} \;, \tag{2.23}$$

with a FWHM equal to the mean seeing for La Palma (1.5 arcsec)

$$a = \frac{1.5''}{2\,\sqrt{ln(2)}} \;. \tag{2.24}$$

The position of the PSF maximum is centered within the central pixel of the superpixel. Integrating the PSF over the superpixel angular surface, we obtain for the INT WFC a value of $f_{psf} = 0.87$.
The rate at which photons are collected within detection element is then given by

$$S = S_0 f_{psf} 10^{-0.4m}, \tag{2.25}$$

where m is the apparent magnitude of the source in the relevant band. Next, we define m_{bg} as the apparent magnitude of the background light detected on the superpixel. The background light contains the light of the stars in the

target galaxy as well as the sky background (moon, zodiac light, foreground stars etc). The rate at which background photons are collected is then

$$S_{bg} = S_0 10^{-0.4 m_{bg}} = S_0 \left(10^{-0.4 m_{gal}} + 10^{-0.4 m_{sky}}\right), \tag{2.26}$$

where m_{gal} is the apparent magnitude of the target galaxy and m_{sky} is the apparent magnitude of the night sky background. The background does not suffer a degradation in magnitude due to the PSF. Now, we assume that an integration of duration t_{int} is performed and during this epoch a star is lensed and magnified by an excess magnification $A(u) - 1 = f(u^2)$. Furthermore, we assume that the noise level is approximately twice the statistical photon fluctuation (Poisson statistics), a level obtained by the AGAPE collaboration (Ansari et al., 1997). Thus, the signal-to-noise ratio (S/N) in a single sample is

$$\begin{aligned} Q :&= \frac{N_{sig}}{2\sqrt{N_{bg}}} = \frac{S f(u^2) t_{int}}{2\sqrt{S_{bg} t_{int}}} \\ &= \frac{f(u^2)}{2} \sqrt{S_0 t_{int}} \; \frac{f_{psf} 10^{-0.4m}}{\sqrt{10^{-0.4 m_{gal}} + 10^{-0.4 m_{sky}}}} \; . \end{aligned} \tag{2.27}$$

A more common quantity than the apparent magnitude of the whole resolution element is the surface brightness μ_{gal} of the target galaxy and μ_{sky} of the night sky background. μ_{gal}, usually given in mag arcsec^{-2}, depends on the line of sight and can be adopted from measurements described in the literature. For the night sky background we adopt a constant value of $\mu_{sky} = 21.9$ mag arcsec^{-2}. Thus, the S/N becomes

$$Q = \frac{f(u^2)}{2} \sqrt{\frac{S_0 t_{int}}{\Omega_{sp}}} \; \frac{f_{psf} 10^{-0.4m}}{\sqrt{10^{-0.4 \mu_{gal}} + 10^{-0.4 \mu_{sky}}}} \; , \tag{2.28}$$

where Ω_{sp} is the angular area of the superpixel.

The basic idea of the peak threshold is, that we introduce a threshold S/N Q_0 and demand that for the detection of a pixel lensing event, the S/N at the peak of the lightcurve shall be larger than Q_0. The impact parameter at the peak magnification is of course $u = \beta$. The threshold minimum impact parameter β_T is obtained by putting $Q = Q_0$. We obtain

$$f\left(\beta_T^2\right) = \frac{2 Q_0}{f_{psf}} \sqrt{\frac{\Omega_{sp}}{S_0 t_{int}}} \; \frac{\sqrt{10^{-0.4 \mu_{gal}} + 10^{-0.4 \mu_{sky}}}}{10^{-0.4 m(M)}}, \tag{2.29}$$

where M is now the absolute magnitude of the source star. The relation between apparent and absolute magnitude $m(M)$ is given by

$$m(M) := M + (m - M)_{gal} \; , \tag{2.30}$$

where we have neglected extinction by interstellar dust. $(m-M)_{gal}$ is the distance modulus of the target galaxy.
If $A \gg 1$, we have $f(u^2) \approx 1/u$ and hence in this regime

$$\beta_T \approx \sqrt{\frac{S_0 t_{int}}{\Omega_{sp}}} \frac{f_{psf}}{2Q_0} \frac{10^{-0.4m(M)}}{\sqrt{10^{-0.4\mu_{gal}} + 10^{-0.4\mu_{sky}}}} \ . \tag{2.31}$$

The exact expression for β_T is obtained using $f^{-1}(x) = 2f(2x)$ and this gives

$$\beta_T = \sqrt{2\ f\left[\frac{4Q_0}{f_{psf}} \sqrt{\frac{\Omega_{sp}}{S_0 t_{int}}} \frac{\sqrt{10^{-0.4\mu_{gal}} + 10^{-0.4\mu_{sky}}}}{10^{-0.4\left[M+(m-M)_{gal}\right]}}\right]} \ . \tag{2.32}$$

Noise level threshold

Another definition for the threshold minimum impact parameter β_T is obtained following Kerins et al. (2001).
Again, we first have to give some definitions. The excess photon count ΔN_{sp} falling on the superpixel due to an ongoing pixel lensing event is

$$\Delta N_{sp} := N_{bg}(A_{sp} - 1) = f_{psf} N_s (A - 1) \ . \tag{2.33}$$

Here N_s and N_{bg} are the source and background photon counts in the absence of lensing. A_{sp} is the superpixel magnification factor and is the observable analogue of A. The baseline photon count is

$$N_{bg} = N_{gal} + N_{sky} \ , \tag{2.34}$$

where N_{gal} is the contribution from the surface brightness of the target galaxy and N_{sky} is the photon count of the night sky background. f_{psf} is the fraction of the seeing disc already defined in the peak threshold formalism. Note that in pixel lensing A and N_s cannot be measured separately, whilst only N_{bg} and A_{sp} can be determined. Now, let σ be the superpixel noise. In the noise level threshold formalism a signal is regarded statistically significant if it occurs at a level 3σ above the background photon count N_{bg}. We define a threshold noise level σ_T, determined by the superpixel flux stability. Melchior (1999) obtained a flux stability level of 0.1-0.3% for our superpixel on INT WFC. We therefore adopt, following Kerins et al. (2001), a threshold noise level of

$$\sigma_T = 2.5 \times 10^{-3}\ N_{bg} \ . \tag{2.35}$$

For a pixel lensing event to be detected we require thus a superpixel excess photon count $\Delta N_{sp} \geq 3\sigma_T / N_{bg}$ giving a threshold magnification of

$$A_T = 1 + 0.0075\ \frac{N_{bg}}{f_{psf} N_s} \ . \tag{2.36}$$

This can be translated into a threshold for the minimum impact parameter

$$\beta_T = \sqrt{2f\left(2\ \frac{0.0075 N_{bg}}{f_{psf} N_s}\right)}\ . \tag{2.37}$$

The crucial step is now to find N_s and N_{bg}. If the source star has an apparent magnitude m, we have $N_s \propto 10^{-0.4m}$ and if μ_{gal} and μ_{sky} are the surface brightnesses of the target galaxy and the night sky background respectively, we get

$$N_{bg} \propto \Omega_{sp}(10^{-0.4\mu_{gal}} + 10^{-0.4\mu_{sky}})\ , \tag{2.38}$$

where Ω_{sp} again is the angular surface of the superpixel. We finally arrive to the threshold minimum impact parameter

$$\beta_T = \sqrt{2f\left[2\ \frac{0.0075\ \Omega_{sp}\ \left(10^{-0.4\mu_{gal}} + 10^{-0.4\mu_{sky}}\right)}{f_{psf} 10^{-0.4\left[M+(m-M)_{gal}\right]}}\right]}\ . \tag{2.39}$$

We are now ready to compare the two definitions of β_T. While in classical microlensing, all events with $\beta \leq 1$ can be detected, in pixel lensing only events with $\beta \leq \beta_T$ are magnified enough to be seen. The threshold minimum impact parameter β_T is a function of the absolute magnitude of the source star and of the surface brightness of the background light. This can be understood intuitively, because the brighter the source star and the more fainter the background light, the better the source star can be 'resolved' during an eventual microlensing event and thus the larger β_T will be.
But β_T depends also largely on several parameters of the telescope CCD-system and the seeing of the observing site.
The comparison of the two formulas (2.32) and (2.39) shows that the ratio between the two thresholds depends again on the absolute magnitude of the source M and the surface brightness of the target galaxy μ_{gal}. Fig. 2.1 shows that the dependence on the M is little important particularly for the fainter stars. In Fig. 2.2 it can be seen that the noise level threshold β_T is smaller than the peak threshold β_T within the brighter parts of the target galaxy, whereas at the outskirts of the target galaxy the noise level threshold is larger.

2.3 Optical Depth

The probability of a given star being microlensed is quite small. The optical depth to microlensing is a measure of this probability. It represents the mean number of lenses whose Einstein rings encompass a given source star. To compute this mean number for a given star, which we define as its optical depth τ_{opt}, we simply integrate over the line of sight from the observer to

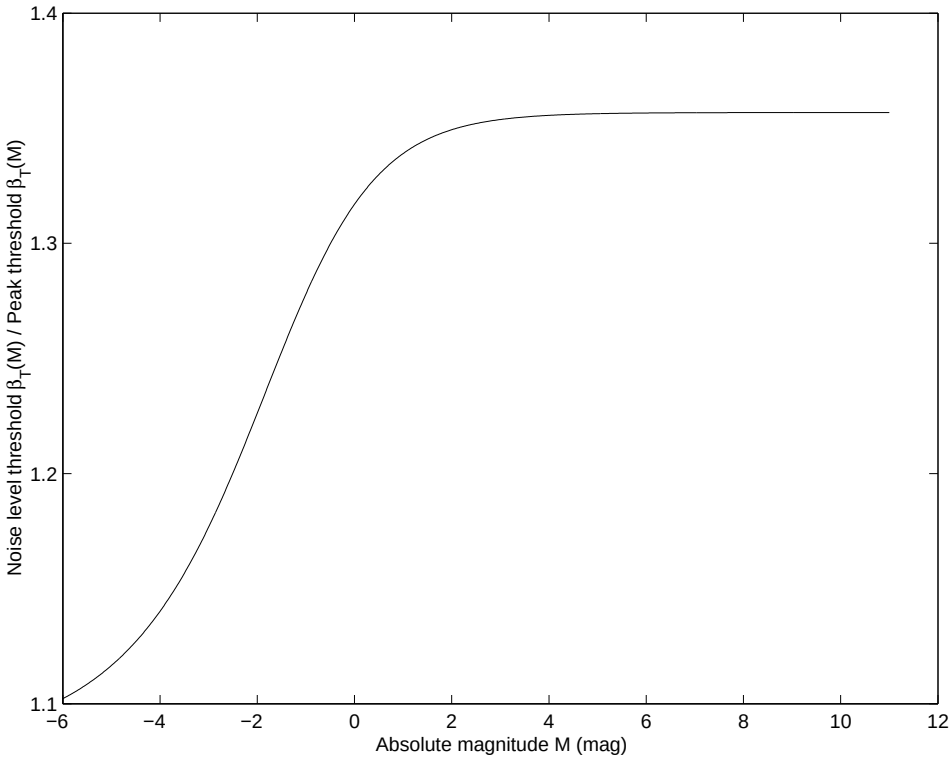

Figure 2.1: Ratio of the two threshold impact parameters (2.39)/(2.32) as a function of the absolute magnitude M of the source star. The surface brightness of the galaxy is set at $\mu_{gal} = 19$ mag arcsec^{-2}.

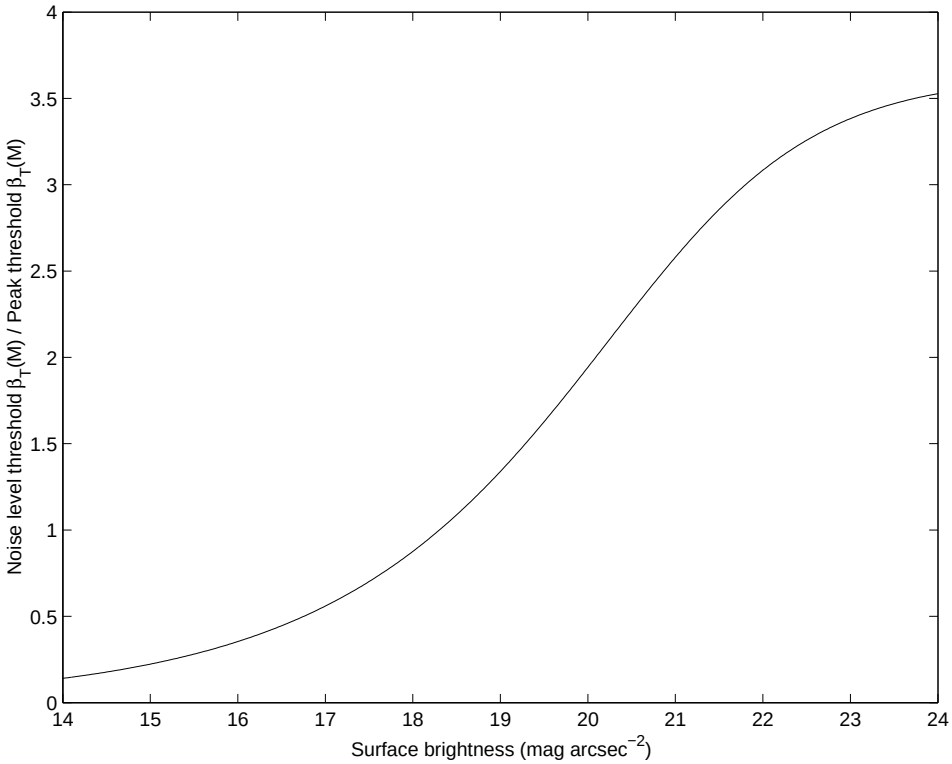

Figure 2.2: Ratio of the two threshold impact parameters (2.39)/(2.32) as a function of the surface brightness μ_{gal} of the target galaxy. The absolute magnitude of the source is set equal to 1 mag.

the star and over the mass function $\left(dN/dM\right)$ of the lenses[1],

$$\begin{aligned}\tau_{opt} : &= \int dM \left(\frac{dN}{dM}\right) \int_0^{D_{os}} dD_{ol}\ n_l(D_{ol})\ R_E^2 \pi \\ &= \frac{4\pi G}{c^2} \int dM M \frac{dN}{dM} \int_0^{D_{os}} dD_{ol}\ n_l(D_{ol}) \frac{D_{ol}(D_{os}-D_{ol})}{D_{os}}\ ,\end{aligned} \tag{2.40}$$

where $n_l(D_{ol})$ is the number density of the lenses along the line of sight. Integrating over the mass function, we get the mean mass $< M >$, which multiplied by the number density gives the mass density of the lenses. We thus see that the optical depth is independent of the mass function of the lenses, and depends only on the total mass density of the lenses,

$$\tau_{opt} = \frac{4\pi G D_{os}^2}{c^2} \int_0^{D_{os}} dD_{ol}\ \rho_l(D_{ol})\ \frac{D_{ol}(D_{os}-D_{ol})}{D_{os}}. \tag{2.41}$$

The optical depth to microlensing is typically very small, less than 10^{-6}. This result indicates that it is necessary to monitor rich fields of stars ($\approx 10^7$ stars) in order to detect microlensing events with a reasonable probability. Eq. (2.41) is only valid under the assumption that all the source stars lie at the same distance. If we consider e.g. self-lensing this assumption is no longer acceptable. In this case we have to integrate not only on the distance of the lens but also on the distance of the source. Therefore in this case, the optical depth is given by

$$\begin{aligned}\tau_{opt} = \frac{4\pi G}{c^2} &\int_0^{\infty} dD_{os}\rho_s(D_{os}) \int_0^{D_{os}} dD_{ol}\rho_l(D_{ol})\ \frac{D_{ol}(D_{os}-D_{ol})}{D_{os}} \\ &\times \left(\int_0^{\infty} dD_{os}\rho_s(D_{os})\right)^{-1}.\end{aligned} \tag{2.42}$$

2.3.1 Optical depth estimations

In practice, the optical depth is measured as follows (cf. Gondolo 1999). Consider a microlensing survey, that monitors N_* stars during the time t_{obs}. When a microlensing event occurs, the full width at half maximum time duration of the event t_{fwhm}, the unlensed flux of the source star F and the excess flux at the peak ΔF_{max} are measured. From (2.14) and (2.8), the minimum impact parameter β and the peak magnification A_{max} can immediately be calculated. The Einstein time t_E can then be calculated using the relation (2.16).

The optical depth in classical microlensing is then usually estimated as

$$< \tau_c >= \frac{\pi}{2} \frac{1}{N_* t_{obs}} \sum_{events} \frac{t_E}{\epsilon(t_E)}. \tag{2.43}$$

[1]The mass function is the number of lenses per unit mass as a function of their mass.

The detection efficiency $\epsilon(t_E)$ is the fraction of microlensing events (with $\beta < 1$) with Einstein time t_E that can be detected by the used telescope-CCD system and under the observational circumstances at the observation site. Typical values for the efficiency are $\epsilon = 0.2 - 0.3$.
The optical depth estimator (2.43) is based on the relation

$$\int_{\beta<1} t_E dN_* d\Gamma = \frac{2}{\pi} N_* \ < \tau_c >, \tag{2.44}$$

where

$$< \tau_c >:= \frac{1}{N_*} \int \tau dN_* \tag{2.45}$$

and dN_* is the differential number of monitored stars and $d\Gamma = \big(2\tau/\pi t_E\big) d\beta$ is the differential event rate per source. The factor $\pi/2$ is simply the mean fraction of the Einstein time that the source star is inside the Einstein radius. The differential number of classical microlensing events is $dN_c := t_{obs} N_* d\Gamma_c$ and therefore

$$\sum_{events} \frac{t_E}{\epsilon(t_E)} = \int_{\beta<1} \frac{t_E}{\epsilon(t_E)} dN_c^* = \int_{\beta<1} t_E dN_c = \frac{2}{\pi} t_{obs} N_* < \tau_c > \ . \tag{2.46}$$

In a pixel lensing experiment, the flux of the source star and the minimum impact parameter can usually not be disentangled. In this case the Einstein time of the events remain unknown. The only informations we have, are the full width at half maximum time t_{fwhm} and the excess flux at the peak ΔF_{max}.
However, it is possible to estimate the optical depth without using the Einstein time. The new optical depth estimator is based on a relation similar to (2.44), proved by Gondolo (1999)

$$\int t_{fwhm} \ \Delta F_{max} \ dN_* d\Gamma = \frac{2}{\pi} I F_{tot} < \tau_p >, \tag{2.47}$$

where F_{tot} is the total flux of the monitored source stars and

$$< \tau_p >: = \frac{1}{F_{tot}} \int F \tau dN_* \ , \tag{2.48}$$

$$I : = \int_0^\infty w(\beta) f(\beta^2). \tag{2.49}$$

Using $t_{fwhm} = t_E w(\beta)$ and $\Delta F_{max} = F f(\beta^2)$, the proof of (2.47) becomes trivial.

The optical depth in pixel lensing $< \tau_p >$ is only equal to the classical optical depth $< \tau_c >$, if the luminosity function of the source stars is independent of the source position, because in this case the average over

the source flux in the definition of $< \tau_p >$ is independent of the average over the source stars. If every microlensing event could be detected, (2.47) immediately gives an estimator for the optical depth, namely

$$< \tau_p >= \frac{\pi}{2It_{obs}F_{tot}} \sum_{\text{events}} t_{fwhm}\Delta F_{max}. \tag{2.50}$$

This estimator would be the correct one, if all occurring events are detected as well. It does therefore not depend on the source luminosity function. However, we know that in pixel microlensing only those events $\beta \leq \beta_T$ are detected. There, the luminosity function of the source stars comes into play. Microlensing events with faint source stars are only detected, if β is very small. On the other hand the luminosity function states that the number of bright stars is much smaller than the number of fainter stars.
We can therefore restrict the integral in (2.47) to events with $\beta \leq \beta_T$ and we obtain

$$< \tau_p >= \frac{\pi}{2It_{obs}F_{eff}} \sum_{\text{events}} t_{fwhm}\Delta F_{max}, \tag{2.51}$$

where we have defined an effective flux

$$F_{eff} := \frac{1}{I} \int \bar{\Phi}(F)F \int_0^{\beta_T(F)} d\beta w(\beta) f(\beta^2)\ dF. \tag{2.52}$$

The luminosity function $\bar{\Phi}(F)$ is here the number of stars per unit flux.
If the luminosity function is known, the effective flux F_{eff} can be calculated directly. Another possibility is to measure in addition the so-called surface brightness fluctuation (SBF) flux (defined in Tonry & Schneider 1988) during the pixel lensing experiment.

$$\bar{F} := \frac{\int F^2 \bar{\Phi}(F) dF}{\int F \bar{\Phi}(F) dF}. \tag{2.53}$$

$\bar{F}$ can be measured by characterizing the pixel-to-pixel variations of the surface brightness of a galaxy image. The ratio F_{eff}/F_{tot} is an almost universal function of $\bar{F}$ (cf. Gondolo 1999). The deviations from this universal behavior for various luminosity function are never larger than 30%.

2.4 Rate of microlensing events

The optical depth is a static quantity. In order to detect a microlensing event, the brightness of the source star must appreciably change in time over which it is monitored. We would like to calculate the rate at which sources enter the Einstein rings of lenses. The lenses will have some velocity distribution $f(\mathbf{v})$ in the rest frame of the galaxy. The microlensing tube

will have some transverse velocity $\mathbf{v}_t$ in this frame. The differential rate of microlensing events is

$$d\Gamma = \left(\frac{dN}{dM}\right) dM(2R_E d\beta)\big(f(\mathbf{v}-\mathbf{v}_t)v_\perp d^3\mathbf{v}\big)dD_{ol} \ , \tag{2.54}$$

where β is the minimum impact parameter and $v_\perp$ is the transverse velocity of the lenses. We make a change of variable to the dimensionless mass $\mu := M/M_\odot$ and write

$$R_E = r_E \sqrt{\mu \ \frac{D_{ol}(D_{os}-D_{ol})}{D_{os}}} \ , \tag{2.55}$$

with $r_E := \sqrt{4GM_\odot/c^2}$. We obtain

$$d\Gamma = \left(\frac{dN}{d\mu}\right)\sqrt{\mu}\ d\mu(2r_E d\beta)\big(f(\mathbf{v}-\mathbf{v}_t)v_\perp d^3\mathbf{v}\big)\ \sqrt{\frac{D_{ol}(D_{os}-D_{ol})}{D_{os}}}\ dD_{ol} \ . \tag{2.56}$$

Because very little is known about the MACHO mass function, we usually assume that the mass distribution of the lenses is independent of their position in M31 or the Galaxy (factorization hypothesis)

$$\left(\frac{dN}{d\mu}\right) = \left(\frac{dN_0}{d\mu}\right)\ H_l(D_{ol}) \ , \tag{2.57}$$

where $H_l(D_{ol}) := \rho_l(D_{ol})/\rho_{l,0}$. The lens number density per unit mass, $\big(dN_0/d\mu\big)$, is normalized as follows

$$\int_{\mu_{min}}^{\mu_{max}} \left(\frac{dN_0}{d\mu}\right)\mu\ d\mu = \frac{\rho_{l,0}}{M_\odot} \ . \tag{2.58}$$

We choose a Maxwellian velocity distribution for the lenses, which will be a reasonable approximation. This distribution is characterized by one parameter, the dispersion velocity v_l,

$$\begin{aligned} f(\mathbf{v}-\mathbf{v}_t) &= \frac{1}{(\pi v_l^2)^{3/2}}\ \exp\!\left(-\frac{|\mathbf{v}-\mathbf{v}_t|^2}{v_l^2}\right) \\ &= \frac{1}{(\pi v_l^2)^{3/2}}\ \exp\!\left(-\frac{v_x^2+v_\perp^2+v_t^2-2v_t v_\perp\cos\alpha}{v_l^2}\right) \ , \end{aligned} \tag{2.59}$$

where v_x is the velocity of the lens along the line of sight and α the angle the transverse velocity $v_\perp$ makes with the velocity of the microlensing tube v_t. With $d^3\mathbf{v} = v_\perp dv_\perp dv_x d\alpha$ (cylindrical coordinates), we can perform the integrals in v_x and α. The former is a Gaussian integration giving $\sqrt{\pi}v_l$ and the latter yields a modified Bessel function the first kind (of order 0)

$$I_0(x) := \frac{1}{\pi}\ \int_0^\pi e^{x\cos\beta}d\beta \tag{2.60}$$

and an additional factor 2. There remains a single velocity integral over $v_\perp$

$$d\Gamma = 4r_E d\beta \, \frac{dN_0}{d\mu}\sqrt{\mu}\, d\mu \, \left(\frac{v_\perp^2}{v_l^2} \exp\left(-\frac{v_\perp^2 + v_t^2}{v_l^2}\right) I_0\left(\frac{2v_\perp v_t}{v_l^2}\right) dv_\perp \right) \\ \times \left(H_l(D_{ol}) \, \sqrt{\frac{D_{ol}(D_{os} - D_{ol})}{D_{os}}} dD_{ol} \right) . \tag{2.61}$$

It is convenient to define dimensionless velocities $v := v_\perp / v_l$ and $\eta := v_t / v_l$. With these definitions, the new differential rate is given by

$$d\Gamma = 4r_E v_l \left(\frac{dN_0}{d\mu} \right) H_l(D_{ol}) \sqrt{\frac{\mu D_{ol}(D_{os} - D_{ol})}{D_{os}}} v^2 e^{-v^2 - \eta^2} \\ \times I_0\big(2\eta v\big) dD_{ol} dv d\beta d\mu \ . \tag{2.62}$$

Note, that the (dimensionless) transverse velocity of the microlensing tube η, generally depends on the distance D_{ol}, the transverse velocity of the observer (the sun) $\mathbf{v}_{\odot\perp}$ and the transverse velocities of the sources $\mathbf{v}_{s\perp}$

$$\boldsymbol{\eta} = \left(1 - \frac{D_{ol}}{D_{os}}\right) \frac{\mathbf{v}_{\odot\perp}}{v_l} + \frac{D_{ol}}{D_{os}} \frac{\mathbf{v}_{s\perp}}{v_l} \ . \tag{2.63}$$

2.4.1 Differential rate in classical microlensing

In classical microlensing we require for an event to be detected a minimum impact parameter $\beta \leq 1$, which corresponds to a magnification at maximum of $A_{max} \geq 1.34$. Thus, the integration over β becomes trivial. The integration goes from 0 to the impact paramater threshold for a detectable event $\beta_T = 1$. Hence, the differential rate in classical microlensing is

$$d\Gamma_c = 4r_E v_l \left(\frac{dN_0}{d\mu} \right) H_l(D_{ol}) \sqrt{\frac{\mu D_{ol}(D_{os} - D_{ol})}{D_{os}}} v^2 e^{-v^2 - \eta^2} \\ \times I_0\big(2\eta v\big) dD_{ol} dv d\mu \ . \tag{2.64}$$

2.4.2 Differential rate in pixel lensing

In pixel lensing the upper limit of the β integration in (2.62) is the threshold minimum impact parameter $\beta_T(M)$. Thus, the differential pixel lensing event rate is given by

$$d\tilde{\Gamma}_p(M) = 4r_E v_l \beta_T(M) \, \left(\frac{dN_0}{d\mu} \right) \, H_l(D_{ol}) \sqrt{\frac{\mu D_{ol}(D_{os} - D_{ol})}{D_{os}}} v^2 e^{-v^2 - \eta^2} \\ \times I_0\big(2\eta v\big) dD_{ol} dv d\mu \\ = \beta_T(M) \ d\Gamma_c \ . \tag{2.65}$$

If we performed the integrations we would obtain an event rate in units of number of events per unit time and per observed star. This event rate would depend on the absolute magnitude of the source star. This is not very meaningful in pixel lensing, since the source stars are not resolved and their absolute magnitude are unknown. $d\tilde{\Gamma}$ is therefore integrated over the luminosity function to average over the absolute magnitude of the sources. We then obtain a pixel lensing event rate in units of number of events per unit time and per angular surface element of the observed field.
Let us therefore define the pixel lensing event rate by

$$\Gamma_p := \Gamma_c \int dM \tilde{\Phi}(M) \beta_T(M) \ , \tag{2.66}$$

where Γ_c is the classical microlensing rate, calculated from (2.64). The function $\tilde{\Phi}(M)$ is defined as the number of stars per unit magnitude and per unit angular surface. $\tilde{\Phi}(M)$ can be expressed in terms of a conventional luminosity function $\Phi(M)$ (number density of stars per unit magnitude), by using the simple, but important, fact, that the surface brightness of the target galaxy μ_{gal} is nothing but the integrated light of all stars per unit angular surface

$$\int dM \tilde{\Phi}(M) 10^{-0.4\left[M+(m-M)_{gal}\right]} = 10^{-0.4\mu_{gal}}, \tag{2.67}$$

which yields

$$\tilde{\Phi}(M) = \frac{\Phi(M)\ 10^{-0.4\mu_{gal}}}{\int dM'\ \Phi(M')\ 10^{-0.4(M'+(m-M)_{gal})}}. \tag{2.68}$$

Inserting this into (2.66) finally leads to the desired pixel lensing event rate

$$\Gamma_p = \Gamma_c\ 10^{-0.4\mu_{gal}}\ \frac{\int dM \Phi(M)\ \beta_T(M)}{\int dM'\ \Phi(M')\ 10^{-0.4(M'+(m-M)_{gal})}}. \tag{2.69}$$

where $\beta_T(M)$ is given by (2.32) or (2.39). Note, that Γ_p has to be considered as a strict theoretical upper limit to the observed event rate and cannot be compared directly with observations, since it tends to overestimate the true pixel lensing rate, because it assumes perfect sensitivity to all event durations, and also stable observing conditions.
To complete this section we examine (2.69) further for our two definitions of $\beta_T(M)$, the peak threshold and the noise level threshold:

Peak threshold

For the peak threshold the integrand in the numerator of (2.69) becomes maximal at an absolute source magnitude $M \approx 1$ (see Fig. 2.3). Looking at the Hertzsprung-Russel-Diagram shows, that the lensed stars tend to be

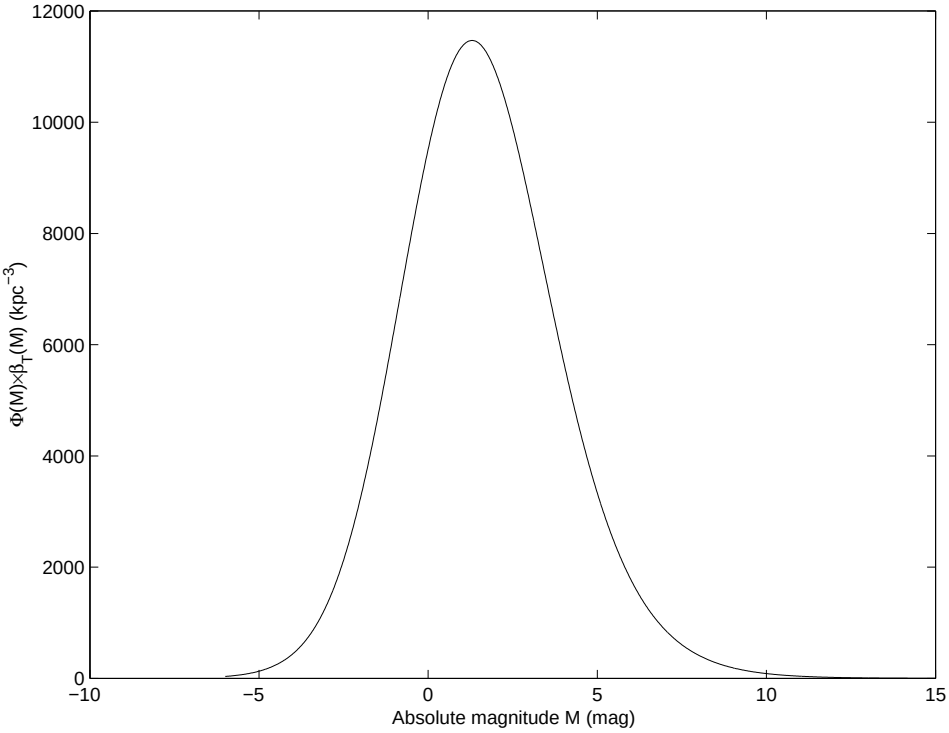

Figure 2.3: $\Phi(M) \times \beta_T(M)$ as a function of the absolute magnitude M of the source star. The surface brightness of the target galaxy is set at $\mu_{gal} = 19$ mag arcsec^{-2}. The maximum lies around $M = 1$.

main sequence A-stars or red giants.

Because for a low magnification event to be detected we would need a very bright source star and such stars do not contribute significantly to the luminosity function, most of the detectable events are expected to have a high magnification $A \gg 10$. We can therefore tentatively use the high magnification approximation (2.31) for $\beta_T(M)$. In this case we obtain

$$\Gamma_p = \Gamma_c \sqrt{\frac{S_0 t_{int}}{\Omega_{sp}}} \frac{f_{psf}}{2Q_0} \frac{10^{-0.4\mu_{gal}}}{\sqrt{10^{-0.4\mu_{gal}} + 10^{-0.4\mu_{sky}}}}. \tag{2.70}$$

The luminosity function has been dropped out, which leads to a first conclusion that the dependence of Γ_p on the luminosity function will only be weak.

Near and within the bulge of the target galaxy the surface brightness of the night sky background can be neglected, which yields

$$\Gamma_p = \Gamma_c \sqrt{\frac{S_0 t_{int}}{\Omega_{sp}}} \frac{f_{psf}}{2Q_0} \sqrt{10^{-0.4\mu_{gal}}}. \tag{2.71}$$

Our second conclusion is that, if we have a constant classical event rate Γ_c, the pixel lensing event rate is basically proportional to the square root of the surface brightness of the target galaxy, a result obtained also by Ansari et al. (1997) and Baltz, Gyuk & Crotts (2002).

Noise level threshold

We also approximate β_T in the noise level threshold for high magnification events and obtain

$$\beta_T(M) \approx \frac{f_{psf}}{0.0075\ \Omega_{sp}} \frac{10^{-0.4[M+(m-M)_{gal}]}}{10^{-0.4\mu_{gal}} + 10^{-0.4\mu_{sky}}}\ . \tag{2.72}$$

Introducing this into (2.69) gives

$$\Gamma_p \approx \Gamma_c \frac{f_{psf}}{0.0075\ \Omega_{sp}} \frac{10^{-0.4\mu_{gal}}}{10^{-0.4\mu_{gal}} + 10^{-0.4\mu_{sky}}}\ , \tag{2.73}$$

which again shows that the functional form of the luminosity function will not have a large influence on the pixel lensing rate. Within the bulge, where the night sky background can be neglected, this reduces to the very simple estimate for the pixel lensing event rate

$$\Gamma_p \approx \Gamma_c \frac{f_{psf}}{0.0075\ \Omega_{sp}}\ . \tag{2.74}$$

In this approximation the classical and the pixel lensing event rates differ only by a numerical factor, which is not the same result as in the peak threshold formalism.

2.5 Dark mass moments

The goal of any observational program, searching for microlensing events, is to extract the mass function of the MACHOs ($dN_0/d\mu$) from the data. The most systematic and clear way is the method of dark mass moments, introduced by De Rújula, Jetzer & Masso (1991). In this section we will discuss this method for classical microlensing and then try to generalize it to the case of pixel lensing.

2.5.1 Dark mass moments in classical microlensing

Consider a classical microlensing experiment that observes N_* resolved stars during a time t_{obs} and has recorded a set of microlensing events. For every event the excess flux at the peak ΔF_{max}, the flux of the source star in the absence of lensing F and the duration of the event t_{fwhm} is measured. From this data we can compute the Einstein time t_E for every event from (2.14) and (2.16). At this point it is convenient to introduce the dimensionless timescale

$$t_c := \frac{v_l}{r_E\sqrt{d}}\, t_E = \frac{v_l}{r_E\sqrt{d}}\, \frac{R_E}{v_\perp} = \frac{1}{v\sqrt{d}} \sqrt{\mu\, \frac{D_{ol}(D_{os}-D_{ol})}{D_{os})}}\ , \tag{2.75}$$

where $v = v_\perp/v_l$. The dispersion velocity of the lens population v_l, the distance from the sun to the centre of the target galaxy d and $r_E = \sqrt{4GM_\odot/c^2}$ are making t_c to a dimensionless number. This new timescale will simplify algebra noticeably. We calculate from the observations the cumulative nth moment of t_c as

$$< t_c^n >:= \sum_{\text{events}} t_c^n. \tag{2.76}$$

These moments are essentially those of the distribution of the observed time durations. The basic idea behind the method of dark mass moments is that the the theoretical expression[2]

$$\int dN_c\ t_c^n = N_* t_{obs} \int d\Gamma_c\ t_c^n \tag{2.77}$$

factorizes into a product of moments of the 'known' distributions $H_l(D_{ol})$ and $f_\perp(v)$ times a moment of the MACHO mass distribution ($dN_0/d\mu$) that can be evaluated by comparison with (2.76).
Unfortunately, it is not that simple, because we have to take into account observational limitations. There is an experimental restriction that affects the observable values of μ in a non-trivial fashion: the limited measurable range in t_{fwhm}

$$t_{min} \le t_{fwhm} \le t_{max}. \tag{2.78}$$

[2] $dN_c := t_{obs} N_* d\Gamma_c$ is the differential number of classical microlensing events.

The limits $t_{min} = \mathcal{O}(\text{tens of min})$ and $t_{max} = \mathcal{O}(\text{yr})$ are set by current technology and by the brevity of human lives. We express this and other experimental restrictions by a sampling efficiency $\epsilon(t_{fwhm})$, that measures the fraction of microlensing events with duration t_{fwhm} that are detected. It can be treated in a first approximation as a step function,

$$\epsilon(t_{fwhm}) = \Theta(t_{fwhm} - t_{min})\ \Theta(t_{max} - t_{fwhm}), \tag{2.79}$$

where Θ is the Heaviside function. The sampling efficiency allows us to characterize the range of MACHO masses, to which a particular experiment has access. To do this, we define

$$dN_c^*(\bar{\mu}) := N_* t_{obs} d\Gamma_c^*(\bar{\mu}), \tag{2.80}$$

where $d\Gamma_c^*$ is defined by (2.64), but with a delta function $\delta(\mu - \bar{\mu})$ instead of the MACHO mass function $(dN_0/d\mu)$. Then, we can introduce the efficiency function

$$\epsilon_0(\bar{\mu}) := \frac{\int dN_c^*(\bar{\mu})\ \epsilon(t_{fwhm})}{\int dN_c^*(\bar{\mu})}, \tag{2.81}$$

that measures the fraction of the total number of microlensing events at a fixed MACHO mass, that can be detected.
As a consequence, the theoretical expression for the *observable* t_c moments is not (2.77), but

$$< t_c^n >:= \int dN_c\ \epsilon_n(\mu)\ t_c^n, \tag{2.82}$$

where the nth efficiency function ϵ_n is defined in analogy to (2.81) by

$$\epsilon_n(\bar{\mu}) := \frac{\int dN_c^*(\bar{\mu})\ \epsilon(t_{fwhm})\ t_c^n}{\int dN_c^*(\bar{\mu})\ t_c^n}. \tag{2.83}$$

The expression (2.82) fortunately does factorize as:

$$< t_c^n >= \frac{4 r_E v_l t_{obs} N_*}{d^{n/2}}\ V(2-n)\ \widehat{D}_{sl}(m)\ \ < \mu^m >, \tag{2.84}$$

with $m := (n+1)/2$ and

$$V(2-n) := e^{-\eta^2}\ \int dv\ v^{2-n}\ I_0(2\eta v) e^{-v^2}, \tag{2.85}$$

$$\widehat{D}_{sl}(m) := \int_0^\infty dD_{os}\ \rho_s(D_{os})\ \int_0^{D_{os}} dD_{ol}\ H_l(D_{ol}) \tag{2.86}$$

$$\times\ \left[\frac{D_{ol}(D_{os} - D_{ol})}{D_{os}}\right]^m\ \left(\int_0^\infty dD_{os}\ \rho_s(D_{os})\right)^{-1}, \tag{2.87}$$

$$< \mu^m >: = \int d\mu\ \epsilon_n(\mu)\ \left(\frac{dN_0}{d\mu}\right)\ \mu^m. \tag{2.88}$$

Comparison of (2.76) and (2.82) then yields the MACHO mass moments $< \mu^m >$. Note, that the mass moments of (2.88) do not weigh $(dN_0/d\mu)$, but the different functions $\epsilon_n(\mu)\big(dN_0/d\mu\big)$. For different values of n the functions ϵ_n are generally not identical. However, in practice this is not a serious problem, if the function $\big(dN_0/d\mu\big)$ peakes in the large region of μ values where $\epsilon_n \approx 1$. In this case, the moments (2.88) *are* the desired moments of the MACHO mass function.
Some of the moments are of particular interest. Of course, the number of events is $< t_c^0 >$. $< \mu^0 >$ is the mean number density of MACHOs and $< \mu^1 >$ is the average mass density of the MACHOs. Thus,

$$f := \frac{\mathrm{M}_\odot}{\rho_{l,0}} \; < \mu^1 > \tag{2.89}$$

is the fraction of the mass density detected in form of MACHOs. The mean MACHO mass is $< \mu^1 > / < \mu^0 > \mathrm{M}_\odot$.

2.5.2 Dark mass moments in pixel lensing

The Einstein time t_E is generally not measurable in pixel lensing. In practice, we have therefore to use another timescale to extract the moments of the dark mass function from the data. Obviously, this will be the full width at half maximum timescale t_{fwhm}. We modify this timescale in the same way like t_E in the previous subsection, to make it dimensionless

$$t_p := \frac{v_l}{r_E \sqrt{d_{gal}}} \; t_{fwhm} \; . \tag{2.90}$$

Since $t_{fwhm} = t_E \; w(\beta)$ (see Appendix A), we get

$$t_p = \frac{1}{v \; \sqrt{d_{gal}}} \sqrt{\mu \; \frac{D_{ol}(D_{os} - D_{ol})}{D_{os}}} \; w(\beta) \; . \tag{2.91}$$

Having the method of Gondolo (1999) in mind, we hope that the flux weighted moments of t_p

$$\int t_p^n \Delta F_{max} dN_p \tag{2.92}$$

factorize again into a product of moments of 'known' distributions times a moment of the MACHO mass distribution like in the previous subsection. The differential number of pixel lensing events in (2.92) is

$$dN_p := \frac{t_{obs} 10^{-0.4 \mu_{gal}}}{\int dM' 10^{-0.4 m(M') \Phi(M')}} \; d\Gamma \Phi(M) dM \; d\Omega_{obs} \; . \tag{2.93}$$

The integrations over the absolute source magnitude M and the angular surface of the observed field Ω_{obs} are nothing else than an integration over

the monitored sources (cf. Gondolo 1999). But first, one has to integrate over the event rate Γ. The differential rate $d\Gamma$ is given in Eq. (2.62). The integration over the event rate contains integrations over the lens velocity v, the lens mass μ, the source and lens positions D_{os} and D_{ol} and the minimum impact parameter β. The β integration is crucial - it is of the form

$$\int_{\beta_{min}}^{\beta_T} d\beta \ \big[w(\beta)\big]^n f(\beta^2) \ , \tag{2.94}$$

where the limits β_T and β_{min} are given by (2.32) and (2.21). Here, it is important to take into account finite source size effects, since if $n \leq 0$, the integral does not exist for $\beta_{min} = 0$. As mentioned in subsection 2.1.1 β_{min} is a function of the lens mass as well. Therefore, Eq. (2.92) will unfortunately not factorize in the desired manner. However, we will ignore this fact and approximate β_{min} by a constant, so that we can proceed in the same way like in the previous subsection.
From the experimental data, the cumulative moments

$$< t_p^n \Delta F_{max} > := \left(\frac{v_l}{r_E\sqrt{d_{gal}}}\right)^n \sum_{events} t_{fwhm}^n \Delta F_{max} \tag{2.95}$$

are calculated. (2.95) is then compared with the theoretical expression[3]

$$< t_p^n >_F := < t_p^n \Delta F_{max} > = \int t_p^n \Delta F_{max} \epsilon_n(\mu) dN_p^*(\mu), \tag{2.96}$$

with the efficiency functions,

$$\epsilon_n(\bar{\mu}) := \frac{\int dN_p^*(\bar{\mu}) \ \epsilon(t_{fwhm}) \ t_p^n}{\int dN_p^*(\bar{\mu}) \ t_p^n}. \tag{2.97}$$

Now, Eq. (2.96) factorizes in a similar manner like (2.84),

$$\begin{aligned} < t_p^n >_F = \frac{4 r_E v_l t_{obs}}{d^{n/2}} \left(\int dM' 10^{-0.4m(M')} \Phi(M')\right)^{-1} \\ \times V(2-n) \ < \mu^m > \int d\Omega_{obs} \left\{10^{-0.4\mu_{gal}} \ \widehat{D}_{sl}(m) \ L(n)\right\}, \end{aligned} \tag{2.98}$$

where V, $\widehat{D}$ and $< \mu^m >$ are defined by (2.85)-(2.88) and

$$L(n) := \int dM \left\{10^{-0.4m(M)} \Phi(M) \int_{\beta_{min}}^{\beta_T(M)} d\beta \ f(\beta^2) \big[w(\beta)\big]^n\right\}. \tag{2.99}$$

Note, that the three factors within the curly brackets of (2.98) depend all on the line of sight. In the case of $L(n)$ this dependence is stuck in $\beta_T(M)$.

[3] $dN_p^*(\mu)$ is the same as dN_p, but with a delta mass function in $d\Gamma$.

Eq. (2.98) is therefore a true triple integration.
Nevertheless, $L(n)$ can be computed in a straightforward manner and thus, comparison of (2.98) and (2.95) leads to the desired mass moments $< \mu^0 >$ and $< \mu^1 >$.
There are a few points in this method, that are not completely satisfactory.

- The moments $< t_p^n >_F$ are very sensitive to the integration limits β_T and β_{min}. For $n = 1$ $L(n)$ depends in particular on the upper limit β_T and for $n = -1$ the lower limit β_{min} is crucial, because for $\beta \ll 1$

$$\frac{f(\beta^2)}{w(\beta)} \propto \frac{1}{\beta^2} \ . \tag{2.100}$$

  Thus in pixel lensing, we have introduced two additional unknown parameters β_T and β_{min}, which have to be estimated.

- As mentioned above, the expression (2.92) does not exactly factorize, since β_{min} depends on the lens mass. It is not clear at this point, how the dark mass moments could be extracted, if we took into account this fact.

- In pixel lensing we have less information than in classical microlensing, because the unlensed flux of the source star cannot be measured. This is a general problem to solve in the transition from classical microlensing to pixel lensing. What we have actually done is the following. We have integrated over the flux of the source stars, but at the same time introduced another quantity, which has to be measured, the luminosity function $\Phi(M)$. This is only meaningful, if the results are not largely dependent on the exact functional form of the luminostiy function.

Chapter 3

Modelling

In this chapter we introduce the models for the mass density and for the velocity distributions of the various components of the target galaxy M31 and of the Milky Way, which we will use for the calculations during the following chapters. The basic parameters of the used models are summarized in Table 3.2. Furthermore, we discuss the adopted mass functions for the different lens objects and the stellar luminosity function for the source stars. Finally, we show the surface brightness profile of M31, that we take from the literature.

3.1 M31: The Andromeda Galaxy

Apart from the Milky Way satellites (LMC, SMC etc.), M31 is the nearest bigger spiral galaxy. Its general characteristics are given in Table 3.1. The Hubble type of M31 is Sb0 and the distance from the sun to the M31 centre is $d = 770$ kpc. The centre of M31 is located near ν Andromedae at $\alpha = 00^h42^m44.3^s$ and $\delta = 41°16'09''$, which corresponds to $l = 121.2°$ and $b = -21.6°$ in galactic coordinates.[1] We use a three-component model for M31, consisting of a stellar bulge (subscript b), a stellar disc (d), and a dark halo (h). Projected onto the sky, the M31 disc shows an elliptical shape. The position angle of the major axis of this apparent ellipse is $\lambda = 37.7°$ and is measured counter-clockwise from the northern direction. The apparent elliptical shape of the disc of M31 is due to the fact that the M31 disc is inclined at $i = 77°$ from edge-on.

[1] The galactic longitude is measured from the Galactic centre ($l = 0°$) ascending in counter-clockwise direction. The galactic latitude is $0°$ in the symmetry plane of the Milky Way disc (galactic equator) and ascending towards the northern Galactic pole located in Coma Berenicis.

M31, the Andromeda Galaxy	
Right ascension	$00^h42^m44.3^s$
Declination	$41°16'09''$
Galactic longitude	121.2°
Galactic latitude	-21.6°
Apparent magnitude	3.8 mag
Distance from the sun	770 kpc
Inclination of the M31 disc	77°
Position angle of the M31 disc major axis	37.7°
Diameter	54 kpc
Apparent angular diameter	4°
Radial velocity	-310 km/s
Luminous mass	$\approx 10^{11}$ $M_\odot$
Total mass	$\approx 10^{12}$ $M_\odot$

Table 3.1: This Table shows some of the most important properties of M31, the Andromeda Galaxy. The first four characteristics are related to the M31 centre. The position angle is measured counter-clockwise from the northern direction. The negative sign of the radial velocity means that M31 moves towards us.

3.1.1 Halo

For the dark halo of M31 we use an axisymmetric oblate spheroid, determined by two parameters, the flatness q_h and the core radius r_c. We will always assume the dark halo to consist to 20% of MACHOs ($f_h = 0.2$), suggested for the Milky Way halo by the observations towards LMC. In cylindrical coordinates with respect to the disc plane (r, φ, z) the density profile is given by

$$\rho_h(r,z) = \rho_{h,0}\ f_h\ \frac{\sqrt{1-q_h^2}}{q_h \arccos(q_h)}\ \frac{r_c^2}{r_c^2 + r^2 + \left(\frac{z}{q_h}\right)^2}. \tag{3.1}$$

The standard halo model we use, is spherical ($q_h = 1$), has a central density $\rho_{h,0} = 2.3 \times 10^8$ $M_\odot$ kpc^{-3}, a core radius $r_c = 2$ kpc and the density profile is cut off at a distance $R_{max} = 200$ kpc from the centre of M31 (cf. Kerins et al. 2001).
If we vary the core radius r_c and the flateness q_h we will also have to change the density normalization $\rho_{h,0}$ (cf. eq. (2-91) of Binney & Tremaine (1987) or Gould 1993). The mass of an oblate halo is smaller than that of a spherical halo, but also the mass distribution is compressed by the oblateness ratio.
For the velocity distribution we take a standard Maxwellian distribution

with dispersion velocity $v_h = \sqrt{2}\sigma_h$

$$f(\mathbf{v})d^3\mathbf{v} = \frac{1}{(\pi v_h^2)^{3/2}} \exp\Big(-\frac{\mathbf{v}^2}{v_h^2}\Big)d^3\mathbf{v}, \tag{3.2}$$

which is already normalized to 1. The velocity dispersion σ_h is determined from the measured rotation speed of the M31 disc under the assumption that the dark halo is a completely virialized system (isothermal sphere) and that the rotation speed remains constant within the halo to large distances. With $v_{M31} = 235$ km/s we obtain

$$\sigma_h = v_{M31}/\sqrt{2} = 166 \text{ km/s}. \tag{3.3}$$

3.1.2 Disc

The M31 stellar disc is modelled by the double exponential disc of Han (1996) with the density profile

$$\rho_d(r,z) = \rho_{d,0} \exp\big(-\frac{r}{h_r}\big) \exp\big(-\frac{|z|}{h_z}\big) \tag{3.4}$$

where the radial and vertical scale heights are $h_r = 6.4$ kpc and $h_z = 0.4$ kpc, respectively. The mass normalization is taken to be $\rho_{d,0} = 3.5 \times 10^8\ M_\odot \text{kpc}^{-3}$ resulting in a total disc mass of $M_d = 6.8 \times 10^{10} M_\odot$ within $r \leq 30$ kpc, $|z| \leq 2$ kpc, where we truncated the disc profile.
The M31 disc stars are assumed to move in circular orbits around the M31 centre. We model the rotation curve of M31 by

$$v_{rot} = \begin{cases} \frac{r}{r_v}\ v_{M31} & r < r_v \\ v_{M31} & r \geq r_v \end{cases}, \tag{3.5}$$

with $v_{M31} = 235$ km/s and $r_v = 1$ kpc. In addition, we superpose a Maxwellian velocity distribution for the disc stars with a velocity dispersion $\sigma_d = 30$ km/s. The motion of the M31 disc stars will be important when considering self-lensing.

3.1.3 Bulge

For the bulge we use an axisymmetric exponential density law similar to the one used by Grenacher et al. (1999) for the bulge of the Milky Way. We are aware that this model is perhaps not suitable for the M31 bulge and might produce unrealistic results for the microlensing quantities in the central region of M31. To get more realistic results, particularly for the self-lensing quantities, one should adopt the bulge models of Kent (1989) or Ruiz (1976) in a next step. However, in this work, we will use for simplicity

$$\rho_b(r,z) = \rho_{b,0} \exp\left[-\Big(\frac{s}{s_e}\Big)^2\right], \tag{3.6}$$

Component	Mass normalization	Scalelengths	Cut-off	σ
M31 halo	2.3×10^8 $M_\odot$kpc^{-3}	$r_c = 2$ kpc	200 kpc	166 km/s
M31 bulge	9.0×10^9 $M_\odot$kpc^{-3}	$s_e = 1$ kpc	8 kpc	100 km/s
M31 disc	3.5×10^8 $M_\odot$kpc^{-3}	$h_r = 6.4$ kpc	30 kpc	30 km/s
		$h_z = 0.4$ kpc	2 kpc	
Milky Way halo	7.9×10^6 $M_\odot$kpc^{-3}	$r_c = 5.6$ kpc	100 kpc	156 km/s

Table 3.2: Parameters adopted for the density and velocity distributions for components of M31 and for the Galaxy. The M31 halo model is from Kerins et al. 2001, but with the possibility of a flattened halo. The disc model is from Han (1996) and the bulge model from Grenacher et al. (1999). Note, that the mass normalization of the Milky Way halo model is the local dark mass density. The dispersion velocities are all taken from Kerins et al. (2001).

where $s^2 = r^2 + \left(\frac{z}{q_b}\right)^2$. We take an effective radius of $s_e = 1$ kpc and an axis ratio of $q_b = 0.8$ and we cut off the profile at a distance of 8 kpc. The density profile is normalized to a total bulge mass within 8 kpc of $M_b = 4 \times 10^{10}$ $M_\odot$ giving $\rho_{b,0} = 9.0 \times 10^9$ $M_\odot$kpc^{-3}. The comparison of our disc and bulge models shows that the mass density of the bulge is the dominant contribution out to a distance of 2 kpc or 9 arcmin from the M31 centre. At larger distances the bulge mass density can be neglected relative to the disc mass density.
Once more, we model the velocity distribution of the bulge by a Maxvellian distribution with a velocity dispersion $\sigma_b = 100$ km/s (Kerins et al. 2001).

3.2 Milky Way halo

When searching for microlensing events due to MACHOs in the haloes of external galaxies, the events due to Galactic MACHOs cannot be neglected. We will assume the Galactic dark halo to be similar to that of M31, because the rotation curves of the discs look very similar. We use the same model as Grenacher et al. (1999) for the Galactic halo (g)

$$\rho_g(r,z) = \rho_{g,\odot}\ f_g\ \frac{\sqrt{1-q_g^2}}{q_g \arccos(q_g)}\ \frac{r_c^2 + r_\odot^2}{r_c^2 + r^2 + \left(\frac{z}{q_g}\right)^2} \tag{3.7}$$

where here $\rho_{g,\odot} = 7.9 \times 10^6$ $M_\odot$ kpc^{-3} is the local dark mass density, q_g is the axis oblateness ratio, $r_\odot = 8.5$ kpc is the distance of the sun from the Galactic centre and the core radius is $r_c = 5.6$ kpc. The density profile is cut off at a radial distance $R_{max} = 100$ kpc from the Galactic centre. In most of the cases we consider only spherically symmetric haloes ($q_g = 1$).
The velocity distribution of the Galactic halo MACHOs is again described

by a Maxwellian distribution with dispersion velocity $\sigma_g = 156$ km/s. The circular motion of the sun $v_\odot = \sqrt{2}\sigma_g = 220$ km/s around the galactic centre will only be considered for the Galactic lenses. For lenses in M31, it can be neglected, since $\frac{D_{ol}}{D_{os}} \approx 0$ in (2.63).

3.3 Lens mass functions

The determination of the mass distribution of the objects, which act as lenses $\left(dN_0/d\mu\right)$ is one of the main aims of microlensing experiments. Thus, one of the questions is how well pixel lensing observables can characterize the MACHO mass. Therefore, we simply model the Galaxy and M31 MACHO mass distribution by a Dirac δ-function. Actually, we assume all the lenses to have the same mass μ_0

$$\left(\frac{dN_0}{d\mu}\right) = \frac{\rho_{l,0}}{M_\odot \mu_0}\, \delta(\mu - \mu_0)\ , \tag{3.8}$$

where we used the normalization condition (2.58).
In the case of self-lensing, the lenses are supposed to be ordinary stars in the bulge or in the disc of M31. Then, we use a broken power law for the stellar mass function with a lower mass cut-off of $\mu_{min} = 0.08$ (hydrogen burning threshold) and an upper cut-off of $\mu_{up} = 1.5$, because stars with larger masses do not act as lenses, since they are seen directly:

$$\left(\frac{dN_0}{d\mu}\right) = \begin{cases} C_1 \mu^{-0.75} & \mu_{min} \leq \mu \leq 0.5 \\ C_2 \mu^{-2.2} & 0.5 \leq \mu \leq \mu_{up}. \end{cases} \tag{3.9}$$

This mass function is normalized with the use of (2.58) and shall be continuos at $\mu = 0.5$, which gives $C_1 = 0.80\ \rho_{l,0}/M_\odot$ and $C_2 = 0.29\ \rho_{l,0}/M_\odot$.
This mass function corresponds closely to the local Solar neighbourhood mass function and is therefore reasonable for stars in the M31 disc, but overestimates the contribution of massive stars in the older bulge (Kerins et al. 2001).

3.4 Luminosity function

We use the luminosity function from Bahcall & Soneira (1980) for both the disc and the bulge of M31. This luminosity function is obtained by a fit for the Milky Way disc, but it should be appropriate for M31, a similar galactic system, as well.

$$\Phi(M) = \begin{cases} \frac{n_* 10^{b(M-M_*)}}{\left[1+10^{-(a-b)c(M-M_*)}\right]^{1/c}} & M_{min} \leq M \leq 15 \\ \Phi(15) = 14.2 \times 10^6\ \mathrm{kpc}^{-3} & 15 \leq M \leq M_{max} \\ 0 & \text{otherwise} \end{cases} \tag{3.10}$$

where $n_* = 4.03 \times 10^6$ kpc^{-3} and

$$M_{min} = -6 \qquad M_{max} = 19 \qquad M_* = 1.28 \tag{3.11}$$

$$a = 0.74 \qquad b = 0.04 \qquad c = 0.29 \tag{3.12}$$

3.5 Surface brightness of M31

For calculating the event rates in pixel lensing we need the surface brightness profile for M31. We adopt the profile along the major axis of M31 given in Kent (1987). Following Kent (1983), it is assumed, that a given isophote can be approximated by an ellipse, such that the overall surface brightness of M31 can be written in the form

$$\mu_{M31} = \mu_{M31}(s) \tag{3.13}$$

where

$$s^2 = \tilde{u}^2 + \frac{\tilde{v}^2}{(1-\epsilon^2)}, \tag{3.14}$$

and

$$\tilde{u} \quad = u\cos\theta + v\sin\theta \tag{3.15}$$

$$\tilde{v} \quad = v\cos\theta - u\sin\theta. \tag{3.16}$$

(u, v) are the coordinates along the major and minor axis of M31, θ is the position angle of the major axis of the ellipse s, and ϵ its ellipticity $(= 1 - b/a)$. With the help of Table III of Kent (1987) we reconstructed the isophotes and the resulting surface brightness profile is shown in Fig. 3.1.

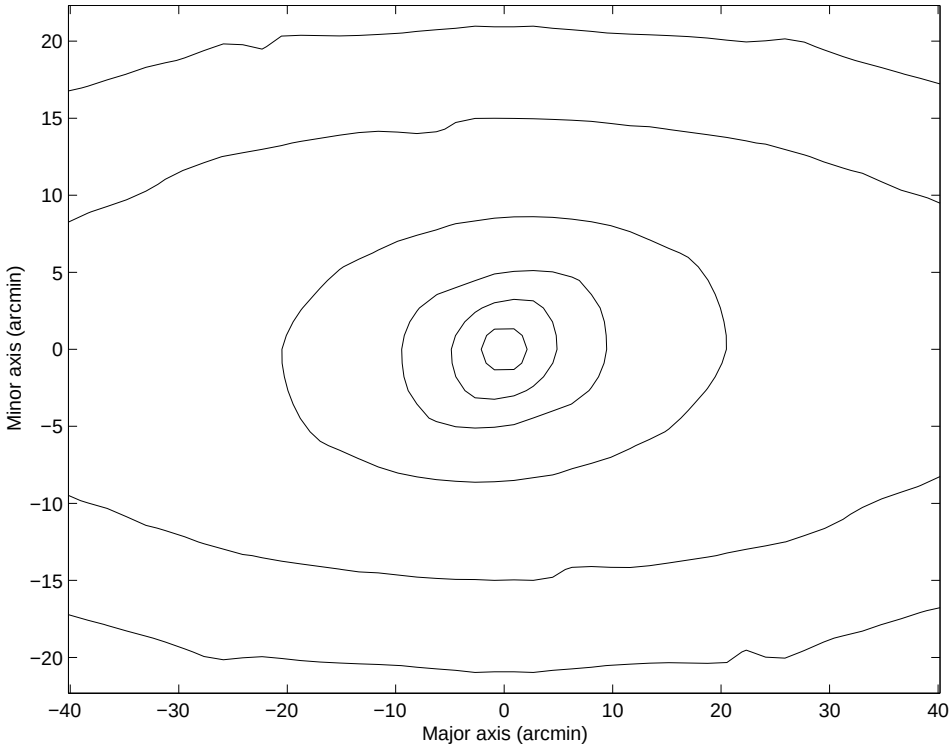

Figure 3.1: Surface brightness profile of both the M31 disc and the M31 bulge. The central surface brightness is 14 mag arcsec^{-2}. Contours are from the centre to the outside 18, 19, 20, 21, 22, 23 mag arcsec^{-2}

Chapter 4

Optical Depth

In this chapter, we will calculate the expected microlensing optical depth towards M31 and we will show a set of optical depth maps for M31. But first, we have to specify the different lens and source components for M31 and for the Milky Way:

- Lenses:
  For the Milky Way only the MACHOs in the halo are important, because the Galactic disc does not contribute significantly. For M31 the main populations are the MACHO halo, the stellar bulge and the stellar disc.
- Sources:
  The source stars are assumed to lie either in the stellar bulge or in the disc of M31.

Thus, we have to compute three different contributions to the optical depth: M31 dark halo, the Galactic halo and self-lensing of M31 stars.

4.1 M31 MACHO halo

For the calculation it is convenient to perform a coordinate transformation from the intrinsic coordinate system in M31 (x, y, z) to a new coordinate system (u, v, w), still centered at the M31 centre, where u and v are the M31 major and minor axis, respectively. w is the line of sight towards M31. Positive values for v reside on the far side of the disc. The coordinate transformation is just a rotation about the inclination angle i and is given by

$$x = u \qquad y = v\cos i + w\sin i \qquad z = w\cos i - v\sin i. \tag{4.1}$$

Then, we translate the coordinate system (u, v, w) along the line of sight by the distance d of M31 to the sun. The new coordinate system (u, v, D), with

$D := d + w$ is then centered at the observer.
We use (2.42) to calculate the optical depth due to the M31 dark halo with

$$\rho_l = \rho_h(D_{ol}) \qquad \rho_s = \rho_d(D_{os}) + \rho_b(D_{os}) \ , \tag{4.2}$$

Averaged over the two observed fields of the POINT-AGAPE collaboration, we obtain for a spherical halo with a 2 kpc core radius, consisting of 20% of MACHOs

$$\tau_h = 6.2 \times 10^{-7}. \tag{4.3}$$

For the northern (N) and the southern field (S), respectively, the optical depths are

$$\tau_h^{(N)} = 4.8 \times 10^{-7} \tag{4.4}$$

$$\tau_h^{(S)} = 7.5 \times 10^{-7}. \tag{4.5}$$

The slightly higher optical depth towards the southern field is explained by the fact, that it is rather located on the far side of the disc, while the northern field lies more or less centered at the major axis.

Let us now investigate the dependence of τ_h on the following parameters of the halo model: the core radius r_c and the flatness q_h. Note, that when varying q_h and r_c, we have also to change the density normalization $\rho_{h,0}$. In Fig. 4.1 we plot the optical depth along the minor axis for different values of q_h and r_c. The most important attribute of the optical depth of the M31 halo lenses is the strong modulation from the near to far side of the M31 disc, which is shown by all four models in Fig. 4.1. The fractional variation in τ_h is most pronounced for less flattened haloes, which is clear from geometry. On the other hand, the models with the larger core radii show a smaller gradient from near to far. In comparison with Fig. 3 of Gyuk & Crotts (2000) we see differences especially at the centre of M31. These differences are due to the fact that we integrated over the source positions as well (see (2.42)).
The optical depth to bulge sources only, peaks nearly[1] at the centre of M31 and is negligible at a distance more than nine arcminutes from the centre. Adding the optical depth for bulge sources to the optical depth for disc sources yields the result in Fig. 4.1.
Variations in core radii and flattening are also reflected in the run of optical depth along the major axis. In Fig. 4.2 we show the optical depth along the major axis displaced by $v = 13'$ on the minor axis (towards the far side of the disc) for the same four halo models (cf. Fig. 4 in Gyuk & Crotts 2000). The central gradients are much larger for the models with the small core radii than for large core radii. Asymptotically, the flattened haloes

[1]The maximum does not lie exactly at the centre of M31, because our bulge is slightly flattened.

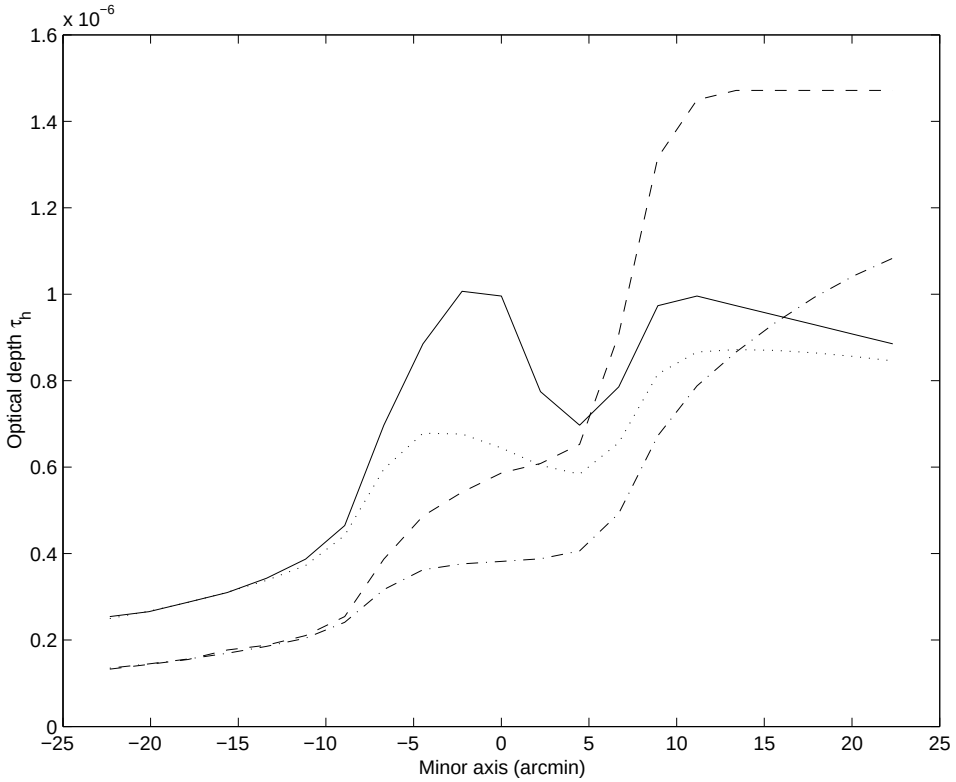

Figure 4.1: M31 halo optical depth along the minor axis for four different halo models with a MACHO fraction of 20%. *Solid line*: $q = 0.3$, $r_c = 1$ kpc. *Dotted line*: $q = 0.3$, $r_c = 5$ kpc. *Dashed line*: $q = 1.0$, $r_c = 1$ kpc. *Dashed-dotted line*: $q = 1.0$, $r_c = 5$ kpc.

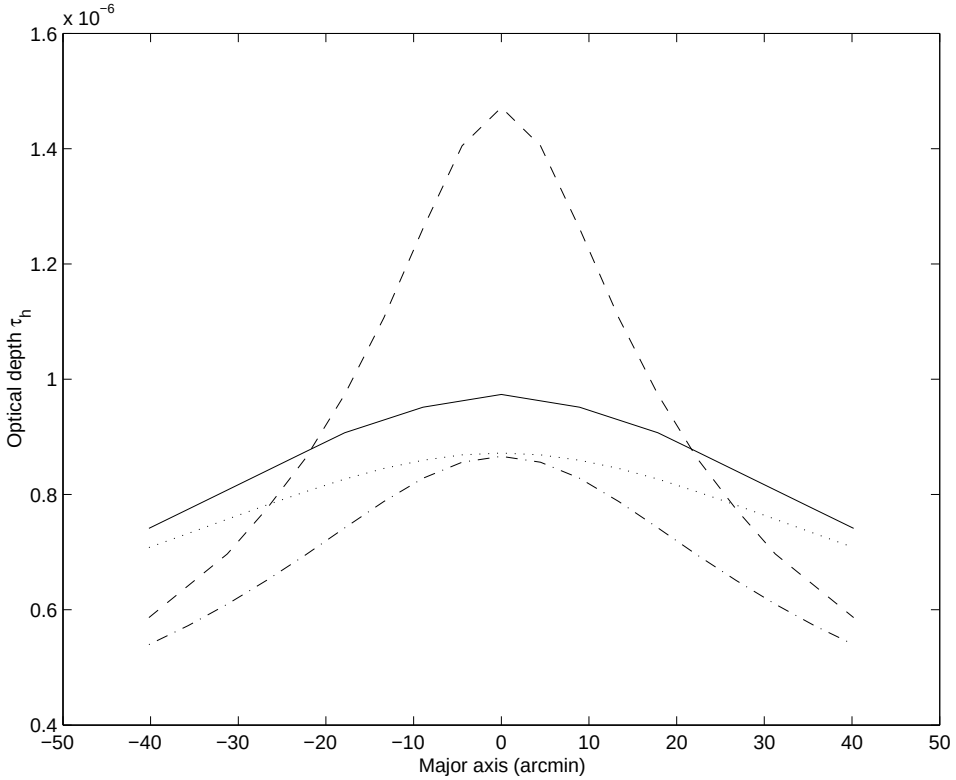

Figure 4.2: M31 halo optical depth along the major axis and offset along the minor axis $v = 13$ arcmin or 3 kpc towards the far side of the disc. The MACHO fraction of the halo is $f_h = 0.2$. *Solid line*: $q = 0.3$, $r_c = 1$ kpc. *Dotted line*: $q = 0.3$, $r_c = 5$ kpc. *Dashed line*: $q = 1.0$, $r_c = 1$ kpc. *Dashed-dotted line*: $q = 1.0$, $r_c = 5$ kpc.

have a larger optical depth, because flatter haloes have a greater density in the Galactic plane. 13 arcmin from the centre, we expect the self-lensing contribution to be small. Therefore, from a microlensing experiment that counts events along the major axis at this position, the halo parameters could be extracted, in principle.

The contour map for the M31 halo contribution is shown in Fig. 4.3. It is clearly seen that the optical depth increases towards the far side of the M31 disc (positive values for the v-axis). The structure of the contours in the centre of M31 comes again from the bulge sources. For bulge sources $< D_{os} >$ is nearly constant near the centre of M31 and so does therefore the optical depth. Our contour map is in quantitative agreement with the one in Fig. 1c of Gyuk & Crotts (2000), if we use the same parameters for the models as they did.[2]

[2]They assumed a halo of 100% MACHOs with a smaller core radius of 1 kpc and a

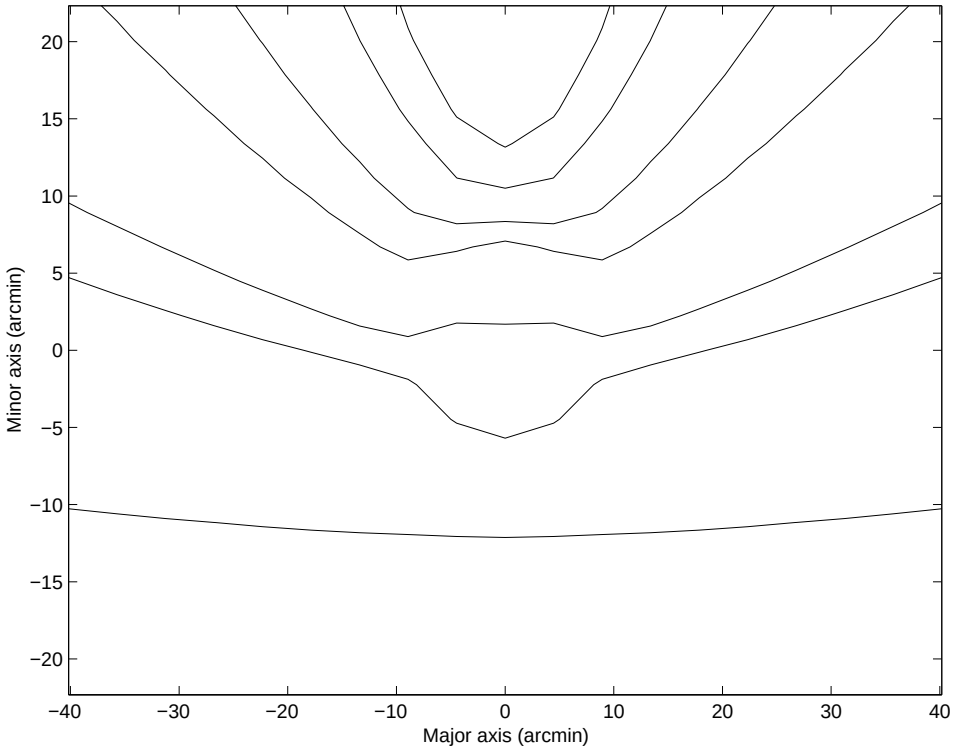

Figure 4.3: Contours of optical depth for a dark halo of M31 with $q = 1$, $r_c = 2$ kpc and a MACHO fraction of 20%. Contours are from bottom to top 0.2, 0.4, 0.5, 0.8, 1, 1.2, 1.3 $\times 10^{-6}$.

4.2 Galactic MACHO halo

The contribution of lenses in the Milky Way halo is again computed with (2.42), but now we put

$$\rho_l = \rho_g(D_{ol}) \qquad\qquad \rho_s = \rho_d(D_{os}) + \rho_b(D_{os}) \ . \tag{4.6}$$

We obtain a constant optical depth over the surface of M31, which is not surprising, since the density of the lenses is almost the same for the different line of sights through the Milky Way halo and the different distances of the source stars has no significant influence. The optical depth to Milky Way MACHOs for a spherical halo with a 5.6 kpc core and a 20% MACHO fraction is

$$\tau_g = 1.7 \times 10^{-7} \ . \tag{4.7}$$

We varied also the core radius and the axis oblateness ratio of the Galactic halo model. We found that a smaller core radius increases the optical depth. The optical depth becomes very large, if the core radius is much smaller than 2 kpc (Fig. 4.4). For a core radius of $r = 2$ kpc ($q_g = 1$, $f_g = 0.2$) we obtain

$$\tau_g = 7.6 \times 10^{-7}. \tag{4.8}$$

The optical depth for haloes with $r_c = 5.6$ kpc and $f_g = 0.2$, but varying flateness q_g is plotted in Fig. 4.5. The optical depth increases when the halo is flattened with a maximum for $q_g = 0.4$,

$$\tau_g = 2.6 \times 10^{-6} \ . \tag{4.9}$$

For higher oblateness ratios ($q_g < 0.4$) the optical depth decreases again: For $q_g = 0.1$ we get

$$\tau_g = 1.4 \times 10^{-7} \ . \tag{4.10}$$

To find constraints on the Milky Way halo parameters, it will be necessary to compare the measured optical depths towards different targets as M31, LMC, SMC and globular clusters.

4.3 Self-lensing

Because our model for the M31 source populations consists of the M31 bulge (b) and the M31 disc (d), there are four possible source/lens (sl) self-lensing configurations: bulge/bulge, disc/bulge, bulge/disc and disc/disc.
We calculate the contribution of each sl-configuration separately with the use of (2.42). The resulting contour maps for each contribution are shown in Fig. 4.6 - Fig. 4.9.

---

slightly bigger mass normalization of 2.7×10^8 $M_\odot kpc^{-3}$. Furthermore, they did not integrate over the source positions as well.

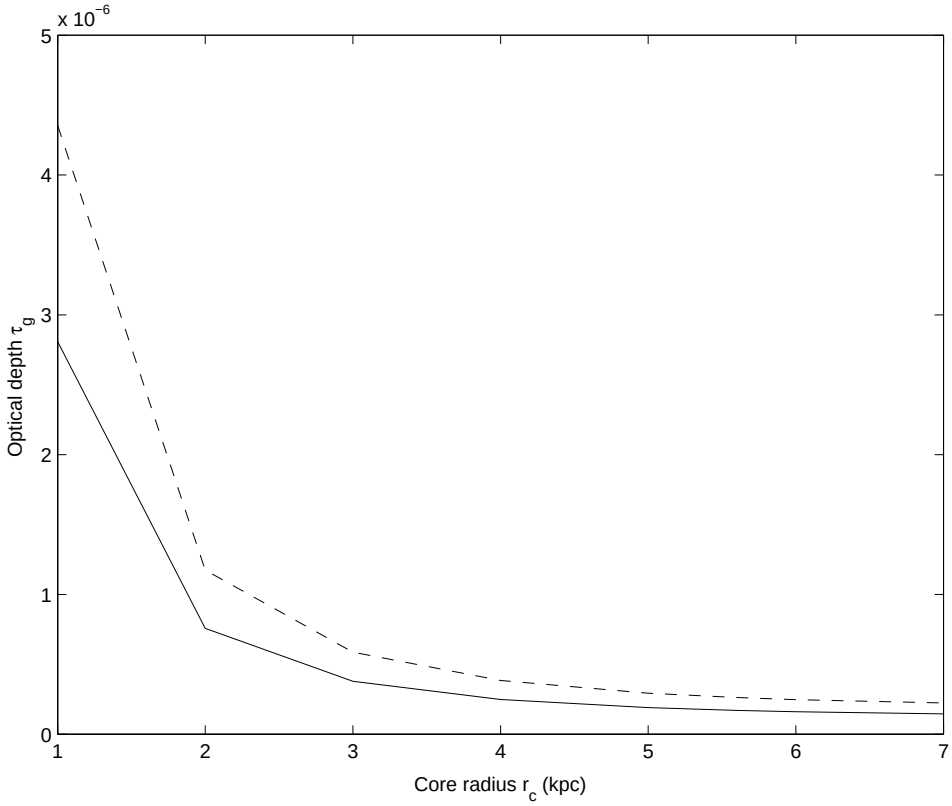

Figure 4.4: Optical depth of the Galactic lenses for different core radii of the Milky Way halo. The solid line shows a spherical halo $q_g = 1$ and the dashed line shows a halo with $q_g = 0.3$. The MACHO fraction is still held at 20%.

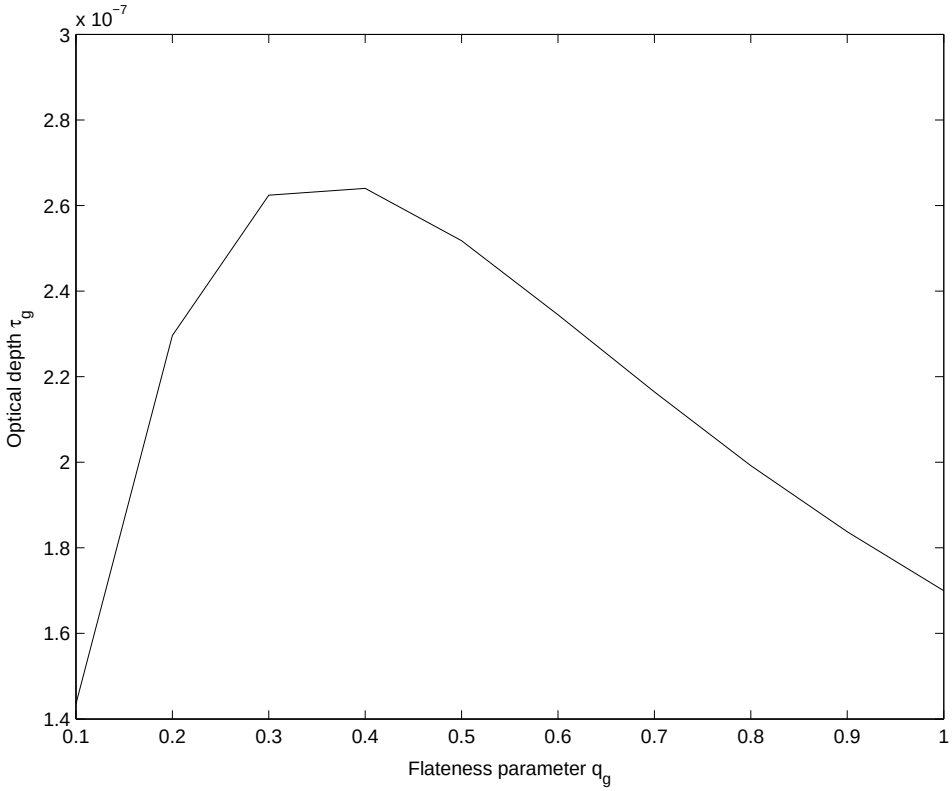

Figure 4.5: Optical depth for MACHOs in the Milky Way as a function of the flatness parameter q_g. The core radius is $r_c = 5.6$ kpc and the MACHO fraction $f_g = 0.2$.

To obtain a total self-lensing optical depth we cannot just add up the four different terms, because their denominators (see (2.42)) are different. We have therefore to take a weighted sum, the weights being evaluated by

$$w_s = \int_0^\infty dD_{os}\rho_s(D_{os}) \left[\int_0^\infty dD_{os}\Big(\rho_b(D_{os}) + \rho_d(D_{os})\Big)\right]^{-1}. \qquad (4.11)$$

The weights depend on the line of sight as well, so we calculate the sum of the four different self-lensing contributions for each line of sight separately to get the contour map for the total self-lensing optical depth (Fig. 4.10). Furthermore, we averaged the self-lensing optical depths over the observed fields of the POINT-AGAPE collaboration (Table 2.2).

4.3.1 Bulge/Bulge

First, we consider the case, where the source star, as well as the lens star, reside in the stellar bulge of M31. The effect of the bulge lenses is highly concentrated towards the centre, as shown in Fig. 4.6. The averaged optical depth over the POINT-AGAPE fields is only $\tau_{bb} = 5.9 \times 10^{-8}$, since they cover a large part of M31 outside the bulge. Thus, the bulge contribution can be effectively removed by deleting the central few arcminutes of M31. On the other hand, the effective source densities are much higher in the central regions, and thus we expect the bulk of the halo events to occur there as well. For the line of sight through the centre of M31 (c), we obtain the large value of

$$\tau_{bb}^{(c)} = 3.7 \times 10^{-6}. \qquad (4.12)$$

4.3.2 Disc/Bulge

The optical depth map for disc/bulge self-lensing is shown in Fig. 4.7. Note, that the maximum value of the optical depth is shifted towards the far side of the disc at about 4', since there the probability to find a disc star behind a bulge star is a little bit larger than at the centre of M31 because of the inclination of the disc. The mean value for the observed fields is $\tau_{db} = 4.3 \times 10^{-8}$. For the southern field it is a little bit larger ($\tau_{db}^{(S)} = 5.9 \times 10^{-8}$) than for the northern field ($\tau_{db}^{(N)} = 2.7 \times 10^{-8}$), because the former is more located on the far side of the disc. Although these mean values are rather small, the optical depth at a particular position can become quite large.

4.3.3 Bulge/Disc

The average optical depth to bulge sources lensed by disc stars is of the same order like the disc/bulge and the bulge/bulge contribution ($\tau_{bd} = 3.2 \times 10^{-8}$).

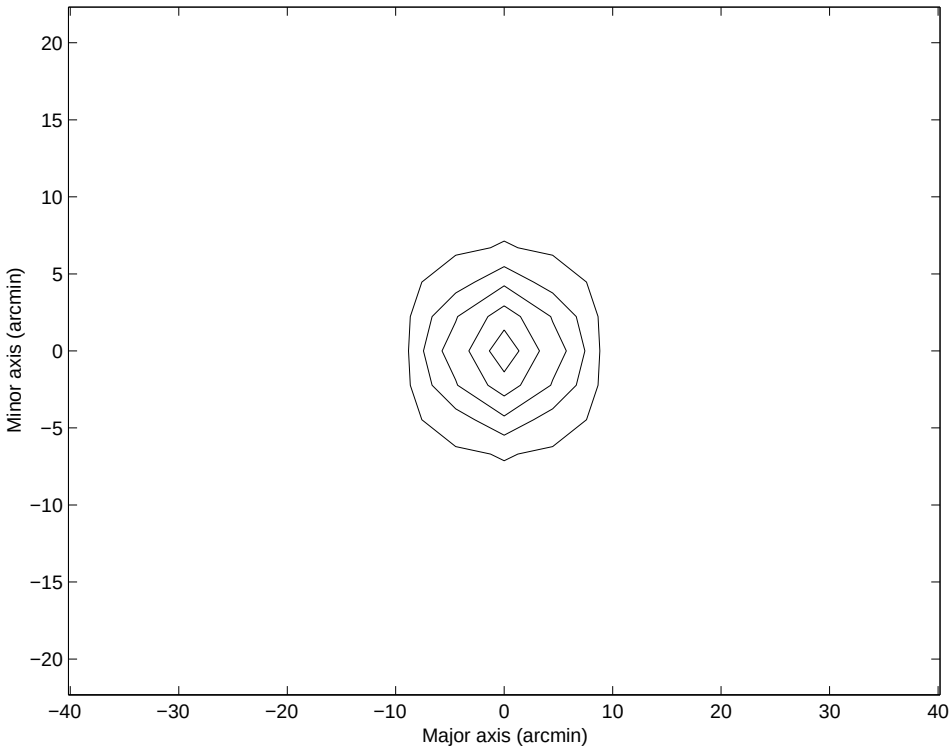

Figure 4.6: Contours of optical depth for the bulge/bulge self-lensing contribution. Contours are from the outside to the centre 1, 5×10^{-7}, 1, 2, 3×10^{-6}.

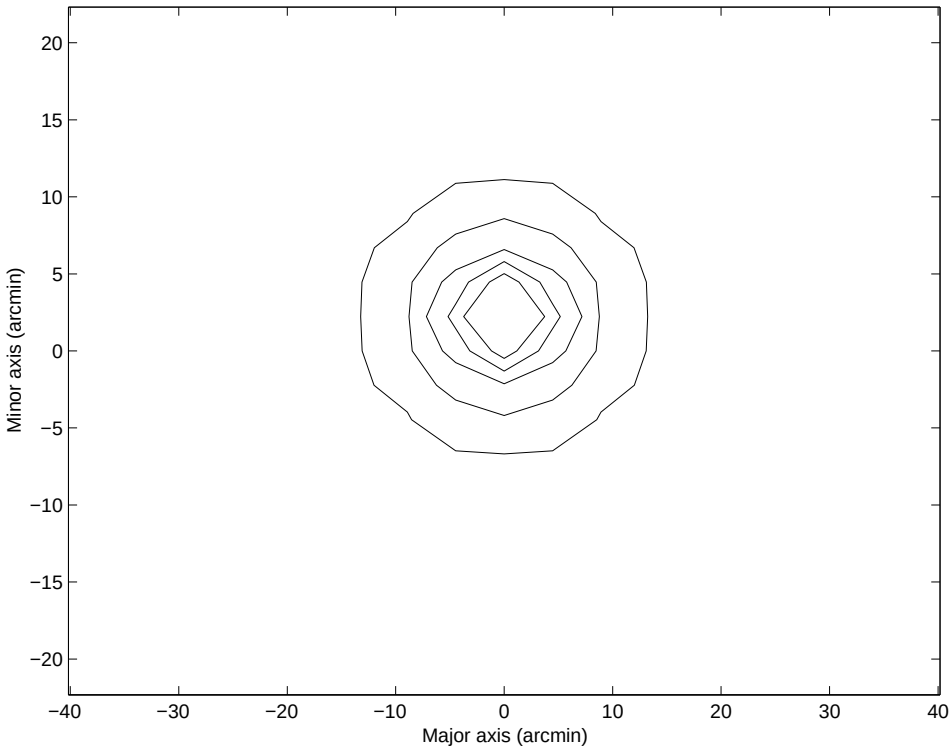

Figure 4.7: Contours of optical depth for the disc/bulge self-lensing contribution. Contours are from the outside to the centre 1×10^{-8}, 4×10^{-7}, 2, 4, 6×10^{-6}.

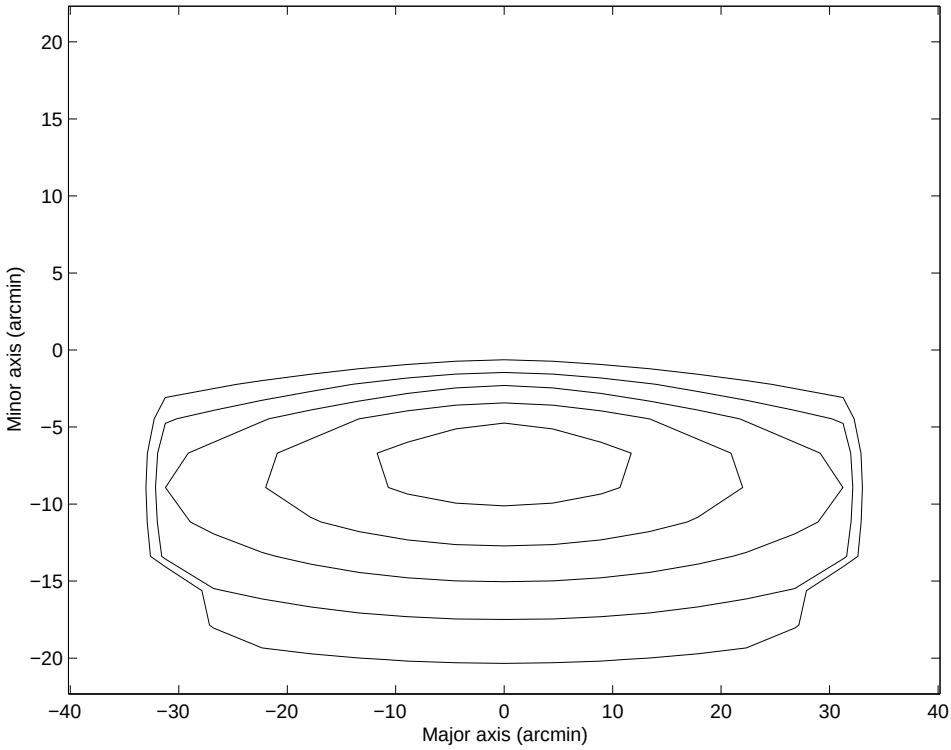

Figure 4.8: Contours of optical depth for the bulge/disc self-lensing contribution. Contours are from the outside to the centre 6, 8×10^{-7}, 1, 1.2, 1.4×10^{-6}.

The contour map is shown in Fig. 4.8. In this case, the maximum value is shifted towards the near side of the disc at about 7', because there bulge stars are more probable to lie behind disc stars. This explains also the higher mean optical depth of the northern field:

$$\tau_{bd}^{(N)} = 5 \times 10^{-8} \tag{4.13}$$

$$\tau_{bd}^{(S)} = 1.4 \times 10^{-8}. \tag{4.14}$$

4.3.4 Disc/Disc

Along the line of sight through the M31 centre we get for disc/disc self-lensing an optical depth of

$$\tau_{dd}^{(c)} = 6.1 \times 10^{-7}, \tag{4.15}$$

which is roughly the same result like that of Gould (1994). The optical depth contour map is shown in Fig. 4.9 and is symmetric relative to the major and

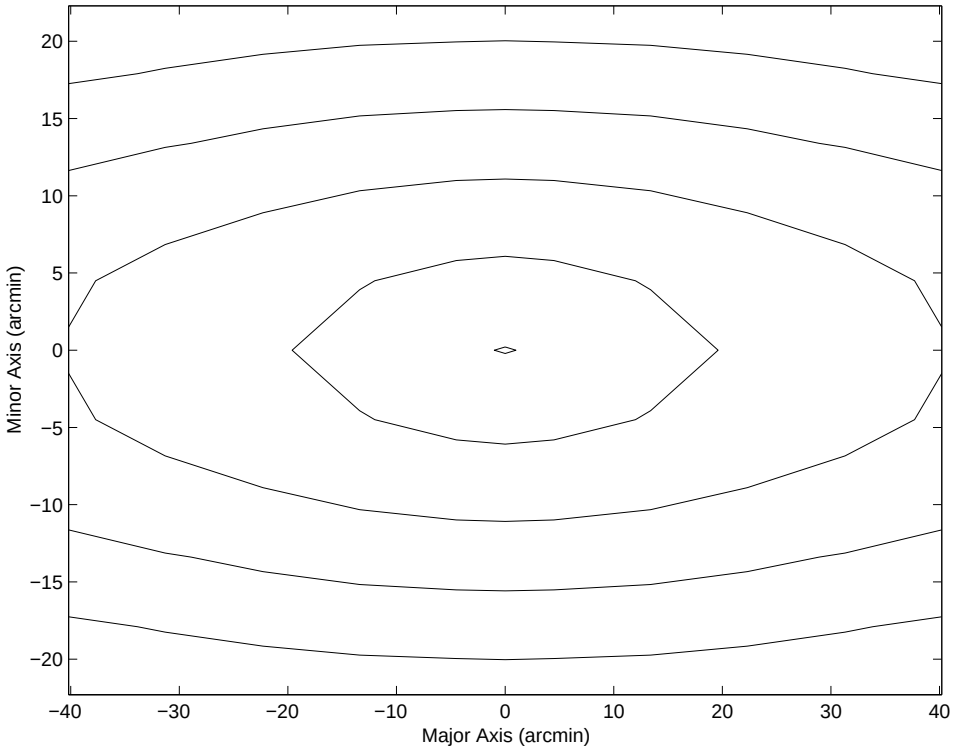

Figure 4.9: Contours of optical depth for the disc/disc self-lensing contribution. Contours are from the outside to the centre 5×10^{-8}, 1, 2, 4, 6×10^{-7}

Source/lens configuration	Northern field	Southern field	Total τ_{sl}
bulge/bulge	6×10^{-8}	5.8×10^{-8}	5.9×10^{-8}
disc/bulge	2.7×10^{-8}	5.9×10^{-8}	4.3×10^{-8}
bulge/disc	5×10^{-8}	1.4×10^{-8}	3.2×10^{-8}
disc/disc	2.2×10^{-7}	1.4×10^{-7}	1.8×10^{-7}
Total self-lensing	3.6×10^{-7}	2.7×10^{-7}	3.1×10^{-7}

Table 4.1: Self-lensing optical depths of the different source/lens configurations averaged over the two observed POINT-AGAPE fields.

minor axis. For the two observed POINT-AGAPE fields, we obtain a mean optical depth of $\tau_{dd} = 1.8 \times 10^{-7}$, which is not negligible compared to the optical depth of the M31 halo. Therefore, even if a microlensing event is found outside of the bulge of M31, disc/disc self-lensing can always be a reasonable alternative.

4.3.5 Total self-lensing optical depth

Taking the weighted sum of the four different self-lensing contributions yields the mean self-lensing optical depth towards the POINT-AGAPE fields presented in Table 4.1. The maximum value for the self-lensing optical depth is obtained along the line of sight throug the centre of M31 with

$$\tau_{sl}^{(c)} = 4.4 \times 10^{-6} \ . \tag{4.16}$$

The contour map for the total self-lensing optical depth is shown in Fig. 4.10. Note, that we have essentially drawn the same contours as in Fig. 4.3. Thus, it is clear, that self-lensing is important particularly within the central 10 arcminutes. Outside of this area, only disc/disc self-lensing is present.

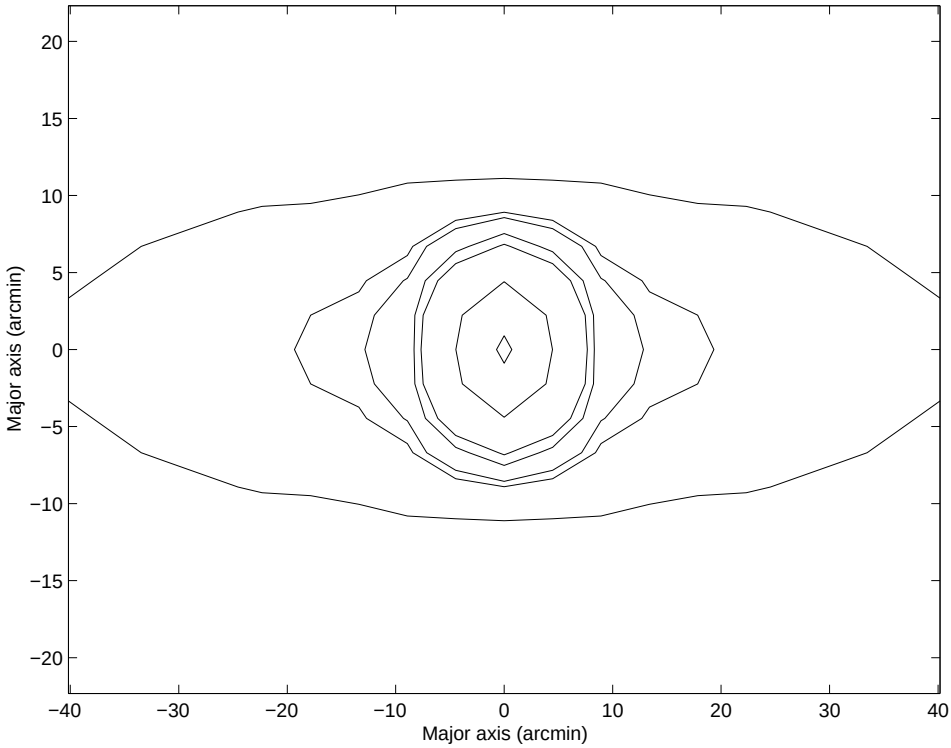

Figure 4.10: Contours of optical depth for the total self-lensing contribution. Contours are from the outside to the centre 0.2, 0.4, 0.5, 0.8, 1, 2, 4×10^{-6}.

Chapter 5

Event Rates

In this chapter we compute the event rates for microlensing towards M31 and provide a set of event rate maps for the different contributions to the total rate. In subsection 5.1 we first calculate the classical microlensing event rates using the theory presented in subsection 2.4 and the modelling of M31 and of the Galaxy described in sections 3.1 and 3.2. In subsection 5.2 we then use the classical rates and generalize them to the case of pixel lensing using the methods given in section 2.2. In addition we calculate the number of expected events for the pixel lensing survey of the POINT-AGAPE collaboration carried out in 1999 and 2000, where two fields in M31 have been monitored using the WFC at the INT telescope during two M31 observing seasons (8 months).

5.1 Classical microlensing rate

The calculations of the classical microlensing rates in this section are all based on (2.64). Like in the previous chapter we calculate the contributions from the three different lens populations separately and finally sum them up to a total event rate. From (2.64) follows that the classical microlensing rate depends on the following properties of the lens population: their mass function $\left(dN_0/d\mu\right)$, their spatial distribution $H_l(D_{ol})$, their dispersion velocity v_l and in addition on the motion of the observer and the sources through the transverse velocity of the microlensing tube η.

5.1.1 M31 MACHO halo

The most important lens population we want to explore are the M31 MACHOs. As discussed in section 3.3 we adopt for the mass function of the MACHO population a delta function

$$\left(\frac{dN_0}{d\mu}\right) = \frac{\rho_{0,h}}{M_\odot \mu_0}\ \delta(\mu - \mu_0)\ , \tag{5.1}$$

where we indroduced the MACHO mass μ_0. Now we can perform the integration over μ in (2.64)

$$\int_0^\infty \left(\frac{dN_0}{d\mu}\right) \sqrt{\mu}\, d\mu = \frac{\rho_{0,h}}{M_\odot \sqrt{\mu_0}} \,. \tag{5.2}$$

In a first approximation we neglect the relative motion of the observer and the sources, so we put $\eta = 0$, which yields

$$\int_0^\infty v^2 e^{-v^2-\eta^2}\, I_0\big(2\eta v\big)\, dv = \int_0^\infty v^2 e^{-v^2}\, dv = \frac{\sqrt{\pi}}{4} \,. \tag{5.3}$$

Like in the calculation of the optical depth we take into account that not all the sources are at the same distance. Thus,we integrate also over the distribution of the source stars (here provided by the M31 disc and bulge). For the double integration over the lens and source distributions we introduce the following shorthand notation[1]

$$\begin{aligned} D_{sl} := & \int_0^\infty dD_{os}\rho_s(D_{os}) \int_0^{D_{os}} dD_{ol}\rho_l(D_{ol}) \sqrt{\frac{D_{ol}(D_{os}-D_{ol})}{D_{os}}} \\ & \times \left(\int_0^\infty dD_{os}\rho_s(D_{os})\right)^{-1} . \end{aligned} \tag{5.4}$$

Inserting (5.2) to (5.4) into (2.64) yields the classical event rate for MACHOs in the M31 halo,

$$\Gamma_{b+d,h} = \frac{\sqrt{\pi}\, r_E}{M_\odot} \frac{v_h}{\sqrt{\mu_0}} D_{b+d,h}, \tag{5.5}$$

where $v_h = \sqrt{2}\sigma_h = 235$ km/s.

In a second step we consider the transverse velocity of the microlensing tube by approximating

$$\eta = \left| \left(1 - \frac{D_{ol}}{D_{os}}\right) \frac{\mathbf{v}_{\odot\perp}}{v_c} + \frac{D_{ol}}{D_{os}} \frac{\mathbf{v}_{s\perp}}{v_c} \right| \approx \frac{v_{s\perp}}{v_c}, \tag{5.6}$$

since for MACHOs in the M31 halo

$$\left(1 - \frac{D_{ol}}{D_{os}}\right) = \mathcal{O}\big(10^{-2}\big). \tag{5.7}$$

Considering the motion of the source stars we have to distinguish between disc sources and bulge sources, because the bulge and the disc clearly show different dynamics.

[1] Using subscripts s for the source population and l for the lens population.

Source stars in the bulge

The Maxwellian distribution for the bulge sources is

$$f(\mathbf{v}_s)d^3\mathbf{v_s} = \frac{1}{(\pi v_b^2)^{3/2}}\ e^{-|\mathbf{v_s}|^2/v_b^2} d^3\mathbf{v_s}, \tag{5.8}$$

with the dispersion velocity $v_b = \sqrt{2}\sigma_b = 141$ km/s. Using cylindrical coordinates $d^3\mathbf{v_s} = v_{s\perp}dv_{s\perp}dv_{s||}d\varphi$, where φ is the angle between $v_\perp$ and $v_{s\perp}$, we can integrate over $v_{s||}$ and φ. We obtain the transverse velocity distribution

$$f_\perp(v_{s\perp})dv_{s\perp} = \frac{2}{v_b^2}\ v_{s\perp}e^{-v_{s\perp}^2/v_b^2}\ dv_{s\perp}. \tag{5.9}$$

It is convenient to change the integration variable to $\eta = v_{s\perp}/v_h$, because η is used in (2.64). This yields the following distribution in η

$$f_\perp(\eta)d\eta = 2\ \left(\frac{v_h}{v_b}\right)^2\ \eta \exp\left[-\left(\frac{v_h}{v_b}\right)^2\eta^2\right]\ d\eta \tag{5.10}$$

and therefore,

$$\Gamma_{bh} = \frac{8r_E}{M_\odot}\ \frac{v_h^3}{v_b^2}\ \frac{D_{bh}}{\sqrt{\mu_0}} \int dv\ \int d\eta\ \eta v^2 I_0(2\eta v)\ e^{-v^2-\eta^2\left[1+\left(v_h/v_b\right)^2\right]}. \tag{5.11}$$

The coupled velocity integration over v and η can be done analytically, since

$$\int dv\ \int d\eta\ \eta v^2 I_0(2\eta v)\ e^{-v^2-\eta^2\left(1+a^2\right)} = \frac{\sqrt{\pi}}{8}\ \frac{\sqrt{1+a^2}}{a^3}. \tag{5.12}$$

and we obtain for the classical event rate for M31 MACHOs lensing bulge stars

$$\Gamma_{bh} = \sqrt{1+\left(\frac{v_h}{v_b}\right)^2}\ \frac{\sqrt{\pi}r_E}{M_\odot}\ \frac{v_b}{\sqrt{\mu_0}}\ D_{bh}. \tag{5.13}$$

We performed a numerical test showing that neglecting the source motions for sources in the bulge yields an about 14% too small event rate.

Source stars in the disc

Let us now consider the case of sources in the M31 disc. The disc stars move in circular orbits around the M31 centre with the velocity $\mathbf{v}_c$. The rotation curve of M31 is given by (3.5).
The Maxwellian velocity distribution of the disc stars has to be shifted by the transverse component $\mathbf{v_{c\perp}}$ of the circular velocity

$$g(\mathbf{v_s})d^3\mathbf{v_s} = \frac{1}{(\pi v_d^2)^{3/2}}\ e^{-|\mathbf{v_s}-\mathbf{v_{c\perp}}|^2/v_d^2}\ d^3\mathbf{v_s}, \tag{5.14}$$

where $v_d = \sqrt{2}\sigma_d \approx 42$ km/s. With cylindrical coordinates, we can integrate over the parallel component of $\mathbf{v_s}$ and over the angle between $\mathbf{v_{s\perp}}$ and $v_{c\perp}$ yielding a modified Bessel function of the first kind (cf. (2.59) and (2.60))

$$g_\perp(v_{s\perp})dv_{s\perp} = 2\frac{v_{s\perp}}{v_d^2}\ I_0\left(2\frac{v_{s\perp}v_{c\perp}}{v_d^2}\right)\ e^{-\left(v_{s\perp}^2+v_{c\perp}^2\right)/v_d^2}\ dv_{s\perp}\ . \tag{5.15}$$

Changing to the integration variable $\eta = v_{s\perp}/v_h$, we obtain the new distribution

$$g_\perp(\eta)\ d\eta = 2\left(\frac{v_h}{v_d}\right)^2\ e^{-v_{c\perp}^2/v_d^2}\ I_0\left(2\eta\frac{v_h v_{c\perp}}{v_d^2}\right)\ \eta\ \exp\left[-\left(\frac{v_h}{v_d}\right)^2\eta^2\right]\ d\eta. \tag{5.16}$$

Therefore the classical event rate for disc stars lensed by M31 MACHOs is

$$\begin{aligned}\Gamma_{dh} = \frac{8r_E}{M_\odot}\ \frac{v_h^3}{v_d^2}\ e^{-v_{c\perp}^2/v_d^2}\ \frac{D_{dh}}{\sqrt{\mu_0}}\ \int dv v^2 e^{-v^2} \\ \times \int d\eta\ I_0(2\eta v)\ I_0\left(2\eta\frac{v_h v_{c\perp}}{v_d^2}\right)\ \eta\ e^{-\eta^2\left[1+\left(\frac{v_h}{v_d}\right)^2\right]}.\end{aligned} \tag{5.17}$$

Finally, we have to calculate the transverse component $v_{c\perp}$ of the circular velocity around the M31 centre of a particular disc source. In the intrinsic coordinate system (x, y, z) of M31 the circular velocity $\mathbf{v_c}$ of a source star at (x, y, z) is

$$\mathbf{v_c} = v_{rot}\ \begin{pmatrix} -y/r \\ x/r \\ 0 \end{pmatrix}, \tag{5.18}$$

where $r = \sqrt{x^2+y^2}$. In the coordinate system of the M31 major and minor axis and the line of sight (u, v, w) we have

$$\mathbf{v_c} = \frac{v_{rot}}{r}\ \begin{pmatrix} -v\cos i - w\sin i \\ u\cos i \\ u\sin i \end{pmatrix}, \tag{5.19}$$

but now $r = \sqrt{u^2+(v\cos i + w\sin i)^2}$. We assume that the source stars reside exactly in the symmetry plane ($z = 0$) of M31, which is a reasonable approximation in this calculation. Thus, we have $w = v\tan i$ and the transverse component of $\mathbf{v_{c\perp}}$ becomes

$$v_{c\perp} = v_{M31}\begin{cases} \frac{1}{r_v}\ \sqrt{v^2(\cos i + \sin i\tan i)^2 + u^2\cos^2 i} & r < r_v \\ \frac{1}{r}\ \sqrt{v^2(\cos i + \sin i\tan i)^2 + u^2\cos^2 i} & r \geq r_v \end{cases} \tag{5.20}$$

The integrations over v and η in (5.17) are performed numerically. We found that neglecting the disc source motion, produces a too small event rate (according to Griest 1991). The error lies between 4% along the major axis, where the disc stars approximately move away from us or towards us, and 45% along the minor axis, where the stars move perpendicular to the line of sight.

5.1.2 Galactic MACHO halo

Since the MACHOs in the Galaxy are expected to be the same kind of objects like the MACHOs in M31, we use again a delta function with the lens mass μ_0 to describe their mass function. The calculation is completely analogous to that in the previos section. We just have to replace the dispersion velocity of the M31 halo by the one of the Milky Way halo $v_g = \sqrt{2}\sigma_g \approx 221$ km/s. The source stars reside again in the M31 bulge and the M31 disc. Neglecting the motion of the microlensing tube ($\eta = 0$) we obtain (cf. (5.5))

$$\Gamma_g = \frac{\sqrt{\pi}\, r_E}{M_\odot}\, \frac{v_g}{\sqrt{\mu_0}}\, D_{d+b,g} \tag{5.21}$$

For a lens mass of $\mu_0 = 0.1$ and our standard spherical halo model with a 20% MACHO fraction and a 5.6 kpc core the rate is

$$\Gamma_g = 1.1 \times 10^{-6} (\mathrm{yr} \times \mathrm{star})^{-1}, \tag{5.22}$$

which is in agreement with Ansari et al. (1997).
In the case of Galactic lenses the motion of the source stars can be neglected, since $D_{ol}/D_{os} = \mathcal{O}\big(10^{-2}\big)$. Thus, we have only to consider the motion of the observer, i.e. the rotation of the sun around the Galactic centre and write

$$\eta = \left| \Big(1 - \frac{D_{ol}}{D_{os}}\Big) \frac{\mathbf{v}_{\odot\perp}}{v_g} + \frac{D_{ol}}{D_{os}} \frac{\mathbf{v}_{s\perp}}{v_g} \right| \approx \frac{v_{\odot\perp}}{v_g}. \tag{5.23}$$

$v_{\odot\perp}$ is the transverse component of the circular velocity of the sun and is given by $v_{\odot\perp} = v_\odot \cos\varphi_{M31}$, where $\varphi_{M31} = 121.2°$ is the Galactic longitude of M31 and $v_\odot = 220$ km/s. The velocity integrations become

$$e^{-\eta^2} \int d\eta \int dv\; I_0\big(2\eta v\big) v^2 e^{-v^2} \approx 0.501 \tag{5.24}$$

and we obtain

$$\Gamma_g = 0.501\, \frac{4\, r_E}{M_\odot}\, \frac{v_g}{\sqrt{\mu_0}}\, D_{d+b,g} = 1.2 \times 10^{-6} (\mathrm{yr} \times \mathrm{star})^{-1}. \tag{5.25}$$

5.1.3 M31 self-lensing

The starting point for calculating the classical rate for self-lensing events is again (2.64)

$$d\Gamma_c = 4 r_E v_l \frac{dN_0}{d\mu} H_l(D_{ol}) \sqrt{\frac{\mu D_{ol}(D_{os} - D_{ol})}{D_{os}}}\, v^2 e^{-v^2-\eta^2} I_0\big(2\eta v\big)\, dD_{ol} dv d\mu \tag{5.26}$$

In the case of self-lensing we *have* to take into account the motion of the sources, particularly if the the source and the lens populations are identical.

Since in self-lensing the lenses are provided by ordinary stars we use the stellar mass function given in (3.9) for $\left(dN_0/d\mu\right)$. We can perform the μ integration ($\mu_{up} = 1.5$, $\mu_{min} = 0.08$)

$$\int_{\mu_{min}}^{\mu_{up}} d\mu \left(\frac{dN_0}{d\mu}\right) \sqrt{\mu} \approx 0.84 \frac{\rho_{l,0}}{M_\odot} , \tag{5.27}$$

and (5.26) becomes

$$\Gamma_{sl} = 0.84 \frac{4 r_E v_l}{M_\odot} D_{sl} \int_0^\infty v^2 e^{-v^2-\eta^2} I_0\left(2\eta v\right) dv. \tag{5.28}$$

If we integrate over the whole mass function ($\mu_{up} = \mu_{max} = 10$), we obtain

$$\int_{\mu_{min}}^{\mu_{max}} d\mu \left(\frac{dN_0}{d\mu}\right) \sqrt{\mu} \approx 1.07 \frac{\rho_{l,0}}{M_\odot} . \tag{5.29}$$

Thus, the error is never larger than 20%, if we change μ_{up}. The microlensing tube velocity η is approximated by (5.6)

$$\eta \approx \frac{v_{s\perp}}{v_l}, \tag{5.30}$$

since for self-lensing $D_{ol}/D_{os} \approx 1$.
Like in the calculation of the self-lensing optical depth we divide the self-lensing event rate up in bulge/bulge, disc/bulge, bulge/disc and disc/disc contributions.

Bulge/bulge

If both the source and the lens are located in the M31 bulge, we use (similar to (5.10)) a Maxwellian distribution for the transverse velocities of the bulge sources (putting $v_h \equiv v_b = \sqrt{2}\sigma_b = 141$ km/s in (5.10)). In terms of the integration variable η, we get

$$f_\perp(\eta)\, d\eta = 2\eta e^{-\eta^2}\, d\eta . \tag{5.31}$$

Using (5.12), the η and v integrations are

$$\int dv \int d\eta\, \eta v^2 I_0(2\eta v)\, e^{-v^2-2\eta^2} = \frac{\sqrt{2\pi}}{8} . \tag{5.32}$$

Thus, the classical event rate for bulge/bulge self-lensing becomes

$$\Gamma_{bb} = 0.84 \frac{\sqrt{2\pi} r_E v_b}{M_\odot} D_{bb} . \tag{5.33}$$

Disc/bulge

If a bulge star is lensing a disc source star, we have to use the Maxwellian velocity distribution for disc stars shifted by the transverse component of the circular velocity $\mathbf{v_{c\perp}}$ ($v_h \equiv v_b$ in (5.16))

$$g_\perp(\eta)\ d\eta = 2\Big(\frac{v_b}{v_d}\Big)^2\ e^{-v_{c\perp}^2/v_d^2}\ I_0\Big(2\eta\frac{v_b v_{c\perp}}{v_d^2}\Big)\ \eta\ \exp\Big[-\Big(\frac{v_b}{v_d}\Big)^2\eta^2\Big]\ d\eta. \quad (5.34)$$

The disc/bulge contribution to self-lensing is

$$\begin{aligned}\Gamma_{db} = 0.84\ \frac{8r_E}{M_\odot}\ \frac{v_b^3}{v_d^2}\ e^{-v_{c\perp}^2/v_d^2}\ D_{db}\ \int dv\ v^2 e^{-v^2} \\ \times \int d\eta\ I_0(2\eta v)\ I_0\Big(2\eta\frac{v_b v_{c\perp}}{v_d^2}\Big)\ \eta\ e^{-\eta^2\left[1+\left(\frac{v_b}{v_d}\right)^2\right]},\end{aligned} \quad (5.35)$$

where $v_{c\perp}$ is given by (5.20).

Bulge/disc

Let us now consider lens stars which belong to the M31 disc population and thus we put $v_l \equiv v_d = \sqrt{2}\sigma_d$ in (5.28), with $\sigma_d = 30$ km/s. For bulge sources their velocity distribution is obtained by replacing v_h by v_d in (5.10)

$$f_\perp(\eta)d\eta = 2\ \Big(\frac{v_d}{v_b}\Big)^2\ \eta\exp\Big[-\Big(\frac{v_d}{v_b}\Big)^2\eta^2\Big]\ d\eta. \quad (5.36)$$

Therefore, the classical bulge/disc self-lensing event rate is given by

$$\Gamma_{bd} = 0.84\sqrt{1+\Big(\frac{v_d}{v_b}\Big)^2}\ \frac{\sqrt{\pi}r_E v_b}{M_\odot}\ D_{bd}, \quad (5.37)$$

where we have again used the analytical integration (5.12).

Disc/disc

The case of disc/disc self-lensing is treated analogous to the case of M31 halo lenses lensing disc stars. The Maxwellian velocity distribution of the disc stars has to be shifted by the transverse component of the circular velocity of the disc stars. Thus, we use (cf. (5.16))

$$g_\perp(\eta)\ d\eta = 2\ e^{-v_{c\perp}^2/v_d^2}\ I_0\Big(2\eta\frac{v_{c\perp}}{v_d}\Big)\ \eta\ e^{-\eta^2}\ d\eta. \quad (5.38)$$

This yields the classical event rate for the disc/disc contribution to self-lensing

$$\begin{aligned}\Gamma_{dd} = 0.84\ \frac{8r_E v_d}{M_\odot}\ e^{-v_{c\perp}^2/v_d^2}\ D_{dd} \\ \times \int dv\ v^2 e^{-v^2}\ \int d\eta\ I_0(2\eta v)\ I_0\Big(2\eta\frac{v_{c\perp}}{v_d}\Big)\ \eta\ e^{-2\eta^2},\end{aligned} \quad (5.39)$$

where $v_{c\perp}$ is taken from (5.20).
The velocity integrations again can be done numerically.

Total self-lensing event rate

The total classical self-lensing event rate is the weighted sum of the four contributions

$$\Gamma_{s-l} = w_b\big(\Gamma_{bb} + \Gamma_{bd}\big) + w_d\big(\Gamma_{dd} + \Gamma_{db}\big), \tag{5.40}$$

with the relative weights already calculated in (4.11).

5.2 Pixel lensing event rates

In this section we use the classical event rates of the previous section to calculate the event rates and the expected number of events for a pixel lensing experiment. We use (2.69) with the peak threshold (2.32) of Baltz & Silk (2000) and the characteristics of the INT observing site at La Palma and of the Wide-field Camera (WFC) (see table 2.2). For the expected number of events we assume that the two INT fields of the POINT-AGAPE collaboration are monitored for two M31 observing seasons ($t_{obs} \approx 8$ months).
The luminosity function and the surface brightness profile of M31 are given in (3.4) and Fig. 3.1, respectively.

5.2.1 M31 MACHO halo

The calculation of the pixel lensing event rate for MACHOs in the M31 halo is now straightforward. For simplicity, we are neglecting the motion of the microlensing tube, because in this case we do not have to distinguish between bulge and disc sources. In Fig. 5.1 we plot the event rate contours for our standard spherical M31 halo with a 20% MACHO fraction, a 2 kpc core and a MACHO mass of $\mu = 0.1$. The near-far asymmetry is still present in the pixel lensing event rate. However, we tested that a flattened halo (e.g. $q = 0.3$) would nearly hide this effect. We also observed that varying the core radius r_c of the halo does only change the shape of the contours near the centre of M31, which will make the measurement of the core radius from pixel lensing to be difficult, because within the bulge the M31 halo lensing will be contaminated by self-lensing. The rate map looks qualitatively very similar to the one presented in Fig. 1 of Baltz, Gyuk & Crotts (2002). Comparing the two maps quantitatively, one should be careful, since in the mentioned paper, the used MACHO mass was 0.422 $M_\odot$.[2] If we do our calculations again with the parameters used in Baltz, Gyuk & Crotts (2002),

[2]They also used a slightly higher dispersion velocity of $v_h = 240$ km/s, a different M31 distance of 795 kpc and a larger density normalization of $\rho_{h,0} = 2.7 \times 10^8$ $M_\odot kpc^{-3}$, but since the rate depends on these quantities linearly, these changes have no significant influence.

Characteristic	MDM 2.4m telescope
Sky background	$\mu_{sky} = 21.0$ mag arcsec^{-2}
Zero point	$m_0 = 25.2$ mag
Exposure time	$t_{int} = 10800\ s$
Worst seeing	1.0"

Table 5.1: Adopted characteristics of the MDM 2.4m telescope used by the MEGA collaboration. For this telescope the magnitudes are given for the R-band

$\mu_0\ [(M/M_\odot)]$	Northern field	Southern field	Total N_{ev}
0.01	109	124	233
0.1	34	39	73
1	11	12	23
10	3	4	7

Table 5.2: Expected number of events from lenses in the M31 halo for different masses MACHO masses μ_0. We assumed that the two INT fields were observed for two seasons lasting 8 months and we used our standard halo model with $r_c = 2$ kpc, $q_h = 1$ and a MACHO fraction of 20%.

the resulting event rate is roughly a factor six smaller. We suppose, that this is due to a difference in the assumed parameters for the telescope-CCD system. Indeed, the rates presented in Baltz, Gyuk & Crotts were adapted to the MDM 2.4m telescope of the MEGA collaboration whose parameters are listed in Table 5.1. The largest difference is the integration time. Using the high magnification approximation (2.70) for the event rate, we see, that this already increases the rate at a factor about 4. We conclude from these observations that the number of effective source stars and thus the pixel lensing event rate is strongly dependent on the parameters of the telescope-CCD system. All these parameters influence the threshold minimum impact parameter β_T for the detectability of a pixel lensing event.

The number of expected events for a two season observation of the INT fields is 73 (34 for the northern and 39 for the southern field) for lens masses of $\mu_0 = 0.1$. It is calculated by integrating the event rate over the angular surface of the observed fields.[3] The number of expected events is shown in 5.2.

5.2.2 Galactic MACHO halo

Since the classical event rate for lenses in the Milky Way is constant across the surface of M31, the pixel lensing event rate for the Galactic halo MA-

[3]In practice, we replaced the integration by a sum of the event rates along discrete line of sights.

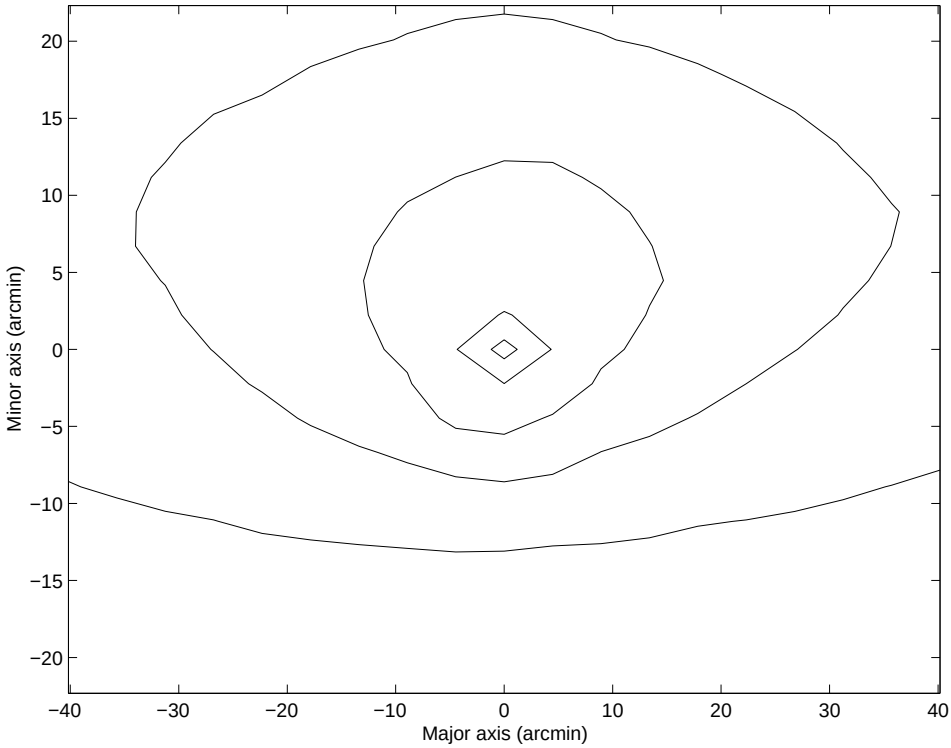

Figure 5.1: Pixel lensing event rates for M31 MACHOs. The rates are given in units of events per year per square arcminute. Contours are from the centre to the outside 2, 0.3, 0.1, 0.03, 0.01 $(\mathrm{yr}\times\mathrm{arcmin}^2)^{-1}$. The M31 halo is taken with $q_h = 1$, $r_c = 2$ kpc and $f_h = 0.2$.

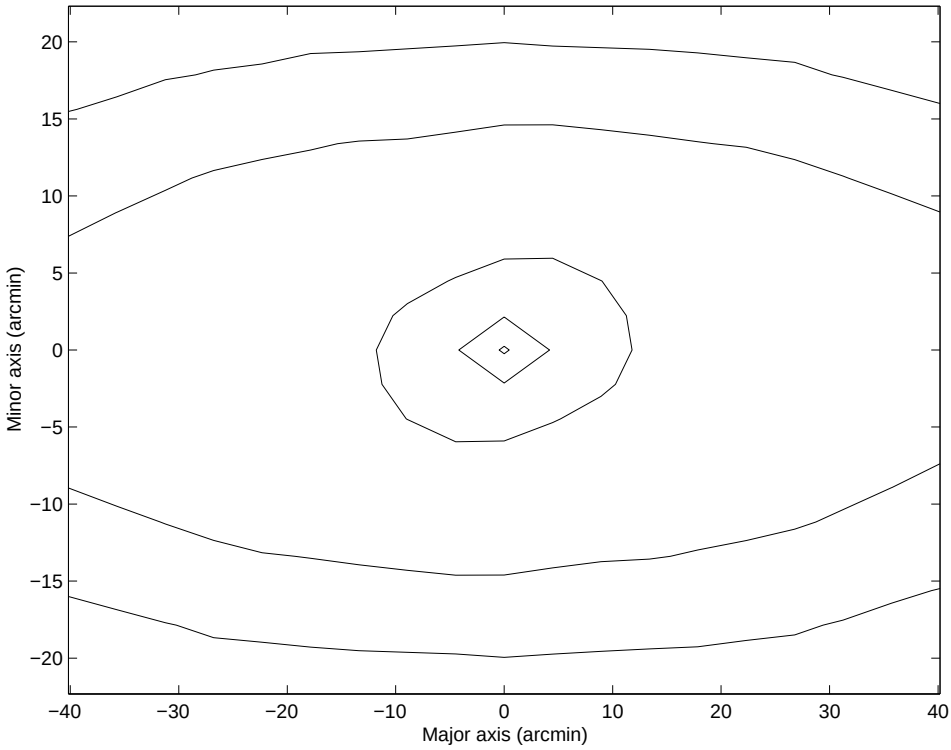

Figure 5.2: Pixel lensing event rates for Milky Way MACHOs. The rates are given in units of events per year per square arcminute. Contours are from the centre to the outside 0.6, 0.1, 0.03, 0.01, 0.005 $(\mathrm{yr}\times\mathrm{arcmin}^2)^{-1}$. The halo is taken with $q_g = 1$, $r_c = 5.6$ kpc and a MACHO fraction of 20%. The mass of the MACHOs is $\mu_0 = 0.1$. Since the optical depth to Galactic halo lensing is quite uniform across M31, the rate only tracks the surface brightness, as expected for (2.71).

CHOs is proportional to the effective number of source stars. In Fig. 5.2 we illustrate a pixel lensing event rate map for the Galactic dark halo, adopting a spherical halo with a 5.6 kpc core and a MACHO fraction of 20%. The lenses are again assumed to have the mass $\mu_0 = 0.1$.
Looking at the approximation (2.71), we see that the rate should be roughly proportional to the square root of the surface brightness of M31, which is in a quite good agreement with Fig. 5.2. We also tested the flattened halo models and observed that varying the flatness q_g only changes the normalization of the contours, but not their shape.
Comparing our results with Fig. 3 of Baltz, Gyuk & Crotts (2002), our event rate is again roughly a factor six or seven smaller for the same reasons as discussed above.

In table 5.3 we list the number of expected events for different MACHO

μ_0 $[(M/M_\odot)]$	Northern field	Southern field	Total N_{ev}
0.01	36	26	62
0.1	11	8	19
1	4	3	6
10	1	1	2

Table 5.3: Expected number of events from lenses in the Milky Way halo for different masses MACHO masses μ_0.

masses. The number of events for M31 halo lenses is almost a factor four bigger than for Galactic halo lenses. This has two reasons: First, the Milky Way halo that we used in the calculations is smaller and less massive than the M31 halo. This is reasonable, since the luminous part of M31 is bigger and more massive than the Milky Way as well. Secondly, the line of sight towards M31 passes only the outer regions of the Milky Way halo, but because of the inclination of the M31 disc the inner denser part of the M31 halo (see also Jetzer 1994 or Baillon et al. 1992).

5.2.3 Self-lensing

The pixel lensing rate for self-lensing is obtained by summing up the four classical contributions (bulge/bulge, disc/bulge, bulge/disc, disc/disc) calculated in section 5.1.3 using the weights (4.11). We show the event rate map for self-lensing in Fig. 5.3. It is clearly seen that self-lensing is largely limited to the central 10 arcminutes, where the bulge is the dominant stellar population. Once again our calculated rates are smaller than the ones shown in Fig. 1 of Baltz, Gyuk & Crotts (2002). The decrease of the event rate along the major axis in the outer regions is due to the circular motion of the disc stars around the M31 centre, which we took into account. In the outer part of M31, only disc/disc self-lensing is important. Along the major axis the source stars are nearly moving away from us, because of the large inclination of the disc, which lowers the event rate.

The number of self-lensing events, divided up to the four contributions, is shown in Table 5.4. The total number of self-lensing events is quite high and comparable to the number of events due to M31 halo lenses. The bulge/bulge contribution clearly dominates self-lensing, since the INT-fields cover a large part of the bulge. But disc/disc self-lensing is important as well, so that it can serve as an alternative to a halo event even in the outer regions of M31. The bulge/disc and disc/bulge contributions are smaller, but show an interesting asymmetry in the two observed fields. We suppose, that this comes from the fact, that the southern field lies at the far side of the disc, so that the bulge is in front of the disc, while the northern field is almost centered on the major axis.

Because self-lensing should occur as well, if the M31 halo does not consist

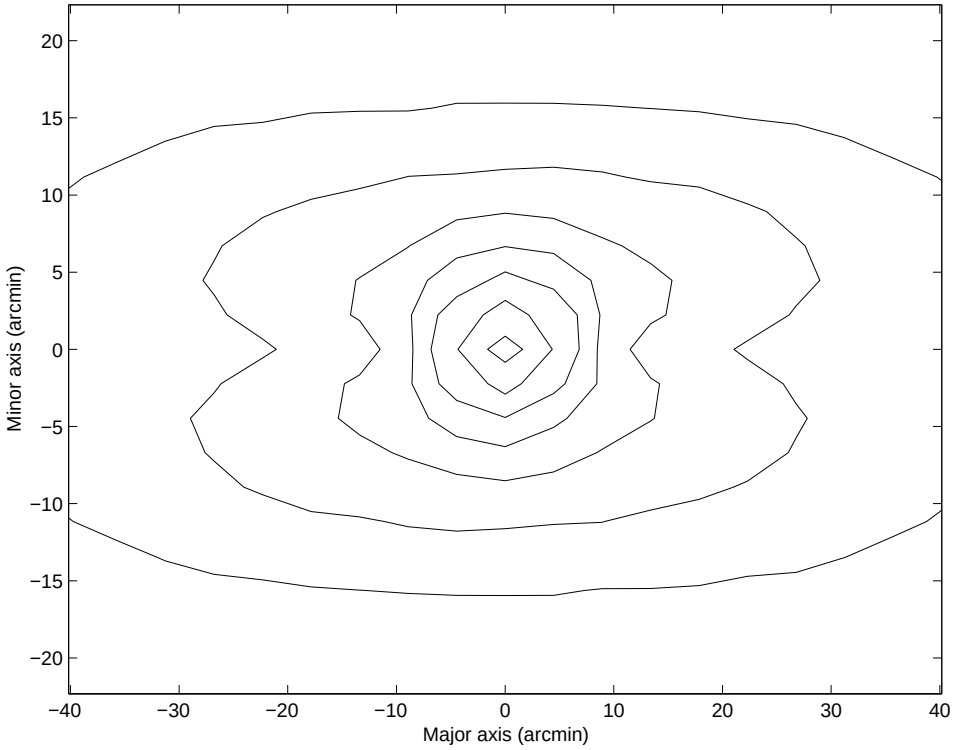

Figure 5.3: Pixel lensing event rates for self-lensing of M31 stars. The rates are given in units of events per year per square arcminute. Contours are from the centre to the outside 10, 1, 0.3, 0.1, 0.03, 0.01, 0.003 $(\mathrm{yr}\times\mathrm{arcmin}^2)^{-1}$.

Source/lens configuration	Northern field	Southern field	Total N_{ev}
bulge/bulge	15	14	29
disc/bulge	4	7	11
bulge/disc	4	2	6
disc/disc	8	5	13
Total self-lensing	31	28	59

Table 5.4: Expected number of events for self-lensing. The number of events for each self-lensing contribution have already been multiplied with the relative weights, so that the total is obtained by just taking the sum.

of MACHOs, the self-lensing events should be found in any case. Since the POINT-AGAPE collaboration found only four events in the considered time span in the observed fields, this result indicates, that our calculation is still too optimistic. There are two quite obvious reasons for this:

- Through our whole calculation we assumed an efficiency function that is identically one. In reality, this is certainly wrong, because for instance certain time durations are largely contaminated by variable stars (Cepheids, Mirae, etc.). Therefore, microlensing candidates with those time durations are often cut off, together with the variable stars. Furthermore, the efficiency function is also a function of position, because in some regions of M31 the background light could be very noisy, or there are disturbing foreground stars or interstellar dust hiding some part of the source stars.

- In our definition of the threshold minimum impact paramter β_T we demanded that only one point at the peak of the lightcurve shall have a given S/N. This is not enough, because one has to see a larger part of the lightcurve to fit it to the Pacyński lightcurve and to measure the time duration of the event. The peak threshold β_T can be improved by either demanding a higher S/N or by requiring that a certain number of the highest points on the lightcurve have a given S/N (see Baltz & Silk 2000). It is also possible to define another criterion for the detectability of pixel lensing events (e.g. Gould 1995, Gould 1996).

5.2.4 Total pixel lensing event rate

To complete this chapter, we add the self-lensing event rate and the halo event rates from the Milky Way and M31. The map for the total pixel lensing event rate is shown in Fig. 5.4. At the centre, the near-far asymmetry due to the inclination of the M31 disc is hidden by self-lensing. In the outer regions, the event rate is dominated by lenses in the M31 halo, and the asymmetry can be seen. The expected number of events are summarized in Table 5.5.

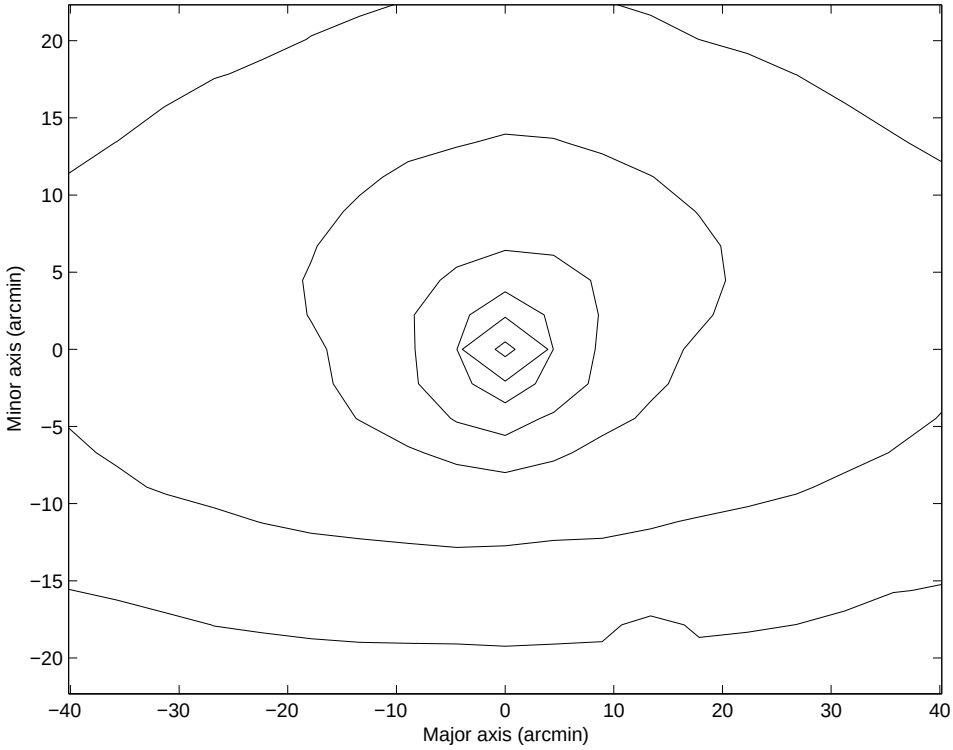

Figure 5.4: Total pixel lensing event rate towards M31. The rates are given in units of events per year per square arcminute. Contours are from the centre to the outside 15, 3, 1, 0.3, 0.1, 0.03, 0.01 $(\mathrm{yr}\times\mathrm{arcmin}^2)^{-1}$.

Contribution	Northern field	Southern field	Total N_{ev}	Total N_{ev}
M31 halo	34	39	73	14
Galactic halo	11	8	19	4
Self-lensing	31	28	59	12
Total N_{ev}	76	75	151	30

Table 5.5: Total expected number of pixel lensing events for a two season survey of the INT fields. The MACHOs in the haloes are assumed to have the mass $\mu_0 = 0.1$. The third column was calculated with our standard threshold S/N $Q_0 = 7$. In the last column, we calculated N_{ev} for a more pessimistic β_T with $Q_0 = 42$.

We also increased the required S/N for a detected event Q_0 from our usual value 7 to 42, a level also used by Baltz & Silk (2000). Looking at (2.70), it is clear that the number of events will depend nearly linearly on Q_0. The last column of Table 5.5 proofs this behavior.

Chapter 6

Comparison with Data

In this chapter we want to compare our theoretical results with the first four reported events of the POINT-AGAPE collaboration. These four events are discussed in Paulin-Henriksson et al. (2002) and we summarize their main characteristics in Table 6.1. Fortunately, the Einstein time of three out of the four events could be determined quite exactly.
In the case of PA-99-N1 the source star has been identified (Aurière et al. 2001) by the Hubble Space Telescope (HST). The PA-99-N1 position lies within a series of five HST WFPC2 archival images.
Since the microlensing event was very red $V - R \approx 1.2$, the source must lie either high up on the giant branch where essentially all stars are resolved by HST, or must be on the main-sequence and so magnified by $A_{max} \approx 10^4$, which is extremely unlikely. Indeed, there is a resolved star with $V = 24.51 \pm 0.12$, $M_V = 0.1$ and $(V - I) = 2.1 \pm 0.16$ at the position of the event, which has a colour compatible with that of the event. The star is an M0-M1 red giant. The probability to find such a star at this position is less than 3% and it has therefore been concluded that the resolved HST object is almost certainly the source star of the event. With these informations in hand, we can determine all the classical microlensing parameters of PA-99-N1. We obtain $\beta \approx 0.06$, $A_{max} \approx 18$ and $t_E = 9.74 \pm 0.7$ days. At the position of PA-99-N1 the M31 halo optical depth ($\tau_h = 3.9 \times 10^{-7}$) and the bulge/bulge contribution ($\tau_{bb} = 3.2 \times 10^{-7}$) are of the same order.
The PA-00-S4 event is of particular interest. On the first sight, it seems to be an excellent candidate for a halo MACHO event, because it lies well outside the projected area of the M31 bulge and it lies on the far side of the M31 disc. The source star is an early A star on the main sequence, which confirms the disc location of the source. Thus, an alternative possibility would be a disc/disc event. However, the event is also only 2'54" from the centre of M32. M32 is a satellite dwarf galaxy of M31, that lies probably in front of M31 (Ford, Jacoby, & Jenner 1978). This suggests, that PA-00-S4 might be an M31/M32 intergalactic event (i.e. the lens being a star in M32). The optical

event	α	δ	ΔR_{max}	t_{fwhm}	t_E
PA-99-N1	$00^h42^m51^s$	$41°23'53''$	20.8 ± 0.13	1.8 ± 0.1	9.74 ± 0.7
PA-99-N2	$00^h44^m20^s$	$41°28'45''$	19.0 ± 0.20	22.0 ± 0.1	91.9 ± 4
PA-00-S3	$00^h42^m30^s$	$41°13'04''$	18.8 ± 0.20	2.2 ± 0.1	12.6 ± 4
PA-00-S4	$00^h42^m29^s$	$40°53'47''$	20.7 ± 0.20	2.1 ± 0.1	128.6^{+143}_{-72}

Table 6.1: Main characteristics of the four microlensing candidates. t_{fwhm} is the full-width at half maximum timescale and t_E the Einstein timescale. Both timescales are given in days. ΔR: magnitude (Johnson/Cousins) of the maximum source flux variation. The source star of PA-99-N1 has been identified on HST archival images, yielding a strong constraint on t_E. For PA-99-N2 and PA-00-S3, the degeneracy between t_E and the source flux could be broken quite efficiently because of good sampling and S/N.

depth due to M31 disc/M32 microlensing is $\tau \approx 1.4 \times 10^{-6}$ (Henriksson et al. 2002) for a distance of 20 kpc between M31 and M32 and a stellar mass-to-light ratio $M/L = 3$ $M_\odot/L_\odot$ for M32. For a MACHO fraction of 20% in the M31 halo we calculated at this position an optical depth of 8×10^{-7}. For Milky Way MACHOs it is only 1.7×10^{-7} and for disc/disc events 1.6×10^{-7}. Unfortunately, PA-00-S4 was also a large magnification event ($A_{max} = \mathcal{O}(10^2)$) and therefore suffers from the degeneracy of the source flux F and the Einstein time t_E, which prevents an accurate determination of either parameter separately.

PA-00-S3 is located only 4' from the centre of M31 and therefore almost certainly a bulge/bulge event. The optical depth for bulge/bulge self-lensing at the position of the event is $\tau_{bb} = 1.2 \times 10^{-6}$, while the M31 halo optical depth is only $\tau_h = 4.7 \times 10^{-7}$.

The most probable candidate for a M31 halo lens is PA-99-N2, since it lies far out (22') from the centre of M31, where bulge/bulge self-lensing is negligible. The M31 halo optical depth is large ($\tau_h = 7.2 \times 10^{-7}$) and the only self-lensing alternative is a disc/disc event. The disc/disc contribution at this position is $\tau_{dd} = 1.5 \times 10^{-7}$.

6.1 Using the Einstein timescale

6.1.1 Optical depth

We use (2.43) and the Einstein times of the four POINT-AGAPE events listed in Table 6.1 to estimate the measured optical depth. We assume a constant efficiency for all events of $\epsilon \equiv 0.2$. We assume further, that both POINT-AGAPE fields were observed for two M31 observing seasons of 4 months ($t_{obs} = 8$ months). Since these events were detected in a pixel lensing experiment, it is a priori not clear, what the meaning of the number of observed stars N_* shall be. The total number of M31 stars within the two

POINT-AGAPE fields can be calculated using the surface brightness profile of M31 and the luminosity function:

$$N_{tot} = \int_{\text{fields}} 10^{-0.4\mu_{M31}} \frac{\int dM\ \Phi(M)}{\int dM'\ 10^{-0.4m(M')}\Phi(M')}\ d\Omega_{obs}\ , \tag{6.1}$$

where Ω_{obs} is the angular surface of the observed fields. N_{tot} is of order $\mathcal{O}(10^{10})$ and is far too large, since not every star in the fields can serve for a detectable pixel lensing event. Therefore, we define an effective number of stars by

$$N_{eff} := \int_{\text{fields}} 10^{-0.4\mu_{M31}} \frac{\int dM\ \Phi(M)\beta_T(M)}{\int dM'\ 10^{-0.4m(M')}\Phi(M')} d\Omega_{obs} \approx 2 \times 10^7. \tag{6.2}$$

Note, that N_{eff} is nothing else than the ratio of the expected number of pixel lensing events occuring in the observed fields and the expected number of classical microlensing events per observed star. Thus, we estimate the optical depth by

$$< \tau_c >= \frac{\pi}{2N_{eff}t_{obs}\epsilon} \sum_{\text{events}} t_E. \tag{6.3}$$

Using all of the four POINT-AGAPE events, we obtain

$$< \tau_c >= 3.3^{+1}_{-1.1} \times 10^{-7}. \tag{6.4}$$

Since the error in the Einstein time of the event PA-00-S4 is so large, we also estimate the optical depth without it, which yields

$$< \tau_c >= 1.5^{+0.2}_{-0.1} \times 10^{-7}. \tag{6.5}$$

6.1.2 Dark mass moments

In this subsection we calculate the dark mass moments for the four POINT-AGAPE events using the measured Einstein times. We distinguish the cases of M31 halo events, Galactic halo events and self-lensing events. We use (2.76) and (2.84) - (2.88) to find the desired mass moments $< \mu^0 >$ and $< \mu^1 >$. For the sampling efficiency we again take $\epsilon(t_{fwhm}) \equiv 0.2$, which gives $\epsilon_n(\mu) \equiv 0.2$ for all n. Like in the previous section we replace the number of observed stars by N_{eff} and obtain from (2.84)[1]

$$\begin{aligned} < t_c^n > = \frac{4r_E v_l t_{obs}\epsilon}{d^{n/2}}\ V(2-n)\ < \mu^m > \int_{\text{fields}} d\Omega_{obs} \Bigg[\widehat{D}_{sl}(m) \\ \times 10^{-0.4\mu_{M31}}\ \frac{\int dM\ \Phi(M)\beta_T(M)}{\int dM'\ 10^{-0.4m(M')}\Phi(M')} \Bigg]. \end{aligned} \tag{6.6}$$

[1] Absolutely the same result is obtained by replacing dN_c by dN_p in (2.82).

Lenses in the M31 halo

The calculation of the dark mass moments is now straightforward, we just solve (6.6) for $< \mu^m >$ and replace $\widehat{D}_{sl}$ by $\widehat{D}_{b+d,h}$. For simplicity we once more neglect the motion of the microlensing tube, so that we do not have to distinguish between sources in the bulge and in the disc. The velocity integrals then simplify to

$$V(2-n) = \int dv\ v^{2-n} e^{-v^2}. \tag{6.7}$$

Taking into account all four events we obtain a mean MACHO mass of

$$< M_{\rm MACHO} >= 0.25^{+0.2}_{-0.1}\ {\rm M}_\odot\ . \tag{6.8}$$

The fraction of MACHOs in the Galactic halo turns out to be

$$f_h = 5.6^{+4}_{-3}\ \%. \tag{6.9}$$

Again, we leave away the event PA-00-S4, because of the inaccurate Einstein time and get

$$< M_{\rm MACHO} > = 0.12^{+0.05}_{-0.01}\ {\rm M}_\odot \tag{6.10}$$

$$f_h = 2.6^{+0.5}_{-0.4}\ \%. \tag{6.11}$$

Lenses in the Galactic halo

Since the Milky Way halo is expected to produce a constant background of microlensing events, every event can in principle be due to MACHOs in the Galactic halo. We have seen that the optical depth of the M31 halo is comparable to the optical depth of the Milky Way halo at certain positions in M31. The calculation of the dark mass moments is the same as before. We have just to replace $\widehat{D}_{sl}$ by $\widehat{D}_{b+d,g}$ in (6.6). In the case of Milky Way lenses we take into account the motion of the sun around the Galactic centre like in the previous chapter. Thus, we put

$$\eta = \frac{v_\odot \cos\varphi_{M31}}{v_g} \tag{6.12}$$

into the velocity moments (2.85). Assuming that all events are Milky Way halo lenses we obtain a MACHO mass of

$$< M_{\rm MACHO} >= 0.2^{+0.2}_{-0.1}\ {\rm M}_\odot\ . \tag{6.13}$$

The MACHO fraction of the Galactic halo is given by

$$f_g = \frac{< \mu^1 >}{\rho_{g,0}} = \frac{< \mu^1 > r_c^2}{\rho_{g,\odot}(r_c^2 + r_\odot^2)}\ . \tag{6.14}$$

We obtain a MACHO fraction of

$$f_g = 12^{+5}_{-3}\ \%. \tag{6.15}$$

Neglecting PA-00-S4 the result is

$$< M_{\rm MACHO} > = 0.1^{+0.03}_{-0.03}\ {\rm M}_\odot \tag{6.16}$$

$$f_g = 5 \pm 2\%. \tag{6.17}$$

Self-lensing

The events PA-99-N1 and PA-00-S3 are probably bulge/bulge events. We therefore want to calculate their mass moments under this assumption. For bulge/bulge events we have to consider the motion of the source stars and (6.6) becomes

$$\begin{aligned} < t_c^n > = \frac{4 r_E v_l t_{obs}}{d^{n/2}}\ \tilde{V}(2-n)\ \ < \mu^m > \ \int_{\rm fields} d\Omega_{obs} \Bigg[\widehat{D}_{bb}(m) \\ \times\, 10^{-0.4 \mu_{M31}}\ \frac{\int dM\ \Phi(M) \beta_T(M)}{\int dM'\ 10^{-0.4 m(M')} \Phi(M')} \Bigg]\ , \end{aligned} \tag{6.18}$$

where now the velocity moments have to be modified because of the distribution (5.31), giving

$$\tilde{V}(2-n) = 2 \int d\eta \int dv\ \Big(\eta v^{2-n} I_0\big(2\eta v\big) e^{-v^2 - 2\eta^2} \Big)\ . \tag{6.19}$$

This integration can be done analytically. We obtain for the mean mass of stars of the two events $< M_* >= 0.26^{+0.2}_{-0.1}\ {\rm M}_\odot$. The POINT-AGAPE collaboration obtained $M_* = 0.54^{+0.1}_{-0.2}\ {\rm M}_\odot$ for PA-99-N1 and $M_* = 0.2\ {\rm M}_\odot$ for PA-00-S3 (Paulin-Henriksson et al. 2002) using different methods for the determination of the mass.

For the other two events PA-99-N2 and PA-00-S4 we investigate the possibility of disc/disc self-lensing. The calculation is just the same as for the bulge/bulge self-lensing except of the velocity moments. Thus, we have

$$\begin{aligned} < t_c^n > = \frac{4 r_E v_l t_{obs}}{d^{n/2}}\ \ < \mu^m > \ \int_{\rm fields} d\Omega_{obs} \Bigg[\widehat{V}(2-n)\ \widehat{D}_{dd}(m) \\ \times\, 10^{-0.4 \mu_{M31}}\ \frac{\int dM\ \Phi(M) \beta_T(M)}{\int dM'\ 10^{-0.4 m(M')} \Phi(M')} \Bigg]\ , \end{aligned} \tag{6.20}$$

but now (cf. (5.38))

$$\begin{aligned} \widehat{V}(2-n) &= 2 e^{-v_{c\perp}^2 / v_d^2} \int d\eta\ \eta I_0\Big(2\eta \frac{v_{c\perp}}{v_d}\Big) e^{-2\eta^2} \\ &\quad \times \int dv\ v^{2-n} I_0\big(2\eta v\big) e^{-v^2} \\ &= \begin{cases} \frac{1}{2} & n = 1 \\ 1 + \frac{1}{2} \left(\frac{v_{c\perp}}{v_d} \right)^2 & n = -1\ , \end{cases} \end{aligned} \tag{6.21}$$

where $v_{c\perp}$ is the transverse component of the circular velocity of the disc stars. Since the velocity moments $\widehat{V}$ depend on the line of sight, we have to take them into the integration over the observed fields. However, we neglect the rotation of the disc in our calculation for simplicity ($v_{c\perp} = 0$).[2] We obtain for the two considered events a mass of $< M_* >= 0.7^{+0.9}_{-0.4}$ $M_\odot$.

6.2 Using the fwhm-timescale

6.2.1 Optical depth

Assuming that only the t_{fwhm}-timescale is measured, we estimate the optical depth using the optical depth estimator (2.51). Since the SBF flux has not been measured, we calculate the effective flux F_{eff} directly using the 'known' luminosity function (3.10). First we have to express F_{eff} in terms of the luminosity function $\Phi(M)$ rather than $\bar{\Phi}(F)$. We obtain

$$\begin{aligned} IF_{eff} &= \int \bar{\Phi}(F)\ F \int_0^{\beta_T} w(\beta) f(\beta^2) d\beta\ dF \\ &= \frac{F_0}{\int dM'\ \Phi(M')\ 10^{-0.4m(M')}} \int 10^{-0.4\mu_{gal}} \\ &\quad \times \int dM\ \Phi(M)\ 10^{-0.4m(M)} \int_0^{\beta_T(M)} d\beta\ f(\beta^2) w(\beta)\ d\Omega_{obs} \\ &\approx 1.082 \times 10^{-2}\ F_0 \end{aligned} \tag{6.22}$$

for the peak threshold. Furthermore, we write[3]

$$\sum_{\text{events}} t_{fwhm} \Delta F_{max} = F_0 \sum_{\text{events}} t_{fwhm} 10^{-0.4\Delta R_{max}}. \tag{6.23}$$

Thus, the constant F_0 cancels out and we obtain for the optical depth using all four POINT-AGAPE events

$$< \tau_p >= 3.9^{+0.7}_{-0.9} \times 10^{-7}, \tag{6.24}$$

and for the three events without PA-00-S4

$$< \tau_p >= 3.8^{+0.8}_{-0.7} \times 10^{-7}. \tag{6.25}$$

The estimated optical depths with the t_{fwhm} timescale are thus in a quite good agreement with the results obtained using t_E.

[2] If we took into account the circular motion of the disc stars, we would obtain a larger mass.

[3] Note, that we make here actually a mistake, since our adopted luminosity function (3.10) is for the V-band and the excess fluxes were measured in the R-band.

6.2.2 Dark mass moments

We now want to test the method developed in 2.5.2. With (2.98) we can calculate the mass moments $< \mu^0 >$ and $< \mu^1 >$. If we take again a constant efficiency of $\epsilon \equiv 0.2$ we obtain

$$\begin{aligned} < t_p^n >_F = & \frac{4 r_E v_l t_{obs} \epsilon}{d^{n/2}} \; V(2-n) \; < \mu^m > \\ & \times \int d\Omega_{obs} \left\{ 10^{-0.4 \mu_{gal}} \; \widehat{D}_{sl}(m) \; L(n) \right\} , \end{aligned} \tag{6.26}$$

where

$$\begin{aligned} L(n) := & \int dM \left\{ 10^{-0.4 m(M)} \Phi(M) \int_{\beta_{min}}^{\beta_T(M)} d\beta \; f(\beta^2) \; \left[w(\beta) \right]^n \right\} \\ & \times \left(\int dM' \; 10^{-0.4 m(M')} \Phi(M') \right)^{-1} . \end{aligned} \tag{6.27}$$

As we have already pointed out in 2.5.2 the L-Moments are very sensitive to the integration limits $\beta_T(M)$ and β_{min}, so that the results we calculate below, have to be considered as a test to investigate the validity of our method. The mean mass density $< \mu^1 >$ is only sensitive of the upper limit β_T, while the mean number density $< \mu^0 >$ depends largely on β_{min}.

Lenses in the M31 halo

We approximate β_{min} in $L(n)$ by assuming, that the source stars all have the same radius $R_* = 20$ $R_\odot$. This value is taken from Table 2.1 knowing that possible source stars peak at $M_V = 1$ (cf. Fig. 2.3) and assuming that most of the source stars are red giants $V - I \approx 1.5$.
For the Einstein radius, we use the estimation in (2.9) and obtain $R_E = 859$ $R_\odot$ for a lens mass of 0.1 $M_\odot$. From (2.21) we then get $\beta_{min} \approx 0.012$. The upper limit β_T is taken from (2.32) with $Q_0 = 7$.
We solve (6.26) for $< \mu^m >$ by replacing $\widehat{D}_{sl}$ by $\widehat{D}_{d+b,h}$. We neglect again the motion of the microlensing tube η in the velocity moments $V(2-n)$. If we assume, that all four detected events of the POINT-AGAPE collaboration are caused by MACHOs in the M31 halo, we obtain the following result

$$< M_{MACHO} > = 0.28^{+0.2}_{-0.1} \mathrm{M}_\odot, \tag{6.28}$$

$$f_h = 35^{+6}_{-8} \; \%. \tag{6.29}$$

The three events without PA-00-S4 lead to

$$< M_{MACHO} > = 0.3^{+0.2}_{-0.1} \; \mathrm{M}_\odot, \tag{6.30}$$

$$f_h = 34^{+7}_{-6} \; \%. \tag{6.31}$$

Lenses in the Galactic halo

For the Galactic halo lenses, we use the same Einstein radius to calculate β_{min}, because the geometrical situation is symmetrical to the situation for M31 halo lenses. Thus, we take again $\beta_{min} = 0.012$. The velocity moments are calculated using (6.12). The mean MACHO mass and the MACHO fraction turn out to be

$$< M_{MACHO} > = 0.2 \pm 0.1 \ \mathrm{M}_\odot, \tag{6.32}$$

$$f_g = 70 \pm 15 \ \%. \tag{6.33}$$

Without PA-00-S4 we get

$$< M_{MACHO} > = 0.23 \pm 0.1 \ \mathrm{M}_\odot, \tag{6.34}$$

$$f_g = 69^{+15}_{-12} \ \%. \tag{6.35}$$

Self-lensing

Finally, we want to investigate the possibility, that PA-99-N1 and PA-00-S3 are bulge/bulge self-lensing events and PA-99-N2 and PA-00-S4 are disc/disc self-lensing events. We again use (2.21) to estimate β_{min}. For self-lensing D_{ls} is typically smaller than for lensing of the haloes, which decreases the Einstein radius. On the other hand, the lens masses in self-lensing are larger, which causes an increment of R_E. We use a lens mass of 0.5 $\mathrm{M}_\odot$ and $D_{ls} = 5$ kpc and $D_{ls} = 10$ kpc for bulge/bulge and disc/disc self-lensing, respectively. We obtain

$$R_E \approx 613 \sqrt{\left(\frac{M}{M_\odot}\right) \frac{D_{ol}(D_{os} - D_{ol})}{D_{os}[\mathrm{kpc}]}} \ R_\odot \approx \begin{cases} 967 \ R_\odot & \text{bulge/bulge} \\ 1362 \ R_\odot & \text{disc/disc} \ . \end{cases} \tag{6.36}$$

This results in

$$\beta_{min} = \begin{cases} 0.0103 & \text{bulge/bulge} \\ 0.0073 & \text{disc/disc} \ . \end{cases} \tag{6.37}$$

In the case of self-lensing the velocity moments have again to be modified, because we have to take into account the motion of the sources.

$$\begin{aligned} < t_p^n >_F = & \frac{4 r_E v_l t_{obs} \epsilon}{(d)^{n/2}} \ \tilde{V}(2-n) \ < \mu^m > \\ & \times \int d\Omega_{obs} \left\{ 10^{-0.4 \mu_{gal}} \ \widehat{D}_{sl}(m) \ L(n) \right\} , \end{aligned} \tag{6.38}$$

where $\tilde{V}$ is given by (6.19). We use $\tilde{V}$ for bulge/bulge and for disc/disc self-lensing, although for disc/disc self-lensing $\tilde{V}$ actually has to be replaced by $\widehat{V}$ from (6.21). However, we neglect again the circular velocity of the disc stars for simplicity, i.e. we put $v_{c\perp} = 0$ in (6.21).

For PA-99-N1 and PA-00-S3 considered as bulge/bulge events, we get a mass of $< M_* >= 0.48^{+0.3}_{-0.2}$ $M_\odot$. If PA-99-N2 and PA-00-S4 are disc/disc events, the mass turns out to be $< M_* >= 0.64^{+0.4}_{-0.2}$ $M_\odot$.

Chapter 7

Summary and Conclusions

The pixel lensing technique makes it possible to detect microlensing events even if the source stars may not be resolved. M31 is an interesting target for applying this technique. The Milky Way halo can be probed for MACHOs along a different line of sight and the results can be compared to the observations towards LMC, SMC, the Galactic centre and globular clusters. Because of the large inclination of the M31 disc, more events should be seen on the far side of the disc than on the near side, since on the far side the line of sight penetrates the denser inner part on the halo. Therefore, microlensing events caused by MACHOs in the M31 halo can be disentangled from Galactic halo and self-lensing events by looking on the far side of the disc. The self-lensing events should be detected anyway, even if there were no MACHOs at all in the haloes of M31 and the Milky Way. In this case, the self-lensing could be used to test the initial mass function (IMF) in the regime of low mass stars ($M < 1$ $M_\odot$), where the IMF is not well known.
One of the various collaborations, that searches for microlensing events towards M31 is POINT-AGAPE. POINT-AGAPE carried out a survey of M31 for pixel lensing during 1999 and 2000 towards two fields in M31. Recently, they reported a subset of four short-timescale microlensing candidates.
Since in the next few years data of much more pixel lensing events will be obtainable, it is essential to relate the various observed pixel lensing quantities (number of events, magnifications, time durations) to the quantities of interest (nature and masses of the lenses, fraction of the dark matter in form of MACHOs etc.). In this work, we have tried to get an insight into this problem.
A crucial issue is the definition of a detectable pixel lensing event, i.e. what physical conditions on the source star (magnitude, background light) and the source/lens geometry (impact parameter) have to be fulfilled, that a pixel lensing event is seen with a given telescope-CCD system. In 2.2 we discussed two rather simple methods to define a pixel lensing event, the peak threshold and the noise level threshold.

Optical depth	τ_{opt} $[10^{-7}]$
M31 halo	6.2
Galactic halo	1.7
Self-lensing	3.1
Estimation using t_E	$3.3^{+1}_{-1.1}$
Estimation using t_{fwhm}	$3.9^{+0.7}_{-0.9}$

Table 7.1: Summary of the calculated and measured optical depths. Note, that estimations with t_E are made with an efficiency of 0.2, the estimations using t_{fwhm} with an efficiency of 1.

An important microlensing quantity is the optical depth. In chapter 4 we calculated the optical depth to the different source/lens configurations theoretically for an up-to-date model of the target galaxy M31. We averaged over the two observed fields of the POINT-AGAPE collaboration. From the data of the four POINT-AGAPE events we estimated the measured optical depth using two methods (cf. subsection 2.3.1).
In Table 7.1 we confront these estimations to the theoretically calculated optical depth. (cf. chapter 6). At this point, it is difficult to accurately interpret these estimated optical depths, since our assumptions on the efficiencies ($\epsilon \equiv 0.2$, $\epsilon \equiv 1$, respectively) were all too simplified. In addition, there have been reported not enough events to build a proper statistics. Furhermore, the four reported POINT-AGAPE events are biased because microlensing candidate events with a time duration larger than 25 days or an excess flux less than a 21 magnitude star were cut away.

In chapter 5 we computed the pixel event rates and the expected number of events for the two year observing program of the POINT-AGAPE collaboration The obtained numbers of expected events are very high compared to only four reported events of the POINT-AGAPE collaboration (see Table 7.2). This indicates that our assumptions for the detectability for an event in a pixel lensing experiment are probably too optimistic. Table 7.2 shows that taking a more pessimistic approach for β_T decreases the expected number of events significantly. If we took into account in addition the experimental efficiency, we could get an expected number of events, which is in a quite good agreement with the four reported events.

The method of dark mass moments (cf. section 2.5) is an elegant way to extract physical quantities like the dark mass density, the MACHO number density, the mean MACHO masses and the fraction of dark matter in form of MACHOs from observational data. Because the Einstein time of the events is needed for the application of this method, we have tried to generalize this method to the pixel lensing case, where in general just the t_{fwhm}-timescale has been measured (see subsection 2.5.2). Our method has the disadvantage

Contribution	Total N_{ev} $Q_0 = 7$	Total N_{ev} $Q_0 = 42$
M31 halo	73	14
Galactic halo	19	4
Self-lensing	59	12
Total N_{ev}	151	30

Table 7.2: Total expected number of pixel lensing events for the POINT-AGAPE survey calculated by our standard approach $Q_0 = 7$ and a more pessimistic approach $Q_0 = 42$.

Contribution	Using t_E	Using t_{fwhm}
M31 halo	0.25	0.28
Galactic halo	0.2	0.2
Self-lensing bulge/bulge	0.26	0.48
Self-lensing disc/disc	0.7	0.64

Table 7.3: Mean lens masses for different assumed locations of the lenses. The masses are given in units of solar masses. The second column is obtained with the classical method of dark mass moments, the last column with the new method. For M31 and the Galactic halo we considered all events, for self-lensing we considered PA-99-N1, PA-00-S3 as bulge/bulge and PA-99-N2, PA-00-S4 as disc/disc events.

that we had to introduce another quantity β_{min}, which is related to the maximum magnification of a pixel lensing event because of the finite size of the source star. β_{min} depends on other unknown quantities (source radius, lens mass, etc.) and has therefore to be estimated as well. In any case the method we developed in subsection 2.5.2 has to be regarded just as a first step in the right direction. The method has certainly to be tested with more observational data and to be improved with more information on the experimental efficiencies and on the luminosity function of the source stars. In sections 6.1.2 and 6.2.2, respectively, we apply both the classical and the new method to the four POINT-AGAPE events. We summarize our results in Table 7.3 and Table 7.4. While for the masses the results of the two methods are in a good agreement, the MACHO fraction obtained by the classical method is systematically a factor 6 higher. The MACHO fraction is in particular dependent on β_T, but not on β_{min}. If we would use a more pessimistic β_T, this would increase the resulting MACHO fractions with both methods. It is therefore not clear at this point, where this discrepancy comes from. One possible answer could be, that in pixel lensing, it is not necessary to proceed from an efficiency of 0.2, because some kind of experimental restriction has already been taken into account in the threshold of the impact parameter β_T. [t]

Contribution	Using t_E	Using t_{fwhm}
M31 halo	5.6	35
Galactic halo	12	70

Table 7.4: Mean MACHO fraction of the M31 halo and the Galactic halo calculated from all four POINT-AGAPE events. The fractions are given in percents. The second column is obtained with the classical method of dark mass moments, the last column with the new method.

Acknowledgments

I would like to thank Prof. Dr. Ph. Jetzer for suggesting the problem, for his support and supervision during my work and for many helpful discussions. I would like to thank also Luigi Mancini for the computer program, written for microlensing towards the LMC, which I could use for my numerical calculations and as well for answering some questions. Finally, I thank Rocco Piffaretti for his help concerning computer problems.

Appendix A

Mathematical Tools

The excess flux of the source star during an ongoing microlensing event is

$$\Delta F(t) = F\ f\left[u^2(t)\right]\ , \tag{A.1}$$

with

$$f(x) := \frac{2+x}{\sqrt{x(4+x)}} - 1\ . \tag{A.2}$$

Often the inverse function $f^{-1}(x)$ is used, for which we proof the following important relation:

Proposition 1. *The inverse of the function f is given by*

$$f^{-1}(x) = f\big(2x\big)\ . \tag{A.3}$$

Proof. We calculate

$$f\Big[2\ f\big(2x\big)\Big]\ . \tag{A.4}$$

Obviously, we have

$$2\ f\big(2x\big) = \frac{4+4x}{\sqrt{4x(2+x)}} - 2\ , \tag{A.5}$$

from which we find

$$
\begin{aligned}
f\Big[2\ f\big(2x\big)\Big] &= \frac{2+\frac{4+4x}{\sqrt{4x(2+x)}}-2}{\sqrt{\left(\frac{4+4x}{\sqrt{4x(2+x)}}-2\right)\left(\frac{4+4x}{\sqrt{4x(2+x)}}+2\right)}} \\
&= \frac{\frac{4+4x}{\sqrt{4x(2+x)}}}{\sqrt{\frac{(4+4x)^2}{4x(2+x)}-4}}-1 \\
&= \frac{4+4x}{\sqrt{(4x+4)^2-16x(2+x)}}-1 \\
&= \frac{4+4x}{4}-1 \\
&= x\ .
\end{aligned}
\tag{A.6}
$$

□

Next, we want to find the relation between the Einstein time t_E and the full width at half maximum time t_{fwhm}:

Proposition 2.

$$
t_{fwhm} = t_E\ w(\beta)\ , \tag{A.7}
$$

where

$$
w(\beta) = 2\ \sqrt{2f\Big[f\big(\beta^2\big)\Big]-\beta^2}\ . \tag{A.8}
$$

Proof. From (A.1), we have

$$
\Delta F_{max} = F\ f\big(\beta^2\big)\ , \tag{A.9}
$$

$$
\frac{\Delta F_{max}}{2} = F\ f\big(u_{1/2}^2\big)\ , \tag{A.10}
$$

where $u_{1/2}$ is the impact parameter, when the excess flux is half of the maximum value. Division of the equations above yields $f(\beta^2) = 2f(u_{1/2}^2)$ and we can solve for $u_{1/2}$ as follows,

$$
u_{1/2}^2 = f^{-1}\left[\frac{f\big(\beta^2\big)}{2}\right] = 2\ f\Big[f\big(\beta^2\big)\Big]\ , \tag{A.11}
$$

where we have used Proposition 1. From (2.12) we have

$$
u_{1/2}^2 = \beta^2 + \left(\frac{t_{fwhm}/2}{t_E}\right)^2, \tag{A.12}
$$

With this determination, it is simple to find t_{fwhm},

$$t_{fwhm} = 2t_E \sqrt{u_{1/2}^2 - \beta^2} = 2t_E \sqrt{2f\left[f(\beta^2)\right] - \beta^2} \ . \qquad \text{(A.13)}$$

□

Appendix B

Calculations

For the calculation of D_{sl} and $\widehat{D}_{sl}(m)$ in (5.4) and (2.86) I used a FORTRAN program from L. Mancini written for microlensing towards LMC. The program applies a simple trapezoidal rule for the integration. The program calculates for instance $D_{b+d,h}$ and $\widehat{D}_{b+d,h}(m)$.
For the integration over the luminosity function in (2.69) I wrote a MATLAB program. Since $\beta_T(M)$ depends on the line of sight, the program calculates

$$\int dM \Phi(M)\ \beta_T(M)\ , \tag{B.1}$$

and its output is a matrix whose entries are the results of the integration above towards different line of sights.
For the integrations of the form

$$\int dv\ v^2 e^{-v^2} \int d\eta\ 2\eta\ I_0\big(2\eta v\big)\ I_0\big(2a(v_{c\perp})\eta\big)\ e^{-b\eta^2} \tag{B.2}$$

in (5.17), (5.35) and (5.39) I first carried out the integration over v, which can still be done analytically, giving

$$\begin{aligned} &\frac{\sqrt{\pi}}{2} \int d\eta\ \eta\ I_0\big(2a(v_{c\perp})\eta\big)\ e^{\eta^2\left(1/2-b\right)} \\ &\quad \times \left[I_0\big(\eta^2/2\big) + \eta^2 \Big(I_0\big(\eta^2/2\big) + I_1\big(\eta^2/2\big) \Big) \right], \end{aligned} \tag{B.3}$$

where I_1 is a modified Bessel function of the first kind with order 1. Then, for the integration over η I wrote a MATLAB program again. Here, the constant a depends on the line of sight, via the transverse circular velocity of the disc stars $v_{c\perp}$. Thus, the output of the program is a matrix again, containing the results for different positions towards M31. A third MATLAB program was written for the computation of $L(n)$ in (2.99). In all MATLAB programs the trapezoidal rule is used for the integration, but I also tested the the programs with the implemented MATLAB routine 'quad', which applies

recursive adaptive Simpson quadrature, and I obtained the same results. For analytical integrations or single numerical integrations I used MAPLE or MATHEMATICA.

Astrophysical constants and units

Speed of light (exact)	$c=2.99792458\times10^{8}$ m s^{-1}
Gravitational constant	$G=6.6726\pm0.0009\times10^{-11}$ $m^{3}kg^{-1}s^{-1}$
Kiloparsec	1 kpc$=3.0856\times10^{19}$ m = 3261 lyr
Solar mass	1 $M_{\odot}=1.989\times10^{30}$ kg
Solar radius	1 $R_{\odot}=6.96\times10^{8}$ m
Solar luminosity	1 $L_{\odot}=3.90\times10^{26}$ W
keV as a temperature	1 keV$=1.1605\times10^{7}$ K
Hubble parameter	$h=H_0/100$ km $s^{-1}Mpc^{-1}$
Density of Universe	$\rho=2.7755\times10^{11}$ Ω h^2 $M_{\odot}Mpc^{-3}$

Bibliography

[1] Ansari R. et al. 1997, A&A **324**, 834

[2] Ansari R. et al. 1999, A&A **344**, L49

[3] Aurière M. et al., 2001, ApJ **553**, L137-L140

[4] Bahcall J.N., Soneira R.M., 1980, ApJ **44**, 73

[5] Baillon P. et al., 1993, A&A **277**, 1

[6] Baltz E. A. & Silk J., 2000, ApJ **530**, 578

[7] Baltz E.A. & Silk J., 2001, MNRAS **323**, L31

[8] Baltz E. A., Gyuk G. & Crotts A., 2002, arXiv:astro-ph/0201054

[9] Binney J. & Tremaine S., 1987, Galactic Dynamics (Princeton Univ. Press)

[10] Calchi Novati S. et al., 2002, A&A **381**, 848

[11] Crotts, A., 1992, ApJ **399**, L43

[12] Crotts A. & Tomaney 1996, ApJ **473**, L87

[13] Crotts et al. 2000, astro-ph/0006282 v2

[14] De Rújula A., Jetzer Ph. & Masso E., 1992, A&A **254**, 99

[15] De Rújula A., Jetzer Ph. & Masso E., 1991, MNRAS **250**, 348

[16] Einstein A., 1936, Science **84**, 506

[17] Ford, H.C., Jacoby G.H. & Jenner D.C. 1978, ApJ **223**, 94

[18] Gondolo P., 1999, ApJ **510**, L29

[19] Gould A. 1993, ApJ **404**, 451-454

[20] Gould A. 1994, ApJ **435**, 573

[21] Gould A. 1995, ApJ **455**, 44

[22] Gould A. 1996, ApJ **470**, 201

[23] Grenacher L. et al., 1999, A&A **351**, 775

[24] Griest K., 1991, ApJ **366**, 412-421

[25] Gyuk G. & Crotts A., 2000, ApJ **535**, 621

[26] Han C., 1996, ApJ **472**, 108

[27] Jetzer Ph. 1994, A&A **286**, 426

[28] Kent S.M., 1987, AJ **94** (2), 306

[29] Kent S.M., 1983, ApJ **266**, 563

[30] Kent S.M., 1989, AJ **97** (6), 1614

[31] Kerins E. J. et al., 2001, MNRAS **323**, 13

[32] Melchior A.-L. 1995, PhD thesis

[33] Melchior A.-L. 1998, A&A **134**, 377

[34] Ostriker J.P., Peebles P.J.E., 1974, ApJ **186**, 467

[35] Paczyński B., 1986, ApJ **304**, 1

[36] Paulin-Henriksson et al. 2002, astro-ph/0207025 v1

[37] Peacock J.A. 1999, Cosmological Physics (Cambridge Univ. Press)

[38] Ruiz M.T., 1976, ApJ **207**, 376

[39] Ruiz M.T., 1976, ApJ **207**, 382

[40] Straumann N., 1974, HPA **47**, 379

[41] Tonry J. & Schneider D.P., 1988, ApJ **96** (3), 807

[42] Walsh D., Carswell R.F. & Weymann R.J. 1979, Nature **279**, 381

[43] Zwicky F., 1933, Helv. Phys. Acta **6**, 110